N-HETEROCYCLIC CARBENE SYNTHESIS TOWARDS SELF-ASSEMBLED MONOLAYERS ON GOLD

by

Jennifer F. McLeod

A thesis submitted to the Department of Chemistry

In conformity with the requirements for

Degree of Master of Science

Queen's University

Kingston, Ontario, Canada

(June, 2019)

Abstract

Modifying surfaces with self assembled monolayers (SAMs) is a simple and effective way to create functional materials. Traditionally compounds containing a thiol head group are used to generate SAMs on gold surfaces. However, a recent discovery by the Crudden lab demonstrated increased bond strength and surface stability of n heterocyclic carbenes (NHCs) to a gold substrate. Here in we report the synthesis and modification of gold surfaces with NHCs containing unique functionality. Chemical synthesis was characterized using nuclear magnetic resonance spectroscopy techniques and SAM formation was analyzed using x-ray photoelectron spectroscopy (XPS). N,N'-Ditolyl-4,5(R,R)-diphenylimidazolium tetrafluroborate (**19**) is a known molecule with chiral functionality about the backbone and successfully formed a SAM on gold with a calculated carbon to nitrogen ratio of 29:2 from XPS analysis results. Iodine (**31**), triflate (**34**), hydrogen bicarbonate (**35**), and tetrafluoroborate (**37**) salts of N,N'-Diisopropyl[2,3-d]imidazoliumnaphthalene were synthesized in order to investigate the π-stacking of the naphthalene backbone when assembled on a gold surface. Unfortunately, from XPS analysis a full monolayer was never achieved. Finally, N,N'-Diisopropylnaphtho[2,3-d]imidazolium-4,9-dione salts: iodine (**48**), triflate (**50**), and tetrafluoroborate (**49**), were synthesized in an attempt to electrochemically probe the redox active quinone moiety once a SAM had formed on a gold surface. Compound **49** formed a monolayer on the gold surface with a carbon to nitrogen ratio of 16:2 from the XPS analysis results and compound **50** has a carbon to nitrogen ratio of 36:2. The electrochemistry experiments were performed using a monolayer of **50** on a gold electrode. The cyclic voltammogram revealed very minor features characteristic of the quinone moiety which indicates low molecular consistent with XPS results.

Acknowledgements

I would like to thank my supervisor Dr. Cathleen Crudden for supporting me (an organic chemistry novice) through a Master's in her lab. I will forever appreciate the skills I have learned from working in an organic chemistry lab. I would like to thank Megan Bruce for all the assistance she provides to all of us. I have no idea how you manage to do it all but we would fall apart without you! I would also like to thank my lab mates who supported me through many a synthesis meeting and helped me with my reactions when all hope was lost. I would also like to thank Dr. Christene Smith for her contagious positive attitude and ability to see the glass half full. Every day was a little brighter with you around and I greatly appreciate your friendship. I would like to thank Dr. Zhe She for his support through the writing process and many lengthy conversations about bikes. I look forward to future rides this summer! Lastly, I would like to thank Josh Clarke for his dedicated friendship and patience. I would not have made it through this degree with out you. You were my rock in hard times and I greatly appreciate all the extra effort you made to help my everyday run a little better and sit with me while I was struggling to learn how to push arrows and solve synthesis problems.

Table of Contents

List of Figures

List of Schemes

List of Tables

List of Abbreviations

BDE	Bond dissociation energy
HREELS	High resolution electron energy loss spectroscopy
NHC	N-heterocyclic Carbene
NMR	Nuclear magnetic resonance
SAM	Self assembled monolayer
SPR	Surface plasmon resonance
STM	Scanning tunneling microscopy
UHV	Ultra high vacuum
XPS	X-ray photoelectron spectroscopy

Chapter 1

Introduction

1.1 N-Heterocyclic Carbenes Overview

1.1.1 A Brief History of Carbenes

Chemistry is an ever-evolving science which has been host to some revolutionary discoveries and continues to grow and adapt to current needs. One of these discoveries was the postulation and isolation of a species known as a carbene, opening new applications of chemistry through all fields from organic to materials chemistry[1].

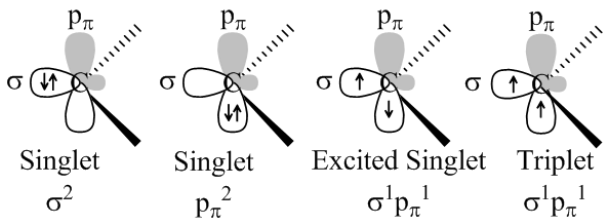

Figure 1-1:[2] Singlet and Triplet Carbene Electronic Configuration. Adapted from Reference 2

A carbene is a neutral compound with a divalent carbon atom containing six electrons in the valence shell and two electrons are found in nonbonding orbitals. As seen in Figure 1-1, carbenes exist in a singlet or triplet state. The singlet state has electrons spin paired in the same orbital (either the σ or p_π), the triplet state exists when the lone pair electrons singly occupy two different, degenerate orbitals with parallel spins.[2,3] Singlet carbenes were the first to become famous as ligands when Fischer synthesized a tungsten carbonyl carbene complex, which later became part of a class of complexes known as Fischer carbene complexes.[4] These carbene complexes are used in several reactions including Diels-Alder and Michael addition reactions.[5,6] Ten years later, triplet carbenes found the spotlight when Schrock created a tantalum carbene complex bearing a triplet carbene.[7] The main application for this carbene complex is as a catalyst

for metathesis reactions.[8] For the purposes of this thesis, a class of singlet carbenes known as N-heterocyclic carbenes (NHCs) will be discussed. NHCs are cyclic singlet carbenes containing at least one nitrogen heteroatom adjacent to the carbenic carbon.

In 1957, Breslow compared the C_2 carbon of a thiazolium salt to the negatively charged carbon on cyanide, suggesting a possible zwitterionic structure analogous to a singlet carbene.[1] In 1962, Wanzlick investigated the nucleophilicity of NHCs, and postulated about the resonance stability of these molecules.[9] He was unable to isolate the carbene, however, he successfully synthesized different imidazolylidene adducts. Figure 1-2 compound **1** illustrates the first heteroatomic carbene to be isolated and characterized, a phosphinocarbene synthesized from the affiliate α-diazophosphine by Bertrand and co-workers in 1988.[10] Following this, the first NHC-based carbene (**2**) was isolated by Arduengo in 1991.[11]

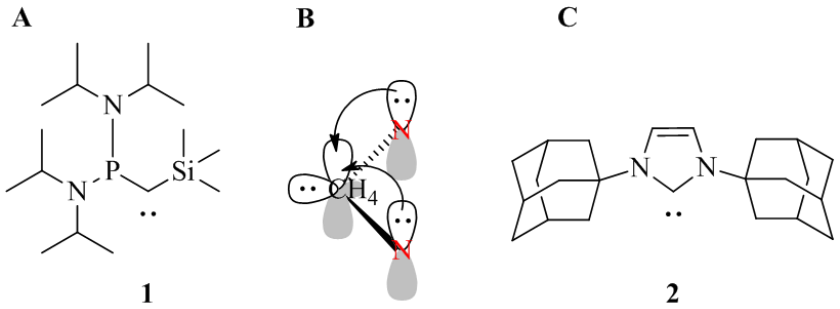

Figure 1-2: NHC Electronics with Notable Carbenes. A Betrand's carbene, B schematic of π-electron donation from nitrogen to carbon, and C Arduengo's carbene .

Typically, a carbene in the triplet state is more stable. However, for NHCs the singlet electronic configuration is more favorable, owing to the donation of electron density of the nitrogens into the empty p-orbital of the carbon as depicted in Figure 1-2B. The high stability of NHC-type carbenes comes from the mesomeric π-donating and σ-withdrawing effects of the adjacent amino groups to stabilize the divalent carbon creating a "push-pull" system that substantially increases carbene stability.[9,12] Sterics also play a role in NHC stability, with larger nitrogen-bound substituents typically conferring more thermal stability. In the case of triplet carbenes, sterics are the dominating factor for stability.[2,3] Additionally, aromaticity when present, is also a contributing factor, increasing the energy gap between the σ and π orbitals, allowing

the NHC to remain in the singlet ground state, however it is by no means required for NHC stability.[13–15] NHCs are also excellent Lewis bases, and create very stable bonds with many metal complexes, which makes transition metal NHC complexes excellent precursors for various catalytic applications.[9,11,16] However, free carbene NHCs are typically only stable under anhydrous conditions, making them more difficult to work with than phosphine-type ligands, requiring a glove box or Schlenk techniques.

NHC metal complexes have been known since the early 1960s and have become a popular choice to replace phosphine-based metal complexes.[2,3] One study by Herrmann and coworkers measured the bond dissociation energies (BDE) for two different phosphine ruthenium complexes, and compared it to the analogous 2,3-dihydro-1*H*-imidazol-2-ylidene ruthenium complex, compound **3**. The NHC–metal bond has a BDE of 18 kcal mol^{-1} larger than the most strongly binding phosphine.[17] Air and moisture stable NHC transition metal complexes have been synthesized as early as 1995. The NHC-palladium catalyst compound **4,** Figure 1-3, described by Herrmann *et al.* was reported to be heat, oxygen, and moisture stable, also surviving boiling THF.[18]

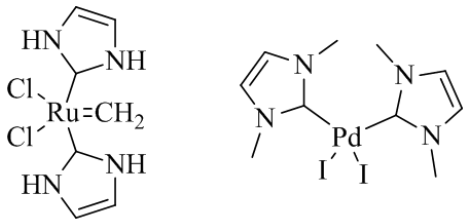

3 **4**

Figure 1-3: Transition Metal Carbene Complexes. **3** Ruthenium - NHC catalyst for metathesis[17], **4** and palladium – NHC catalyst for Heck coupling[18].

The increased stability to the complex by the NHC makes it a popular ligand for robust chemical reactions. In addition to replacing phosphines on metals for catalysis, NHCs have also been known to be suitable capping ligands in various materials applications, as will be discussed below.

Compound **3,** Arduengo's carbene, was the first NHC to be isolated, the structure seen in Figure 1-2 has an imidazole core with two adamantly groups. Since then, countless derivatives of the Arduengo carbene have been created and characterized.[19]

1.1.2 The Use of NHCs in Materials Science

1.1.3.1 Self-Assembled Monolayers

Self-assembled monolayers (SAMs) spontaneously form an organized monolayer of molecules from either solution or vapour phase.[20,21] One of the earliest SAM reports was by Bigelow *et al*. in 1946, who observed the spontaneous monolayer formation of eicosyl alcohol on a pyrex™ Erlenmeyer flask.[22] SAMs are created when a surface active material physisorbs onto a surface and reorder until in its most energetically stable orientation prior to final chemisorption onto the surface.[20] The affinity of the surface active species to the substrate will dictate the SAM stability.

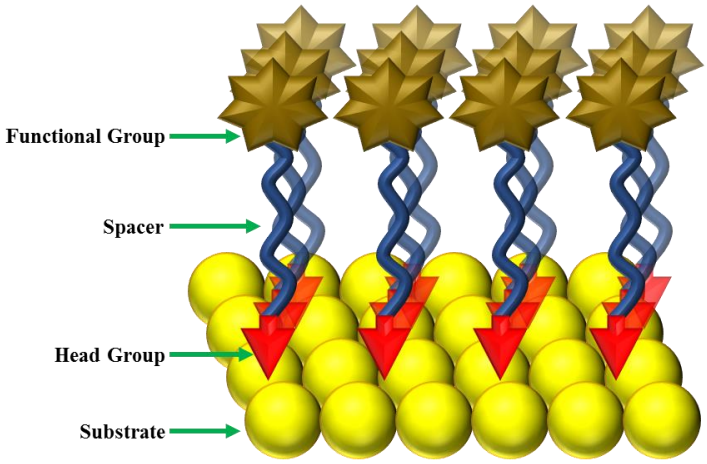

Figure 1-4: Self Assembled Monolayer Schematic

SAMs consists of 4 parts as outlined in Figure 1-5. The first is the surface which will react and support the molecular adsorbate. This surface is called the substrate. The molecule which will be forming the monolayer contains the other three sections of a SAM. There needs to be a surface-active head group, which is the part of the molecule that will react and form a chemical bond with the substrate. Often there will be a spacer between the head group and the terminal functionality. This spacer is traditionally a simple alkyl chain with varying lengths depending on the purpose of the SAM. Finally, there may be some sort of terminal functionality. The functionality is tailored towards the application being used and resides at the opposing end of the molecule from the head group.[21]

For each component of a SAM there is an interface. The border between the head group and the substrate is where the chemistry of SAM formation happens. As mentioned above, the head group will

undergo physisorption then chemisorption to the substrate when energetically stable. The area occupied by the spacer will determine monolayer thickness, stabilize the molecule after chemisorption, and change the optical and conductive properties of the SAM.[21,23] Finally, the boundary between the terminal functional group and surrounding media is where the intended chemistry will happen.

Nuzzo *et al.* discovered the self-assembly of disulfides on gold, generating a whole field of research into thiols as SAMs for gold surfaces.[24] The first use of NHCs as a monolayer on gold appeared in 2011 by Weidner *et al*.[25] In this study, the researchers performed a solution deposition of 1,3-diethylbenzimidazol-2-ylidene onto a (111) gold on silica chip in THF for 24 hours and characterized the product by NEXAFS. After this study, in 2013 Johnson and coworkers investigated the binding of NHCs to a gold surface by flowing free carbenes over a gold surface in a THF solution while concurrently monitoring the surface using a quartz crystal microbalance.[26] Shortly after, Crudden *et al*. were the first to investigate the stability of NHCs on a gold substrate and compare these to thiols in 2014.[27] This study showed that NHCs are stable towards temperature extremes, boiling water, boiling organic solvents, pH extremes, and even 1% hydrogen peroxide.[27] Comparatively, thiol SAMs desorb from a planar gold surface around 70°C, and readily desorb in THF.[23,28,29] Additionally, oxidation of thiol SAMs spontaneously occurs under ambient conditions resulting in thiol desorption from the gold surface.[30–32] Suffice to say that the substantially greater stability of NHC-type SAMs on gold lends a new tool for SAM research.

There are a multitude of applications for the self assembly of molecules onto metal surfaces.[33] One important application is metal protection against corrosion.[33–35] The organization of SAMs on the surface often lends to closely packed assemblies that can protect metal surfaces against corrosion as depicted in Figure 1-5.[33,34] One example by Zhang *et al.* describes the protective abilities of a monolayer of cysteine modified with either dodecylacid or dodecylamine on a copper surface.[34] In this study, the surface resistance was measured using electrochemical impedance spectroscopy, where a higher resistance indicates better stability towards electrochemical oxidation. The researchers concluded that cysteine modified with dodecylacid or dodecylamine provided superior protection than unmodified cysteine.[34]

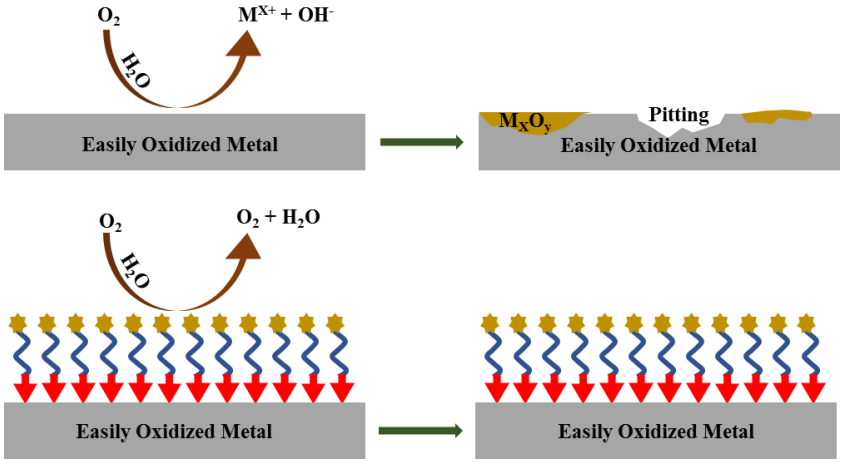

Figure 1-5: Schematic of SAMs for Metal Surface Protection

Another application for SAMs is their use in building sensitive surface plasmon resonance (SPR) sensor chips.[36] In this technique a light source is directed at the surface being investigated and the reflected light is detected and measured. When the light hits the substrate, it induces a surface plasmon which is a wave of electron density that oscillates across the surface. By inducing this surface plasmon a portion of the light which was directed at the metal is absorbed changing the refractive angle of the incident light which the spectrometer detects to identify the amount of light adsorbed by the metal.[36,37] When the surface is modified with a SAM the signal detected will be different than the bare substrate, making it possible to characterize SAM formation. Additionally, if the functional group on the SAM is designed to detect a specific analyte, a biosensor can be conceived which measures the signal difference between bound and unbound analyte as depicted in Figure 1-6.[38]

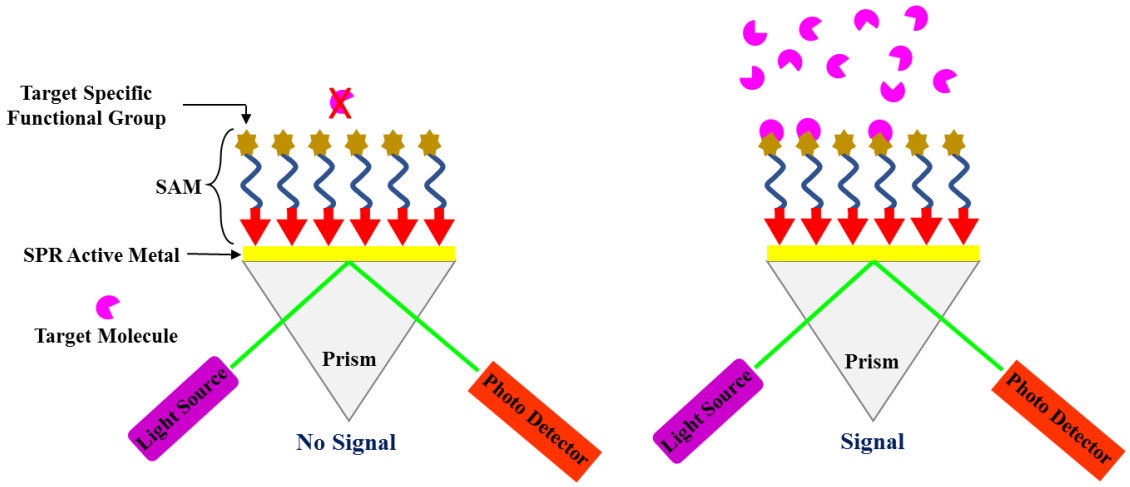

Figure 1-6: Basic Schematic of a Surface Plasmon Resonance SAM Sensor

In 2016 Crudden *et al*. reported on a bench stable technique for NHC SAM formation and applied it to create an NHC analogue for a biotin SPR sensor. When compared to the commercially available thiol based sensor, the NHC chip had greater sensitivity, longer shelf life, better performance at extreme pH levels, and more consistency between measurements.[39] This research highlights the potential to create more durable devices by simply replacing thiols with NHCs in SAMs.

1.1.3.2 NHC Deposition on Metal Surfaces

Solution or vapour phase deposition is possible for both thiol and NHC SAMs.[20,21,39,40] For solution phase deposition, the transport of adsorbate to the solution solid interface is the first step, followed by adsorption of the target molecule in sub monolayer quantity.[20,21] Over time the film reorganizes into a structured densely packed layer known as the SAM.[20,21] The initial *in situ* study of thiol vapour phase deposition was completed in 1996 by Poirier and Pylant, who found that thiol deposition started with island growth, lying flat on the substrate then reconstructed to an organized SAM.[41] Two years later, measuring substrates at various adsorbate concentrations using x-ray techniques yielded results corroborating the previous *in situ* study.[42]

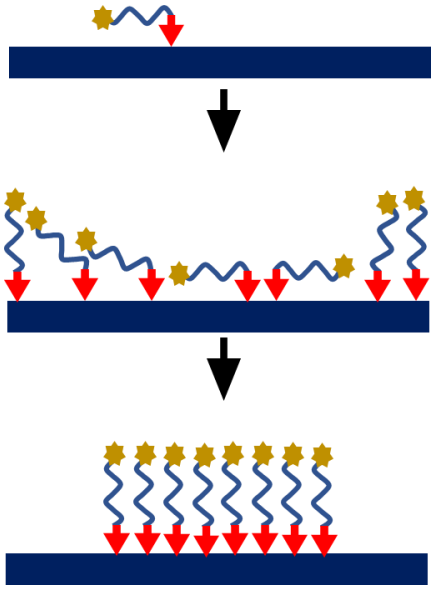

Figure 1-7: Schematic of SAM Formation

There are many factors associated with the stability of thiol SAMs formed by vapour and solution phase deposition. In the solution phase, interaction of the target molecule with solvent can cause decomposition. Cometto *et al*. created sulfur SAMs with dimethyl disulfide.[3] Electrochemical desorption was used to characterize the monolayer showing that immersion times of 1 hour and greater. This technique showed the loss of the signal attributed to the methyl thiolate and the appearance of a desorption current peak attributed to sulfur. Additionally, X-ray photoelectron spectroscopy (XPS) measurements of the surface saw the growth of a sulfur feature at -161eV indicative of atomic sulfur.[43] In another paper, Salvarezza and coworkers created SAMs from 4-mercaptopyridine and found through XPS characterization that ethanolic solutions promote decomposition into atomic sulfur and other poly sulfur species in as little as 10 minutes.[44]

In the case of preparing NHC films, deposition often needs to be carried out under inert atmosphere since carbenes are typically reactive towards H_2O. Another factor which can affect the stability of the molecule or SAM formation is the cleanliness of the substrate. For solution phase deposition, it is important to immerse the substrate in the thiol solution shortly after it has been cleaned so adventitious contaminants have less time to adsorb onto the surface.[20,21] Vapour phase depositions have the advantage of being in ultra-high vacuum, so contaminants are less of an issue. However in this case, SAM precursors must be

volatile enough for in vacuo deposition and must have sufficient thermal stability to withstand any heating required..[20,21,42,45]

When studying the sulfur gold bond of films generated via solution phase and by vapor phase, it is found the vapor phase has a weaker bond to the surface.[46,47] Nuzzo *et.* al observed ultra high vacuum monolayer formation does not involve the cleavage of the S-H bond, allowing the sulfur to desorb more easily from the surface.[47] Thus, solution phase is the favoured method for creating SAMs. In the case of the generation of NHC-based SAMs, a strong base such as KO^{t}Bu, or NaH is needed to prepare the NHC from its protonated salt.[2,27,39] However this process requires the use of either Schlenk techniques or an inert atmosphere glovebox.

The Crudden lab reported a bench-stable solution-phase deposition of imidazolium bicarbonate salts.[39] This was an important advance in the area of NHC deposition since it allows for deposition under ambient conditions without any special precautions. This salt works as a precursor to NHCs since in organic solvents such as methanol, the bicarbonate anion is a strong enough base to deprotonate the carbenic carbon and generate the free carbene, and thus with bicarbonate as the anion, exogenous base is not needed.[48–50] The SAM formed using this technique is as stable as that generated using the free carbene.[27,39] These reports revolutionized the approach to NHC SAM formation, by offering a more accessible technique providing a highly stable SAM. In this thesis, solution phase NHC SAMs will be made with both the free carbene and bench stable methods.

1.1.3.3 NHC SAMs formed on Gold Surfaces

In 2014, Crudden *et al*. investigated the properties of NHCs chemisorbed to gold surfaces, specifically looking at the binding mode, bond strength, and chemical robustness of the resulting film.[27] NHCs were extensively investigated and were shown to form ordered monolayers on the gold surface, binding via the carbeneic carbon. The gold carbon bond strength was measured to be 150 kJ mol^{-1} which is 25 kJ mol^{-1} stronger than the gold thiol bond.[27,45] In subsequent studies, the nature of the wingtip groups was shown to be critical to influence binding mode and bond strength to the surface. If these substituents

were too small, NHCs lie flat on the surface.[40,51,52] Additionally, if the wingtip groups were too bulky, less stable films were formed.[40,51,52]

Despite NHCs forming a strong bond with gold, *in situ* measurements show they may be mobile on the surface.[40,51,52] These two ideas are not, however, incongruent since thiols are also known to bind tightly to the surface and yet still reorganize the surface by weakening the gold-gold bonds.[53,54]

Wang *et al*. proposed this type of restructuring to explain the ordered films they observed, but they tested only highly bulky DIPP-type NHCs, which may preferentially bind to stray gold atoms already at a higher energy.[51] Other applications for NHCs on gold and other metals, include nanoparticles and catalysis as discussed in a Chemical Reviews article by Smith *et. al*.[55]

1.1.3.4 The Use of NHCs in Nanoparticle Synthesis

Transition metal nanoparticles have applications in catalysis, sensing and in bionanotechnology.[56,57]

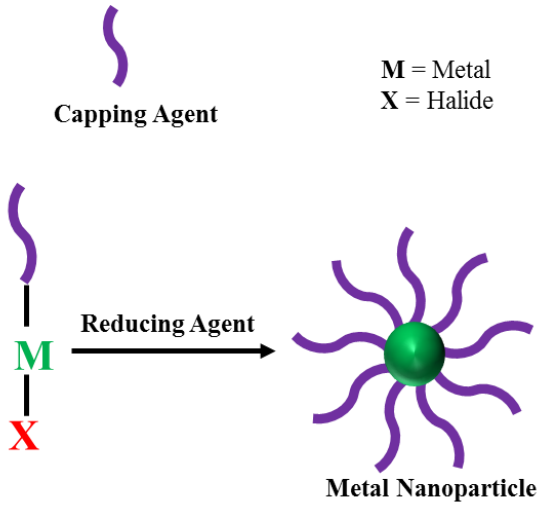

Figure 1-8: Nanoparticle Formation Schematic

To obtain nanosized particles, a capping agent must be used to reduce surface energy and limit growth. As on planar surfaces, thiols are widely used to stabilize nanoparticles.[24,58] However, the high

stability of NHCs on metal surfaces makes them an ideal candidate as surfactants for nanoparticles. The development of NHC-capped nanoparticles is a relatively recent phenomenon stemming from a report by Ott *et al*. where the *in situ* preparation of NHC stabilized nanoparticles was reported in 2005. [59]

There are two standard methods for creating nanoparticles, bottom up, and top down. In the bottom up method, a metal complex containing the desired metal and surfactant are reduced forming the nanoparticle.[60,61] In the top-down method, a pre-formed nanoparticle with a different surfactant will be subjected to ligand exchange with an NHC.[62] Multidentate ligands are widely employed in thiolate-stabilized systems in both the bottom up and top down approaches, and have recently been illustrated with NHCs.[63,64] A study by Man *et al.* investigates the stability of gold nanoparticles functionalized with bidentate NHCs in both the bottom up and top down approaches.[63] The use of alkyl linker on the backbone of the NHC was shown to enhance nanoparticle stability, with the top down approach producing the most stable particles. Interestingly, the nanoparticles prepared with bidenteate NHCs were not significantly more stable than monodentate NHCs.

Reactive NHC metal nanoparticles formed in both the top down and bottom up approaches have been employed in heterogenous catalysis.[55,65] Palladium, ruthenium, and platinum NHC functionalized nanoparticles have all been synthesized and used for catalysis.[66] For example, palladium has been used in the α-arylation of ketones,[67] ruthenium has been employed for hydrogenation of aromatic compounds,[68] and platinum nanoparticles have been reported for the hydrogenation of styrene.[69] However, it should be noted that this list is far from exhaustive. Continued expansion in this area of chemistry has the potential to improve upon current homogeneous catalysis techniques.[55,65]

1.2 Surface Analysis Techniques

1.1.1 X-ray Photoelectron Spectroscopy

X-ray photoelectron spectroscopy (XPS) is a surface analysis technique used extensively in this thesis. XPS works by bombarding a surface with high energy X-rays causing an electron to be ejected from an atomic orbital of an atom laying on the surface of the sample. The electron is detected by the instrument and the binding energy corresponding to a specific element, and the quantum orbital it came from can be determined as depicted in Figure 1-9.[70–73]

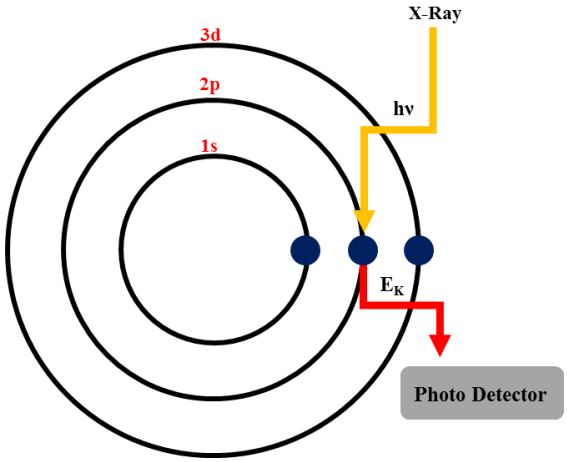

Figure 1-9: XPS Schematic

The first X-ray spectrometer with the capacity to measure binding energies within 1 electron volt was designed by Nordling *et al.* in 1957.[74] In this experiment the researchers evaporated 500 Å of copper onto a 0.5μm sheet of aluminum. When the copper was irradiated with X-rays, the resulting spectrum provided a binding energy consistent with previously reported values. A few years later in 1964, Seigbahn and co workers were able to distinguish chemical bonding between different elements.[75] When comparing the spectra of S, Na_2SO_3, and Na_2SO_4 the scientists noticed a shift in the sulfur peak position. The peak shift is indicative of the different bonds which the sulfur is making. This also lends a tool for deconvolution of more complicated spectra when there are over lapping peaks. Additionally, in the same year this group was able to characterize lighter elements ($Z \leq 12$) which was previously not possible using this technique.[76]

Armed with the ability to identify any element on the periodic table and its oxidation state, XPS is a truly indispensable technique for elemental surface analysis.

1.1.1 Scanning Tunneling Microscopy

Scanning tunneling microscopy (STM) is another surface analysis technique employed to image the morphology of a substrate under investigation. STM was invented in 1982 by Binning, Rohrer, Gerber, and Weibel.[77,78] In their experiment, the (110) surfaces of $CaIrSn_4$ and Au was investigated at angstrom level topology. The lattice space of the Ir metal was measured to be 6.7 Å which is consistent with the estimated value of 6.87 Å from crystallographic data.

STM works by applying a current to an atomically precise tip. Using a piezoelectric tube the tip can approach within angstroms of the surface which causes electrons to tunnel from the substrate generating an image of the topography based of the tunneling current.[79,80] There are two main methods for imaging the surface, constant current and constant height. Constant current is often used for imaging molecules and features on a surface. In this method the current applied to the probe is kept constant resulting in height changes as it moves across the surface.[81] This allows the change in height of the different features on the surface to be measured. Conversely, in the constant height method, the position of the probe in the z axis is kept constant resulting in a changing current as the tip rasters across the surface.[81] This method is often used with atomically flat surfaces since height variation in topology runs the risk of damaging the tip. Using the constant height method can be useful in mixed metal surfaces, as an image can be generated depicting the exact areas containing each respective metal. Figure 1-10 depicts a general schematic of scanning tunneling microscope, and the tunneling of electrons.

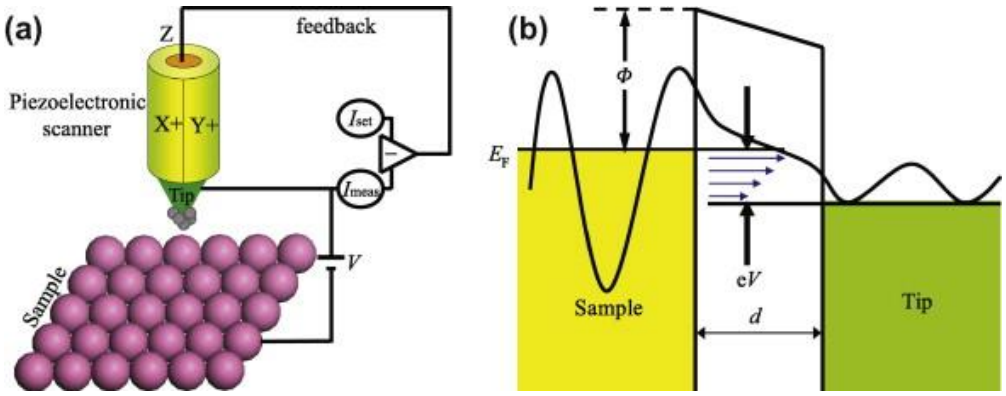

Figure 1-10:[82] (a) General schematic of a scanning tunneling microscope with a circuit describing the constant current method. A voltage V is applied between the tip and the surface generating the tunneling current Imeas. The difference is measured between Imeas and the set point current Iset and fed back to the z piezo control which determines the tip height. (b) Schematic of the tunneling processes between the sample and the tip across a vacuum barrier with width d and height ϕ. Taken from Reference 82.

The images resulting from STM can provide information about surface organization of the SAM, the formation of etch pits and mobility of step edges, etc.[79] It is also possible to do single molecule imaging where the vibrational mode of the molecule can be imaged. Additionally, the effects of surrounding co-adsorbed species and surface defects on the molecules vibrational properties can be investigated.[83,84]

1.1.2 Electrochemical Analysis

Electrochemical studies of SAMs are another valuable way to test film stability and probe electrochemical properties such as electron transfer rates. Electron transfer rates can be evaluated using a range of different techniques such as cyclic and linear sweep voltammetry.[85] The Laviron method and Tafel plots can be used for evaluating the electron transfer rates of SAMs. Crudden and co workers determined the electron transfer rate of a ferrocene tagged NHC SAM to be $9.1 s^{-1}$ which is identical to the comparable thiol SAM.[39,86] In the same study, the electrochemical stability of the NHC SAM was monitored using cyclic voltammetry, where an increase in current signal would indicate monolayer degradation which creates surface defects.

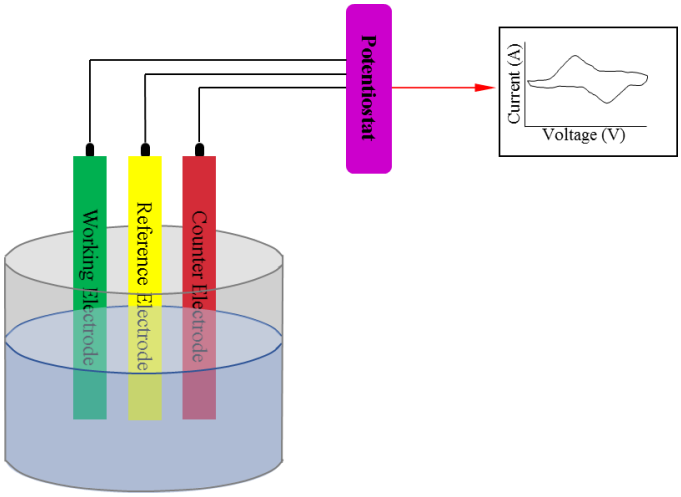

Figure 1-11: Generalized Schematic of Cyclic Voltammetry

1.2.3.1 NHC Structure

The stable NHC structure is in part derived from the wingtip groups attached to the nitrogen atoms adjacent to the carbenic carbon. Steric bulk in these positions helps to kinetically stabilize the molecule.[3] Additionally, an unsaturated backbone contributes to NHC stability as the molecule is now flat which improves π-donation from the nitrogen into the empty carbene p-orbital.[3] Figure 1-12 depicts a range of NHC salts which are used as precursors for forming the free carbene.

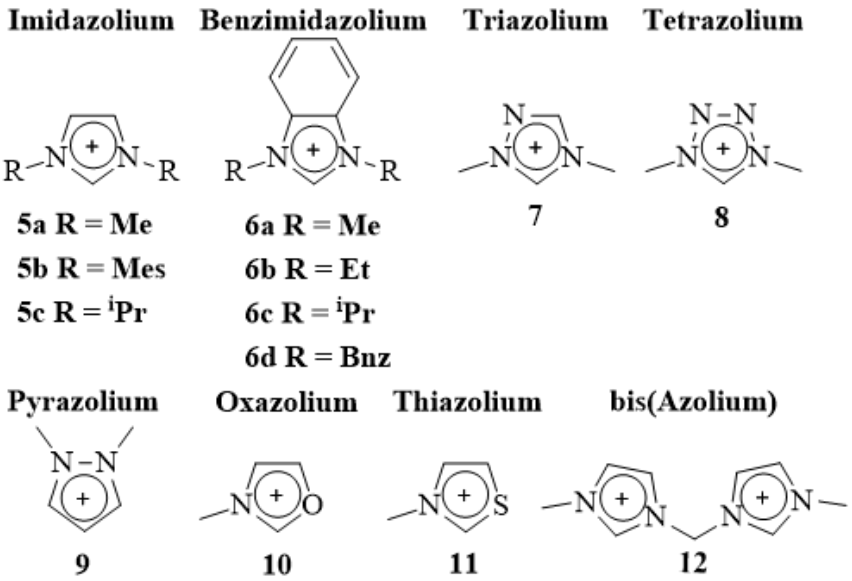

Figure 1-12: Typical NHC Precursors

In this thesis, the variations on structures **5** and **6** will be studied. One key difference between **5c** and **6c** is the pKa of the C_2 proton. In DMSO, the carbenic proton of an imidazolium ion has a pKa of 24, which is higher than benzimidazolium which has a pKa of 18.6.[87,88] Thus it is easier to remove the C_2 proton from the alkylated benzimidazolium forming the benzimidazolylidine carbene that has been largely employed in this thesis.

Substituents on the nitrogen atoms flanking the carbene are called the wingtip groups. The substituents at these positions have implications on the surface binding mode of the NHC. The first thorough study of NHC SAMs in 2014 found that NHCs with bulky wingtip groups such as in IMes **5b**, are less stable than NHC SAMs generated from **6c**[27] A first principles density functional theory study by Tang *et al*. compares different ligands bound to gold and describes the increased stability of bulky NHCs due to the van der Waals interaction with the wingtip groups and gold. [89] With a substituent such as a benzyl group **6d**, one can imagine as the NHC approaches the surface, the wingtip groups can freely rotate about the methylene such that the phenyl rings are parallel with the surface inducing van der Waals interactions and allow for chemisorption outlined in Figure 1-15 B. Conversely, as previously mentioned and illustrated in Figure 1-15 D, having a mesityl group (**5b**) at the wingtip position creates substantial steric bulk with reduced mobility causing difficulties for the carbene to approach the surface and form a chemical bond.[27,51]

In a detailed investigation on the effect of wing-tip size and the orientation of deposited NHCs on a copper surface, our group showed that NHCs **6a** and **6b**, with small wing tip groups lie flat on the surface forming dimeric structures resulting from extraction of a metal atom from the surface, while isopropyl-substituted NHC **6c** stands straight up as previously predicted.[40] These results were obtained using high resolution electron energy loss spectroscopy (HREELS), STM, and complimentary density functional theory studies. The HREELS spectra revealed, among other signals, a peak at 730 cm^{-1} for **6a** and **6b**, characteristic of an out of plane aromatic C-H bending mode. This peak was enhanced relative to solution studies and therefore strongly suggests, due to surface selection rules, that the molecule is oriented normal to the plane of the metal . This was confirmed by the STM images, which showed the molecules lying flat on the surface in dimers, having extracted one metal atom from the bulk. Around the same time, Papageorgiou and coworkers reported the same results for **5a**, the imidazolium version of **6a** using STM alone.[52]

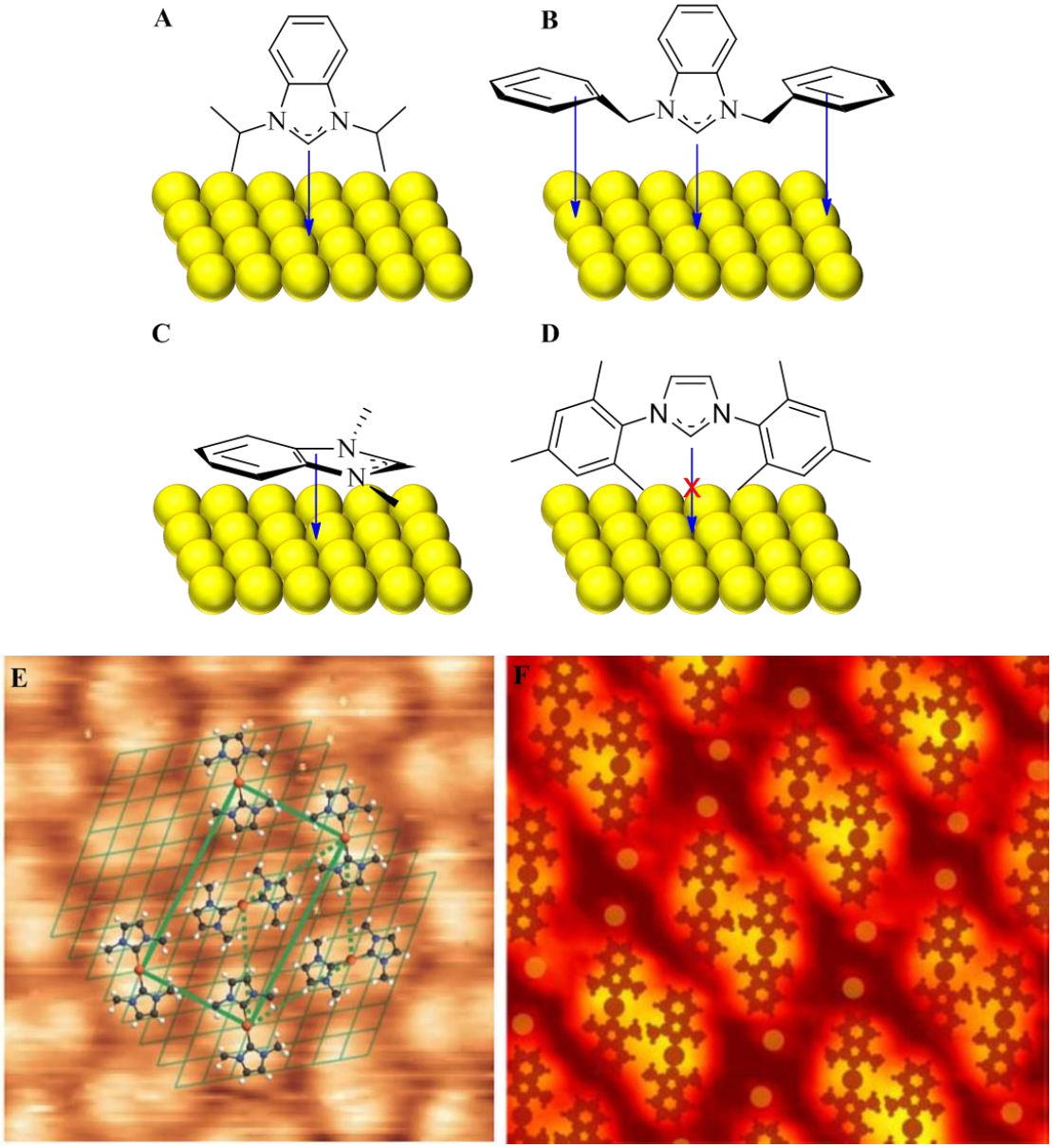

Figure 1-15: Schematic diagram of different carbenes approaching a metal surface **A** perpendicular approach of **6c** to substrate with sufficiently bulky wingtip group. **B** perpendicular approach of 6d to substrate stabilized by aromatic wingtip groups. **C** parallel approach of **5a** to substrate. **D** very bulky wingtip groups of **5b** preventing carbene approach to the substrate. **E**[52] STM image of 5a dimer lying flat on a copper surface. **F**[40] STM image of 6a dimer lying flat on a copper surface. Taken from Reference 52.

In addition to surface orientation, another effect the wingtip groups can have is the intermolecular interactions. If the substituents on the wingtip groups exhibit little intermolecular interaction, the spacing between each NHC moiety will be at least as large as each molecule. However, if the NHC design has significant intermolecular interactions there is potential for a denser film.[90] As previously mentioned, a densely packed film is advantageous for substrate protection of easily oxidizing metals such as silver and

copper.[33–35] Controlling the intermolecular interactions is important for film density control and applications for this technology. The introduction of structures that can lead to ordered surfaces and serve as reporters for redox properties will be studied in this thesis.

1.2.3.2 Redox Active Compounds

Redox active compounds are of interest in a wide variety of applications, from catalysis to cancer research.[91–94] Redox active compounds being used in catalysis is described by Yin *et al.* where a cobalt tungsten complex is made and used to facilitate the electron transfer process required for water oxidation.[94] Additionally, silver nanoparticles generate reactive oxygen species through an electron transfer process which causes cell death and are currently being used as a site specific cancer treatment.[91] As previously mentioned, the Crudden lab created a ferrocene tagged NHC SAM in order to demonstrate the ability to anchor a redox molecule to a surface and probe it electrochemically.[39]

In this thesis, NHC-modified quinones will be examined as redox-active molecules. Quinones are found in nature, where one of the most popular examples is plastoquinone which facilitates the electron transfer for water oxidation in photo system 2.[95] Since quinone species are abundant in the natural world, researching this species and its analogues, to potentially diversify areas requiring these properties are of interest.

In electrochemistry, quinones such as 1,4-benzoquinone (**13**) are reduced to 1,4-hydroxyquinone (**14**) via a two electron reduction in buffered water, or two sequential one electron reductions in aprotic solvents generating the 1,4-quinone dianion (**15**) as illustrated in Figure 1-16.[96–98]

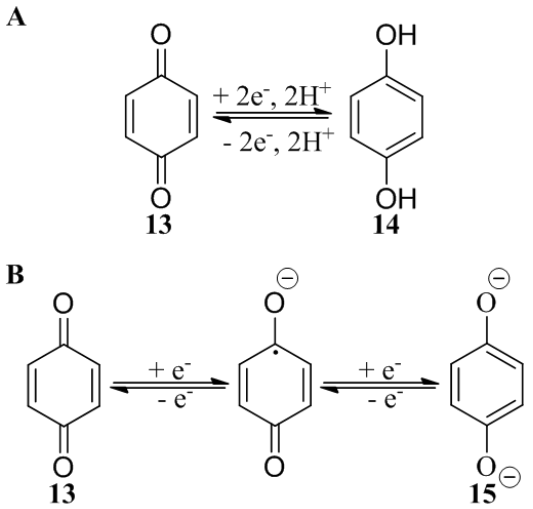

Figure 1-16: 1,4-Benzoquinone redox reactions in A buffered water and B aprotic solvents.

The redox abilities associated with quinone moieties makes them good candidates for applications in the medical field. Quinones are used as antibiotic or anticancer agents, where the electron transfer can form oxygen radicals causing tumor and bacterial death.[99–101] Capasso *et al.* investigated the vegetation waters from the olive oil making process and discovered antibacterial properties.[99] The different compounds in the water were analyzed individually and *o*-quinone was found to be 100% effective at killing *Coryne. michiganense* (+) and *Ps. savastoni* (-) bacteria. Blough and co workers studied the production of hydroxyl radicals from diaziquone and 3,6-dihydro-2,5-bis(aziridinyl)-1,4-benzoquinone which contribute to cell death.[100] It was found that diaziquone produces hydroxy radicals at a rate fast enough to be considered clinically important, 4.7×10^4 molecule $s^{-1}cell^{-1}$ at a concentration of 100 μM with similar results for the other compound.

Additionally, as the drive to remove toxic and rare earth metals from industry strengthens, organic batteries are growing in popularity.[102] The redox properties in quinones make it an ideal candidate as an alternative to their metal counterparts.[103] Lee *et al.* investigated lithium modified 2,3-diamino-1,4-naphthoquinone for use in lithium organic batteries.[103] It was found that the lithium modified 2,3-diamino-1,4-naphthoquinone has a discharge capacity of 250 mAh g^{-1} and a 99% capacity retention after 500 cycles at 0.2*C* . These results rival those of the more commonly used lithium metal oxides.

Thiol based quinone SAMs are being used in sensor technology. The Raouafi research group demonstrated a means for indirect detection of dopamine using a ω-mercaptopropyl naphthoquinone monolayer on a gold electrode using differential pulse voltammetry. [104] They applied this technique to a urine sample containing dopamine and were able to generate a signal demonstrating a practical application for the technique. Another example of current research demonstrates a quinone based mercapto-amine SAM functionalized with an antibody for carcinoiembryonic antigen detection.[105] The resulting sensor had better carcinoiembryonic antigen detection than current methods with a lower detection limit of 0.33 ng mL^{-1}.

The redox activity associated with quinones plays an important part in several areas of research. Examination into NHC quinone monolayers on substrates is another area which needs to be studied with the hopes of improving upon existing devices.

In this thesis, we will examine the effect of different NHC structures on SAM formation. We will examine redox active quinone-containing stuctures, pi-conjugated structures and chiral NHCs.

1.3 References

1. Breslow, R. Rapid deuterium exchange in thiazolium salts. *Journal of the American Chemical Society* **79**, 1762–1763 (1957).
2. Bourissou, D., Guerret, O., Gabbaï, F. P. & Bertrand, G. Stable Carbenes. *Chemical Reviews* **100**, 39–92 (2000).
3. Herrmann, W. A. & Köcher, C. N-Heterocyclic Carbenes. *Angewandte Chemie International Edition in English* **36**, 2162–2187 (1997).
4. Fischer, E. O. & Maasböl, A. On the Existence of a Tungsten Carbonyl Carbene Complex. *Angewandte Chemie International Edition in English* **3**, 580–581 (1964).
5. Licandro, E. *et al.* Michael Addition of Chiral Fischer Aminocarbene Complexes to Nitroolefins: Study on the Effect of the Michael Acceptor Structure on Diastereoselectivity. *Organometallics* **20**, 485–496 (2001).

6. Wulff, W. D. & Yang, D. C. Diels-Alder reactions of Fischer carbene complexes. *Journal of the American Chemical Society* **105**, 6726–6727 (1983).

7. Schrock, R. R. Alkylcarbene complex of tantalum by intramolecular .alpha.-hydrogen abstraction. *Journal of the American Chemical Society* **96**, 6796–6797 (1974).

8. Grubbs, R. H. & Brunck, T. K. Possible intermediate in the tungsten-catalyzed olefin metathesis reaction. *Journal of the American Chemical Society* **94**, 2538–2540 (1972).

9. Wanzlick, H. W. Aspects of Nucleophilic Carbene Chemistry. *Angewandte Chemie International Edition in English* **1**, 75–80 (1962).

10. Igau, A., Grutzmacher, H., Baceiredo, A. & Bertrand, G. Analogous α,α'-bis-carbenoid, triply bonded species: synthesis of a stable λ^3-phosphino carbene-λ^5-phosphaacetylene. *Journal of the American Chemical Society* **110**, 6463–6466 (1988).

11. Arduengo, A. J., Kline, M., Calabrese, J. C. & Davidson, F. Synthesis of a reverse ylide from a nucleophilic carbene. *Journal of the American Chemical Society* **113**, 9704–9705 (1991).

12. Carter, E. A. & Goddard, W. A. Relation between singlet-triplet gaps and bond energies. *The Journal of Physical Chemistry* **90**, 998–1001 (1986).

13. Boehme, C. & Frenking, G. Electronic Structure of Stable Carbenes, Silylenes, and Germylenes. *Journal of the American Chemical Society* **118**, 2039–2046 (1996).

14. Regitz, M. Stable Carbenes—Illusion or Reality? *Angewandte Chemie International Edition in English* **30**, 674–676 (1991).

15. Heinemann, C., Müller, T., Apeloig, Y. & Schwarz, H. On the Question of Stability, Conjugation, and "Aromaticity" in Imidazol-2-ylidenes and Their Silicon Analogs. *Journal of the American Chemical Society* **118**, 2023–2038 (1996).

16. Kuhn, N., Kratz, T. & Henkel, G. A stable carbene iodine adduct: secondary bonding in 1,3-diethyl-2-iodo-4,5-dimethylimidazolium iodide. *Journal of the Chemical Society, Chemical Communications* 1778 (1993). doi:10.1039/c39930001778

17. Weskamp, T., Kohl, F. J., Hieringer, W., Gleich, D. & Herrmann, W. A. Highly Active Ruthenium Catalysts for Olefin Metathesis: The Synergy of NHeterocyclic Carbenes and Coordinatively Labile Ligands. *Angewandte Chemie International Edition* **38**, 2416–2419

18. Herrmann, W. A., Elison, M., Fischer, J., Köcher, C. & Artus, G. R. J. Metal Complexes of N-Heterocyclic Carbenes—A New Structural Principle for Catalysts in Homogeneous Catalysis. *Angewandte Chemie International Edition in English* **34**, 2371–2374 (1995).

19. Arduengo, A. J., Harlow, R. L. & Kline, M. A stable crystalline carbene. *Journal of the American Chemical Society* **113**, 361–363 (1991).

20. Schwartz, D. K. Mechanisms and Kinetics of Self-Assembled Monolayer Formation. *Annual Review of Physical Chemistry* **52**, 107–137 (2001).

21. Love, J. C., Estroff, L. A., Kriebel, J. K., Nuzzo, R. G. & Whitesides, G. M. Self-Assembled Monolayers of Thiolates on Metals as a Form of Nanotechnology. *Chemical Reviews* **105**, 1103–1170 (2005).

22. Bigelow, W. C., Pickett, D. L. & Zisman, W. A. Oleophphobic Monolayers. I. Films Adsorbed from Solution in Non-Polar Liquids. 26

23. Srisombat, L., Jamison, A. C. & Lee, T. R. Stability: A key issue for self-assembled monolayers on gold as thin-film coatings and nanoparticle protectants. *Colloids and Surfaces A: Physicochemical and Engineering Aspects* **390**, 1–19 (2011).

24. Nuzzo, R. G. & Allara, D. L. Adsorption of bifunctional organic disulfides on gold surfaces. *Journal of the American Chemical Society* **105**, 4481–4483 (1983).

25. Weidner, T. *et al*. NHC-Based Self-Assembled Monolayers on Solid Gold Substrates. *Australian Journal of Chemistry* **64**, 1177 (2011).

26. Zhukhovitskiy, A. V., Mavros, M. G., Van Voorhis, T. & Johnson, J. A. Addressable Carbene Anchors for Gold Surfaces. *Journal of the American Chemical Society* **135**, 7418–7421 (2013).

27. Crudden, C. M. *et al.* Ultra stable self-assembled monolayers of N-heterocyclic carbenes on gold. *Nature Chemistry* **6**, 409–414 (2014).

28. Schlenoff, J. B., Li, M. & Ly, H. Stability and Self-Exchange in Alkanethiol Monolayers. *Journal of the American Chemical Society* **117**, 12528–12536 (1995).

29. Bain, C. D. *et al.* Formation of monolayer films by the spontaneous assembly of organic thiols from solution onto gold. *Journal of the American Chemical Society* **111**, 321–335 (1989).

30. Lee, M.-T., Hsueh, C.-C., Freund, M. S. & Ferguson, G. S. Air Oxidation of Self-Assembled Monolayers on Polycrystalline Gold: The Role of the Gold Substrate. *Langmuir* **14**, 6419–6423 (1998).

31. Vericat, C., Benitez, G. A., Grumelli, D. E., Vela, M. E. & Salvarezza, R. C. Thiol-capped gold: from planar to irregular surfaces. *Journal of Physics: Condensed Matter* **20**, 184004 (2008).

32. Schoenfisch, M. H. & Pemberton, J. E. Air Stability of Alkanethiol Self-Assembled Monolayers on Silver and Gold Surfaces. *Journal of the American Chemical Society* **120**, 4502–4513 (1998).

33. Meth, S. *et al.* Siloxane-based thin films for corrosion protection of stainless steel in chloride media. *Journal of Applied Electrochemistry* **41**, 885–890 (2011).

34. Zhang, D.-Q., Gao, L.-X., Cai, Q.-R. & Lee, K. Y. Inhibition of copper corrosion by modifying cysteine self-assembled film with alkylamine/alkylacid compounds. *Materials and Corrosion* **61**, 16–21 (2010).

35. Jennings, G. K., Yong, T.-H., Munro, J. C. & Laibinis, P. E. Structural Effects on the Barrier Properties of Self-Assembled Monolayers Formed from Long-Chain ω-Alkoxy- *n* -alkanethiols on Copper. *Journal of the American Chemical Society* **125**, 2950–2957 (2003).

36. Anker, J. N. *et al.* Biosensing with plasmonic nanosensors. *Nature Materials* **7**, 442 (2008).

37. Willets, K. A. & Van Duyne, R. P. Localized Surface Plasmon Resonance Spectroscopy and Sensing. *Annual Review of Physical Chemistry* **58**, 267–297 (2007).

38. Stephenson-Brown, A. *et al.* Glucose selective Surface Plasmon Resonance-based bis-boronic acid sensor. *The Analyst* **138**, 7140 (2013).

39. Crudden, C. M. *et al.* Simple direct formation of self-assembled N-heterocyclic carbene monolayers on gold and their application in biosensing. *Nature Communications* **7**, 12654 (2016).

40. Larrea, C. R. *et al.* N-Heterocyclic Carbene Self-assembled Monolayers on Copper and Gold: Dramatic Effect of Wingtip Groups on Binding, Orientation and Assembly. *ChemPhysChem* **18**, 3536–3539 (2017).

41. Poirier, G. E. & Pylant, E. D. The Self-Assembly Mechanism of Alkanethiols on Au(111). *Science* **272**, 1145–1148 (1996).

42. Schreiber, F. *et al.* Adsorption mechanisms, structures, and growth regimes of an archetypal self-assembling system: Decanethiol on Au(111). *Physical Review B* **57**, 12476–12481 (1998).

43. Cometto, F. P. *et al.* Decomposition of Methylthiolate Monolayers on Au(111) Prepared from Dimethyl Disulfide in Solution Phase. *The Journal of Physical Chemistry C* **114**, 10183–10194 (2010).

44. Ramírez, E. A. *et al.* Complex Surface Chemistry of 4-Mercaptopyridine Self-Assembled Monolayers on Au(111). *Langmuir* **28**, 6839–6847 (2012).

45. Lavrich, D. J., Wetterer, S. M., Bernasek, S. L. & Scoles, G. Physisorption and Chemisorption of Alkanethiols and Alkyl Sulfides on Au(111). *The Journal of Physical Chemistry B* **102**, 3456–3465 (1998).

46. Ulman, A. Formation and Structure of Self-Assembled Monolayers. *Chemical Reviews* **96**, 1533–1554 (1996).

47. Nuzzo, R. G., Zegarski, B. R. & Dubois, L. H. Fundamental studies of the chemisorption of organosulfur compounds on gold(111). Implications for molecular self-assembly on gold surfaces. *Journal of the American Chemical Society* **109**, 733–740 (1987).

48. Baek, K. Y., Jo, J. H., Moon, J. H., Yoon, J. & Lee, J. Y. Systematic Strategy for Designing Immidazolium Containing Precursors To Produce *N* -Heterocyclic Carbenes: A DFT Study. *The Journal of Organic Chemistry* **80**, 1878–1886 (2015).

49. Fèvre, M. *et al.* Imidazolium Hydrogen Carbonates versus Imidazolium Carboxylates as Organic Precatalysts for N-Heterocyclic Carbene Catalyzed Reactions. *The Journal of Organic Chemistry* **77**, 10135–10144 (2012).

50. Fèvre, M. *et al.* Imidazol(in)ium Hydrogen Carbonates as a Genuine Source of *N* -Heterocyclic Carbenes (NHCs): Applications to the Facile Preparation of NHC Metal Complexes and to NHC-Organocatalyzed Molecular and Macromolecular Syntheses. *Journal of the American Chemical Society* **134**, 6776–6784 (2012).

51. Wang, G. *et al.* Ballbot-type motion of N-heterocyclic carbenes on gold surfaces. *Nature Chemistry* **9**, 152–156 (2017).

52. Jiang, L. *et al.* N-Heterocyclic carbenes on close-packed coinage metal surfaces: bis-carbene metal adatom bonding scheme of monolayer films on Au, Ag and Cu. *Chemical Science* **8**, 8301–8308 (2017).

53. Sondag-Huethorst, J. A. M., Schonenberger, C. & Fokkink, L. G. J. Formation of Holes in Alkanethiol Monolayers on Gold. *The Journal of Physical Chemistry* **98**, 6826–6834 (1994).

54. Schoenenberger, C., Sondag-Huethorst, J. A. M., Jorritsma, J. & Fokkink, L. G. J. What Are the 'Holes' in Self-Assembled Monolayers of Alkanethiols on Gold? *Langmuir* **10**, 611–614 (1994).

55. Smith, C. A. *et al.* N-Heterocyclic Carbenes in Materials Chemistry. *Chem. Rev.* (In press).

56. Yeh, Y.-C., Creran, B. & Rotello, V. M. Gold nanoparticles: preparation, properties, and applications in bionanotechnology. *Nanoscale* **4**, 1871–1880 (2012).

57. Wang, J., Zhang, L., Peng, F., Shi, X. & Leong, D. T. Targeting Endothelial Cell Junctions with Negatively Charged Gold Nanoparticles. *Chemistry of Materials* **30**, 3759–3767 (2018).

58. Brust, M. Synthesis of Thiol-derivatised Gold Nanoparticles in a Two-phase Liquid-Liquid System. 2

59. Ott, L. S., Cline, M. L., Deetlefs, M., Seddon, K. R. & Finke, R. G. Nanoclusters in Ionic Liquids: Evidence for *N* -Heterocyclic Carbene Formation from Imidazolium-Based Ionic Liquids Detected by ^{2} H NMR. *Journal of the American Chemical Society* **127**, 5758–5759 (2005).

60. Vignolle, J. & Tilley, T. D. N-Heterocyclic carbene-stabilized gold nanoparticles and their assembly into 3D superlattices. *Chemical Communications* 7230 (2009). doi:10.1039/b913884f

61. Hsu, S. J., Hsu, K. M., Leong, M. K. & Lin, I. J. B. Au(I)-benzimidazole/imidazole complexes. Liquid crystals and nanomaterials. *Dalton Transactions* 1924 (2008). doi:10.1039/b717787a

62. Hurst, E. C., Wilson, K., Fairlamb, I. J. S. & Chechik, V. N-Heterocyclic carbene coated metal nanoparticles. *New Journal of Chemistry* **33**, 1837 (2009).

63. Man, R. W. Y. *et al.* Ultrastable Gold Nanoparticles Modified by Bidentate *N* -Heterocyclic Carbene Ligands. *Journal of the American Chemical Society* **140**, 1576–1579 (2018).

64. Garg, N., Carrasquillo-Molina, E. & Lee, T. R. Self-Assembled Monolayers Composed of Aromatic Thiols on Gold: Structural Characterization and Thermal Stability in Solution. *Langmuir* **18**, 2717–2726 (2002).

65. Astruc, D., Lu, F. & Aranzaes, J. R. Nanoparticles as Recyclable Catalysts: The Frontier between Homogeneous and Heterogeneous Catalysis. *Angewandte Chemie International Edition* **44**, 7852–7872 (2005).

66. Zhukhovitskiy, A. V., MacLeod, M. J. & Johnson, J. A. Carbene Ligands in Surface Chemistry: From Stabilization of Discrete Elemental Allotropes to Modification of Nanoscale and Bulk Substrates. *Chemical Reviews* **115**, 11503–11532 (2015).

67. Ranganath, K. V. S., Kloesges, J., Schäfer, A. H. & Glorius, F. Asymmetric Nanocatalysis: N-Heterocyclic Carbenes as Chiral Modifiers of Fe3O4/Pd nanoparticles. *Angewandte Chemie International Edition* **49**, 7786–7789 (2010).

68. Gonzalez-Galvez, D. *et al.* NHC-stabilized ruthenium nanoparticles as new catalysts for the hydrogenation of aromatics. *Catal. Sci. Technol.* **3**, 99–105 (2013).

69. Baquero, E. A., Tricard, S., Flores, J. C., de Jesús, E. & Chaudret, B. Highly Stable Water-Soluble Platinum Nanoparticles Stabilized by Hydrophilic N-Heterocyclic Carbenes. *Angewandte Chemie International Edition* **53**, 13220–13224 (2014).

70. Powell, C. J. Elemental binding energies for X-ray photoelectron spectroscopy. *Applied Surface Science* **89**, 141–149 (1995).

71. Turner, N. H. & Schreifels, J. A. Surface Analysis: X-ray Photoelectron Spectroscopy and Auger Electron Spectroscopy. *Analytical Chemistry* **72**, 99–110 (2000).

72. Boehm, H. . Surface oxides on carbon and their analysis: a critical assessment. *Carbon* **40**, 145–149 (2002).

73. Hollander, J. M. & Jolly, W. L. X-ray photoelectron spectroscopy. 8 (1970).

74. Nordling, C., Sokolowski, E. & Siegbahn, K. Precision Method for Obtaining Absolute Values of Atomic Binding Energies. *Physical Review* **105**, 1676–1677 (1957).

75. Hagström, S., Nordling, C. & Siegbahn, K. Electron spectroscopic determination of the chemical valence state. *Zeitschrift für Physik* **178**, 439–444 (1964).

76. Nordling, C., Hagström, S. & Siegbahn, K. Application of electron spectroscopy to chemical analysis. *Zeitschrift für Physik* **178**, 433–438 (1964).

77. Binnig, G., Rohrer, H., Gerber, C. & Weibel, E. Tunneling through a controllable vacuum gap. *Applied Physics Letters* **40**, 178–180 (1982).

78. Binnig, G., Rohrer, H., Gerber, C. & Weibel, E. Surface Studies by Scanning Tunneling Microscopy. *Physical Review Letters* **49**, 57–61 (1982).

79. Feuchtwang, T. E. & Cutler, P. H. Tunneling and Scanning Tunnel Microscopy: a Critical Review. *Physica Scripta* **35**, 132–140 (1987).

80. Park, S. & Quate, C. F. Scanning tunneling microscope. *Review of Scientific Instruments* **58**, 2010–2017 (1987).

81. Leemput, L. E. C. van de & Kempen, H. van. Scanning tunnelling microscopy. *Reports on Progress in Physics* **55**, 1165–1240 (1992).

82. Song, C.-L. & Hoffman, J. E. Pairing insights in iron-based superconductors from scanning tunneling microscopy. *Current Opinion in Solid State and Materials Science* **17**, 39–48 (2013).

83. B. C. Stipe, M. A. Rezaei & W. Ho. Single-Molecule Vibrational Spectroscopy and Microscopy. *Science, New Series* **280**, 1732–1735 (1998).

84. Ho, W. Single-molecule chemistry. *The Journal of Chemical Physics* **117**, 11033–11061 (2002).

85. Werner, W. S. M. Electron transport in solids for quantitative surface analysis. *Surface and Interface Analysis* **31**, 141–176 (2001).

86. Eckermann, A. L., Feld, D. J., Shaw, J. A. & Meade, T. J. Electrochemistry of redox-active self-assembled monolayers. *Coordination Chemistry Reviews* **254**, 1769–1802 (2010).

87. Bordwell, F. G. Equilibrium acidities in dimethyl sulfoxide solution. *Accounts of Chemical Research* **21**, 456–463 (1988).

88. Bruice, T. C. & Schmir, G. L. Imidazole Catalysis. II. The Reaction of Substituted Imidazoles with Phenyl Acetates in Aqueous Solution. *Journal of the American Chemical Society* **80**, 148–156 (1958).

89. Tang, Q. & Jiang, D. Comprehensive View of the Ligand–Gold Interface from First Principles. *Chemistry of Materials* **29**, 6908–6915 (2017).

90. Janiak, C. A critical account on π–π stacking in metal complexes with aromatic nitrogen-containing ligands. *Journal of the Chemical Society, Dalton Transactions* 3885–3896 (2000). doi:10.1039/b003010o

91. Sims, C. M. *et al.* Redox-active nanomaterials for nanomedicine applications. *Nanoscale* **9**, 15226–15251 (2017).

92. Grieshaber, D., MacKenzie, R., Voros, J. & Reimhult, E. Electrochemical Biosensors - Sensor Principles and Architectures. 59 (2008).

93. Jacob, A., Roy, T., Kaicharla, T. & Biju, A. T. Metal-Free, Brønsted Acid-Catalyzed Formal [3+2] Annulation of Quinone Monoacetals with 2-Naphthols. *The Journal of Organic Chemistry* **82**, 11269–11274 (2017).

94. A Fast Soluble Carbon-Free Molecular Water Oxidation Catalyst Based on Abundant Metals. 5

95. Foyer, C. H. & Noctor, G. Redox Regulation in Photosynthetic Organisms: Signaling, Acclimation, and Practical Implications. *Antioxidants & Redox Signaling* **11**, 861–905 (2009).

96. Bailey, S. I. & Ritchie, I. M. A cyclic voltammetric study of the aqueous electrochemistry of some quinones. *Electrochimica Acta* **30**, 3–12 (1985).

97. Bauscher, M. & Maentele, W. Electrochemical and infrared-spectroscopic characterization of redox reactions of p-quinones. *The Journal of Physical Chemistry* **96**, 11101–11108 (1992).

98. Quan, M., Sanchez, D., Wasylkiw, M. F. & Smith, D. K. Voltammetry of Quinones in Unbuffered Aqueous Solution: Reassessing the Roles of Proton Transfer and Hydrogen Bonding in the Aqueous Electrochemistry of Quinones. *Journal of the American Chemical Society* **129**, 12847–12856 (2007).

99. Capasso, R. *et al.* Antibacterial polyphenols from olive oil mill waste waters. *Journal of Applied Bacteriology* **79**, 393–398 (1995).

100. Li, B., Gutierrez, P. L., Amstad, P. & Blough, N. V. Hydroxyl Radical Production by Mouse Epidermal Cell Lines in the Presence of Quinone Anti-Cancer Compounds. *Chemical Research in Toxicology* **12**, 1042–1049 (1999).

101. Tandon, V. K., Singh, R. V. & Yadav, D. B. Synthesis and evaluation of novel 1,4-naphthoquinone derivatives as antiviral, antifungal and anticancer agents. *Bioorganic & Medicinal Chemistry Letters* **14**, 2901–2904 (2004).

102. Muench, S. *et al.* Polymer-Based Organic Batteries. *Chemical Reviews* **116**, 9438–9484 (2016).

103. Lee, J., Kim, H. & Park, M. J. Long-Life, High-Rate Lithium-Organic Batteries Based on Naphthoquinone Derivatives. *Chemistry of Materials* **28**, 2408–2416 (2016).

104. Hammami, A., Sahli, R. & Raouafi, N. Indirect amperometric sensing of dopamine using a redox-switchable naphthoquinone-terminated self-assembled monolayer on gold electrode. *Microchimica Acta* **183**, 1137–1144 (2016).

105. Pavithra, M., Muruganand, S. & Parthiban, C. Development of novel paper based electrochemical immunosensor with self-made gold nanoparticle ink and quinone derivate for highly sensitive carcinoembryonic antigen. *Sensors and Actuators B: Chemical* **257**, 496–503 (2018).

Chapter 2

Results and Discussion

2.1 Introduction

Metal surface modification by means of SAMs is a growing field with potential applications in sensor technology and corrosion protection.[1–5] Specifically, when investigating the modification of gold surfaces, Crudden *et al*. demonstrated a robust method for creating NHC monolayers with stability towards extreme conditions and duration for months on a benchtop.[4,6] As a means of expanding the tool box of NHCs used for surface modification, the synthesis and deposition of three analogues to the ones discussed by Crudden *et al*.[4,6], was carried out. Figure 2-1 depicts the carbenes synthesized and deposited onto gold films in this thesis.

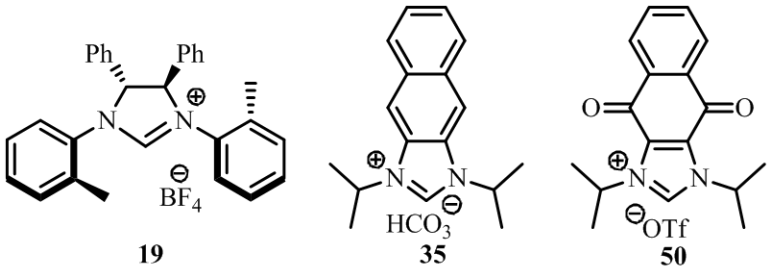

19 **35** **50**

Figure 2-1: Synthesized Carbene Salts

The following carbenes were chosen for their unique properties. Compound **50** contains a quinone moiety which has unique redox properties allowing for a wide range of uses. Some of the applications associated with quinones include electron transfer processes which can contribute to vibrancy in dyes, and anti-cancer properties in medicine.[7,8] Compound **19** is a chiral compound that is known to be a highly effective ligand as a chiral metathesis catalyst.[9] When appended to the surface via the C_2 carbon the chirality associated with the backbone presents an opportunity for heterogenous stereoselective catalysis and chiral surface formation.[10,11] Compound **35** is aromatic with an additional benzannulation to the backbone, designed to test the effect that increased π-π interactions have on the potential to form a well organized

densely packed monolayer. The unique features encompassed in these molecules augment the variety of NHCs already prepared by the Crudden lab.

SAM creation is traditionally achieved via solution deposition, in which a substrate is placed in a solution containing the target molecule and left for a predetermined amount of time.[12] During this time, the target molecule physisorbs onto the substrate, moves around until it reaches an energetically stable conformation then chemisorbs.[12] Vapour phase deposition is another method of forming SAMs.[12] In this method, the substrate is placed in a vacuum chamber, and the target molecule is vapourized then flowed through the chamber forming a monolayer on the substrate.[13]

X-ray photoelectron spectroscopy (XPS) is a method that is employed to analyze the elemental composition of monolayers. If the target molecule is known, a ratio between the abundance of the expected elements can be determined then compared with experimentally obtained results, where the signals can be deconvoluted and compared with literature data. Another method which can be employed for surface analysis is scanning tunneling microscopy (STM). This technique allows the researcher to image the surface topology of the sample allowing for the packing and orientation of the molecules on the surface to be determined. Electrochemical testing can also be performed to characterize SAMs. By running voltammetry and impedance experiments, current suppression and increased resistance with respect to a bare gold electrode can provide information about SAM formation.

2.2 Synthetic Routes

Synthesis of the target molecules illustrated in Figure 2-1 were adapted and developed from literature procedures.[4,6,9] NHCs can be synthesized in many ways. The general approach employed in this research involves synthesis of the appropriate diamine, then ring closing using either formic acid or triethylorthoformate followed by introduction of the appropriate wing tip groups.[9,14]

2.1.1 N,N'-ditolyl-4,5(R,R)-diphenylimidazolium tetrafluoroborate

The synthesis of molecule **19** was achieved following the prep outlined by Seiders *et. al.*[15]

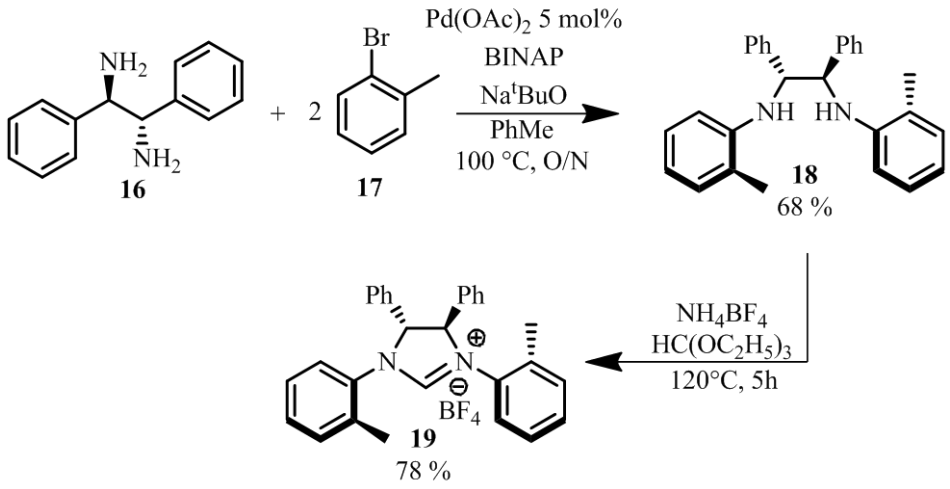

Scheme 2-1: N,N'-ditolyl-4,5(R,R)-diphenylimidazolium tetrafluoroborate Synthetic Scheme

As depicted in Scheme 1, the first step involves forming the functionalized diamine **18** through a Buchwald-Hartwig cross coupling reaction of diamine **16** with aryl halide **17**. Compound **18** was characterized by ^{1}H NMR and found to be the desired compound by comparison with literature values. Compound **18** was then subjected to triethyl orthoformate in the presence of ammonium tetrafluoroborate affording the ring closed product **19**. In the reports by Crudden et al.[4], to form the free carbene for monolayer creation in a bench stable way, the counterion for the carbene precursor should be exchanged for bicarbonate using a hydroxide resin. Attempts were made to form the bicarbonate salt, however the compound decomposed on the resin. Recent findings by Dr. Christene Smith, a recent graduate of the Crudden group, suggest that deposition can occur in methanol without introducing the hydrogen carbonate analogue, although these studies need further confirmation.[16]

2.1.2 N,N'-diisopropylnaphthalene[2,3-d]imidazolium salt

The synthesis of molecule **35** was achieved following procedures outlined by Grobler et. al[14], and Crudden et al.[4,6] Initially, attempts at synthesizing **35** involved first synthesizing **24**. A triflation of compound **20**, was performedyielding **22** in 66% yield.[17] An attempt to synthesize **24**via a Buchwald-Hartwig cross coupling between **23** and **22** was carried out.[18] However, **24** was never obtained, with the reaction leading to reagent decomposition.

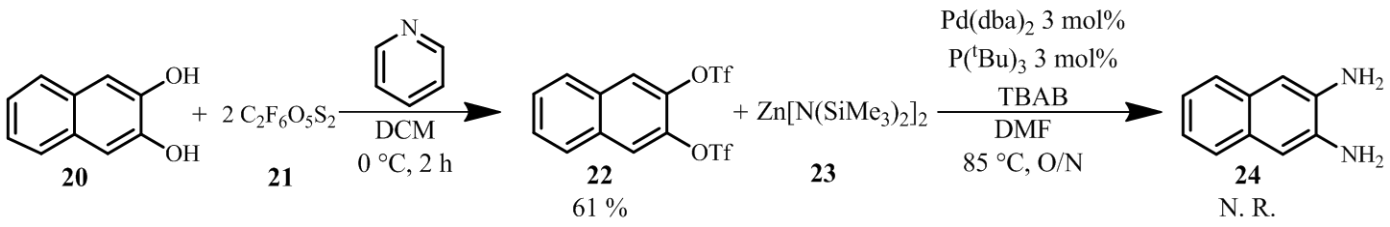

Scheme 2-2: 2,3-diaminonaphthalene Synthetic Scheme

Since the previously mentioned cross coupling reaction was unsuccessful, another cross coupling reaction was employed to directly cross couple isopropyl amine (**25**) to **22** in order to synthesize **26**. Following a report by Nolan and coworkers resulted in a mixture of starting material **22**, and trace product **26**.[19]

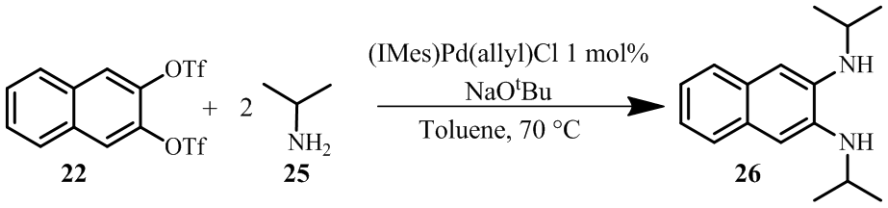

Scheme 2-3: 2,3-diisopropylaminenaphthalene Synthetic Scheme

Since the synthesis of **24** and **26** failed to produce desired product, we decided to purchase **24** from a chemical supplier. With the diamine in hand, ring closing was achieved using formic acid at reflux.[14] Compound **31** was characterized by ^{1}H NMR and is consistent with the reported spectra.[14] Substitution of the first isopropyl group onto the nitrogen was carried out the same way as described by the Crudden group for other carbene salts, using 2-bromopropane (**28**) and Cs_2CO_3 in acetonitrile to afford compound **29**.[6] Here the expected septet representing the CH of the isopropyl is seen in the ^{1}H NMR spectrum at a shift of 4.74, ppm and the corresponding doublet representing the two CH_3 groups of the isopropyl is seen at 1.70 ppm. Since the molecule is no longer symmetrical, the aromatic region in the ^{1}H NMR spectrum is now represented by a multiplet at 7.42 ppm integrating for two protons, which correspond to the protons on C_7 and C_8.

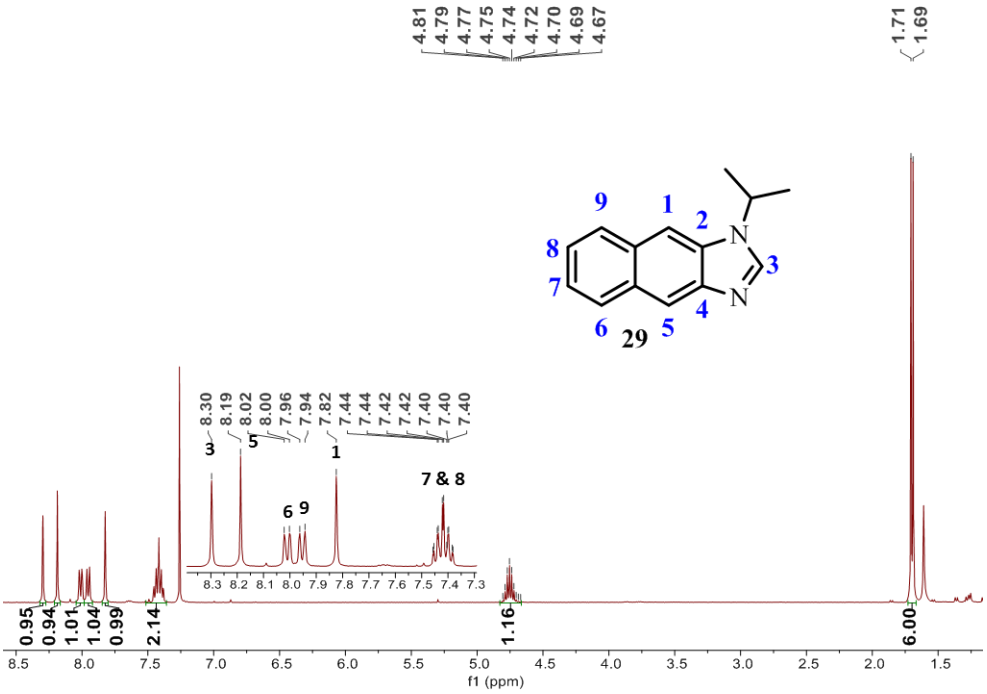

Figure 2-2: N-isopropylnaphthalene[2,3-d]imidazole ^{1}H NMR

The addition of the second isopropyl group to the nitrogen was achieved by two methods both described by the Crudden lab in relation to other carbene salts.[4,6] Compound **31** was prepared by heating **29** and 2-iodopropane in a pressure tube depicted in Scheme 4. Upon ^{1}H NMR analysis, the aromatic region becomes symmetrical again with a doublet of doublets at 7.67 ppm and 8.20 ppm corresponding to the protons on C_7, C_8, and C_6, C_9, respectively.

Since **31** is a salt, a more polar solvent is required to dissolve the compound for NMR analysis, in this case deuterated methanol was used, which results in rapid proton exchange at the carbenic carbon resulting in the absence of this proton in the spectra.

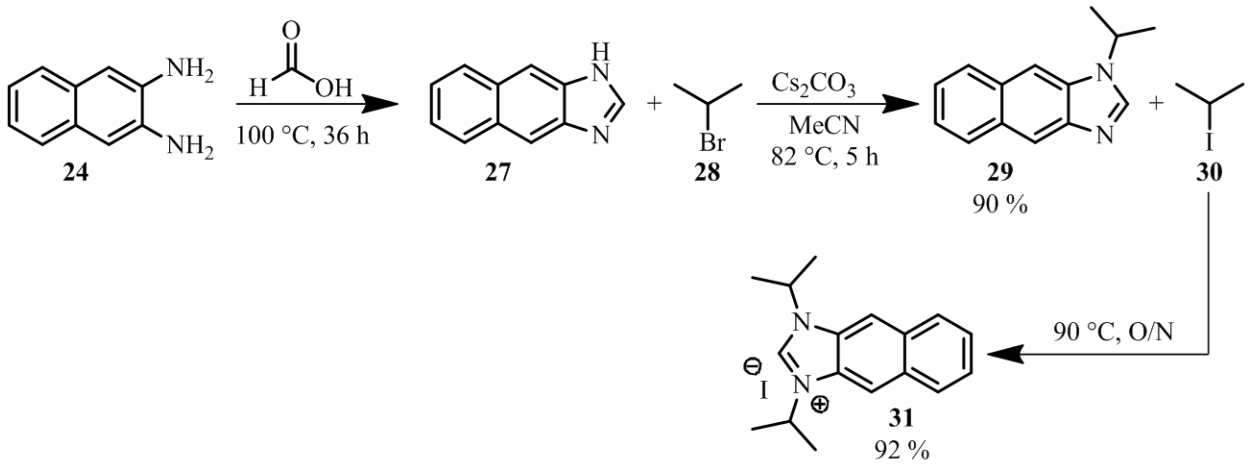

Scheme 2-4: N,N'-diisopropylnaphthalene[2,3-d]imidazolium Iodide Synthesis

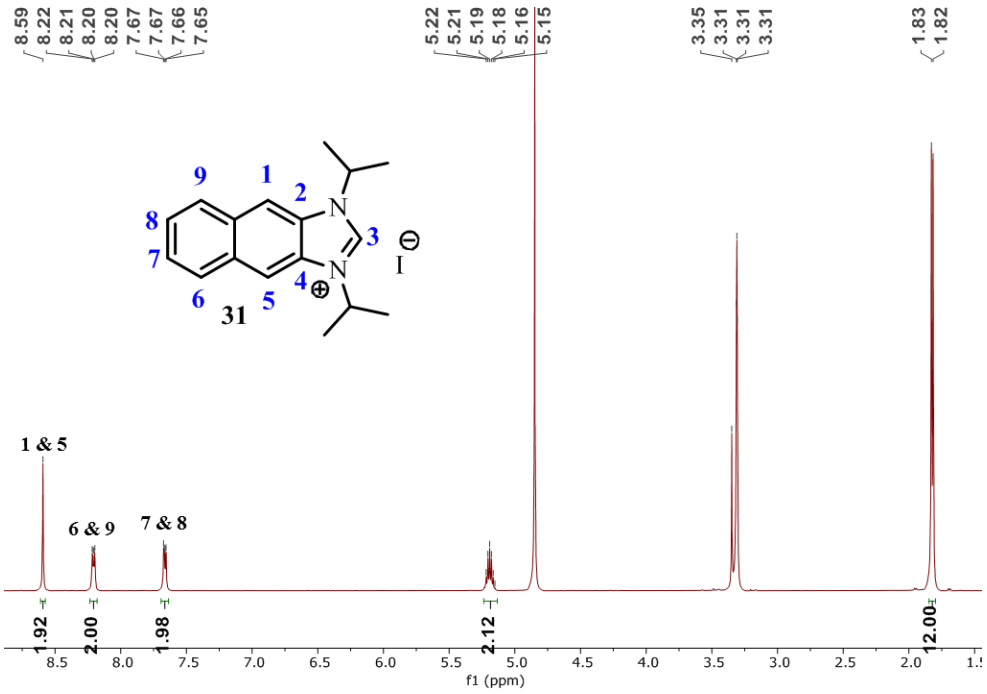

Figure 2-3: N,N'-diisopropylnaphthalene[2,3-d]imidazolium Iodine salt ^{1}H NMR Spectrum

Compound **34** was prepared using the method outlined by Crudden *et al.*[4] where isopropyl triflate is made *in situ* prior to reacting with the carbene. The resulting ^{1}H NMR spectrum closely resembled that of **31** with two doublets of doublets at 7.65 ppm and 8.07 ppm corresponding to the protons on C_7, C_8 and C_6, C_9 respectively. A singlet is observed at 8.22 ppm integrating to two protons, corresponding to the protons on C_1 and C_5, and another singlet 9.99 ppm integrating to one proton, corresponds to the carbenic

proton. The ^{19}F NMR spectrum in Figure 2-5 reveals a singlet at -78.29 ppm which is consistent with the fluorine in a triflate anion.

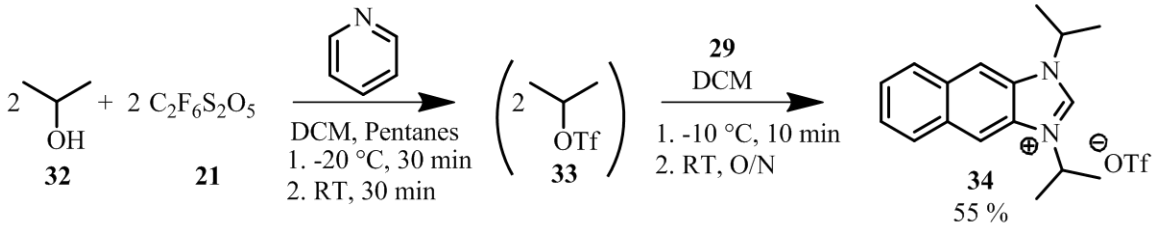

Scheme 2-5: NN'-diisopropylnaphthalene[2,3-d]imidazolium Triflate (**34**) Synthesis

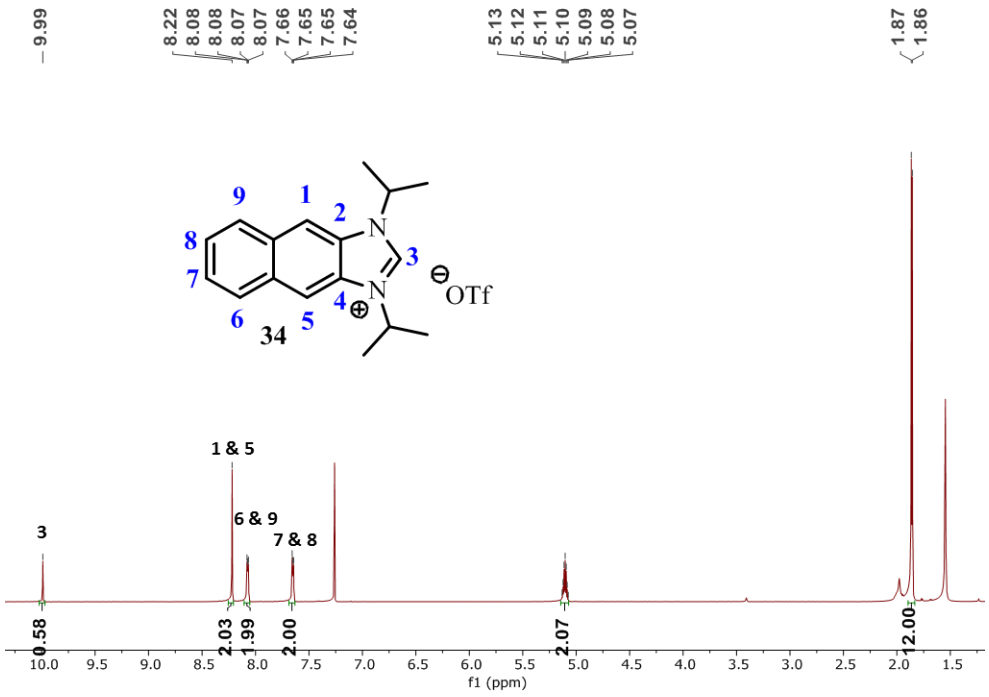

Figure 2-4: N,N'-diisopropylnaphthalene[2,3-d]imidazolium Triflate salt ^1H NMR Spectrum

The bicarbonate salt, compound **35** was prepared using the bicarbonate resin described in a paper by Crudden *et al.*[4] The resin exchange was monitored by ^1H NMR and powder XPS. Powder XPS was used to confirm the iodine anion had been successfully replaced by the bicarbonate anion after the resin exchange procedure. Since iodine is NMR silent, it is not possible to monitor the exchange using NMR. However,

when exchanging the triflate anion for the bicarbonate anion, ^{19}F NMR spectroscopy can be employed to observe the loss of the triflate signal. The ^{1}H NMR spectra are identical to that of **31** since methanol was used as a solvent for this compound. Despite being soluble in chloroform, methanol is used since chloroform can be slightly acidic and may cause decomposition of bicarbonate salts.

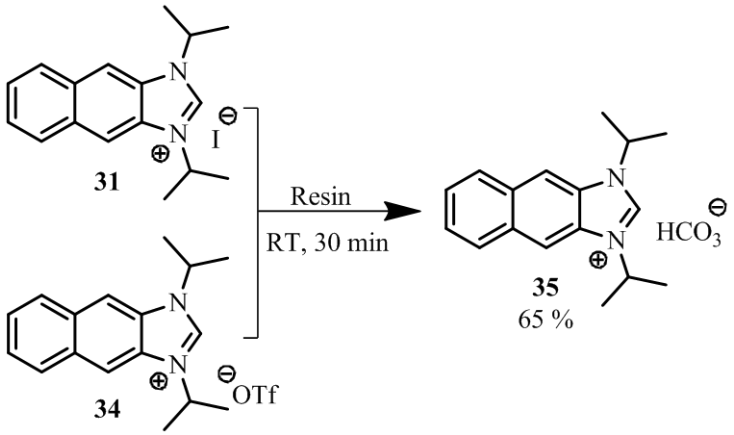

Scheme 2-6: N,N'-diisopropylnaphthalene[2,3-*d*]imidazolium **31** and **34** anion exchange to **35**

Finally, tetrafluoroborate salt **37** was also synthesized using the method of Weber *et al.*[20], who employed Cs_2CO_3 base in the alkylating step as described by Crudden *et al.*[4] and ring closing with $NH_4^+BF_4^-$ and triethylorthoformate as described by Sieders *et al.*[9], Scheme 7. ^{19}F NMR analysis confirmed the structure of **37**, as shown in Figure 2-5.

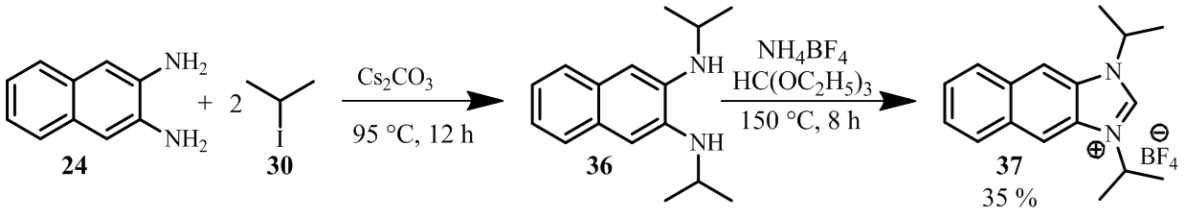

Scheme 2-7: N,N'-diisopropylnaphthalene[2,3-d]imidazolium Tetrafluoroborate Synthesis

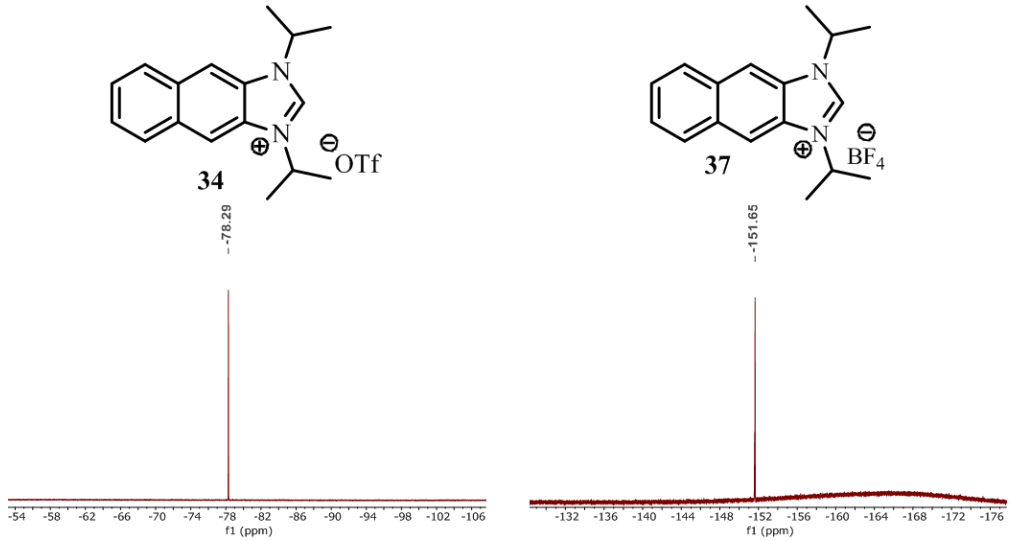

Figure 2-5: N,N'-diisopropylnaphthalene[2,3-d]imidazole OTf^- and BF_4^- ^{19}F NMR Spectra

2.1.3 N,N'-diisopropyl[2,3-d]imidazolium-1,4-dionenaphthalene salt

The synthesis of molecule **50** was achieved using preparations outlined by Lee *et al.*[21] and Crudden *et al.*[4,6] Initially the synthesis was attempted following papers by Pompeo *et al.*[22] and Dunsford *et al.*[23]; however, changing the 2,6-diisopropyl phenyl groups on the formamidine to isopropyl reduced the nucleophilicity of the nitrogen leading to an incomplete reaction. The desired product was produced once in < 10% yield and was not reproducible. Instead **40** is consistently the resultant product from the reaction.

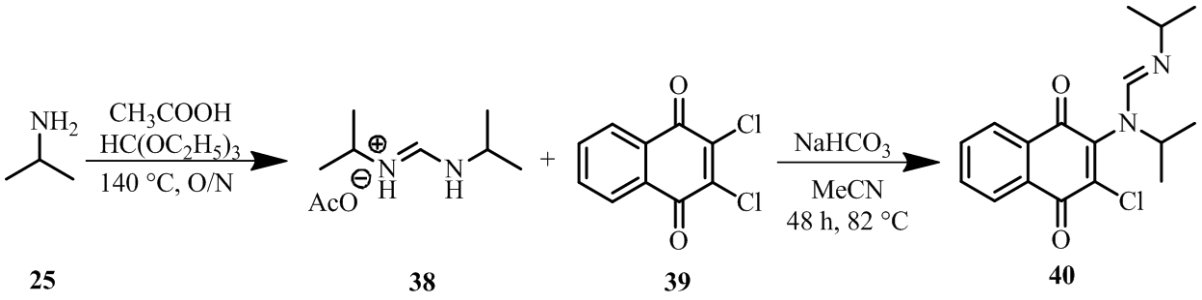

Scheme 2-8: First Synthesis Attempt for N,N'-diisopropyl[2,3-d]imidazolium-1,4-dionenapthalene salt

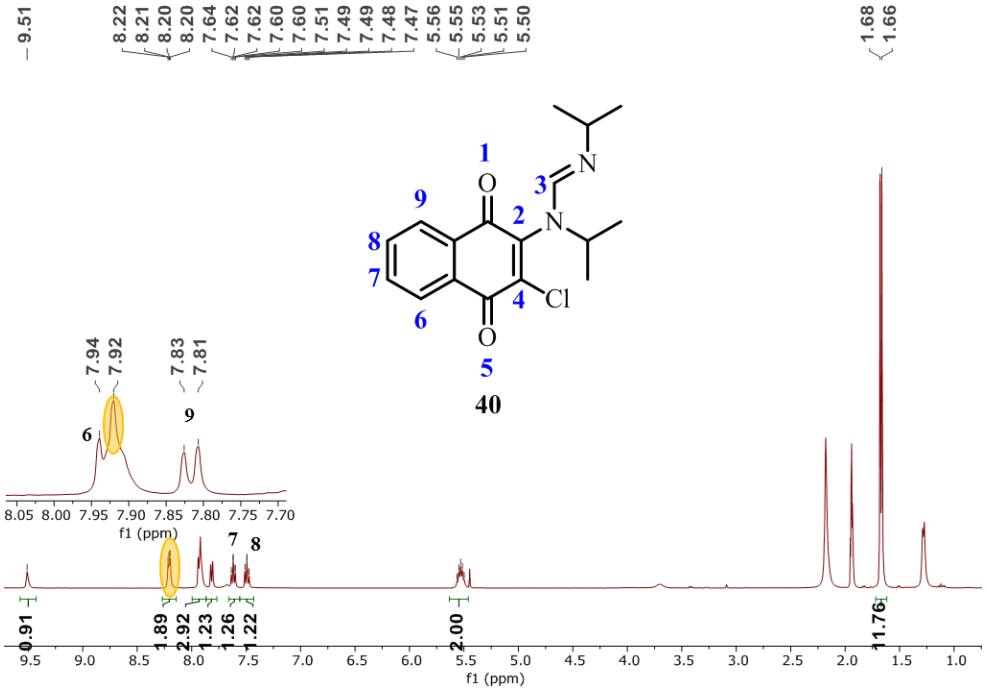

Figure 2-6: ^{1}H NMR Spectrum of compound **40** where the peaks associated with compound **39** are highlighted in yellow

Inspired by a report from Saravanakumar *et al*. on the substitution of Cl with N^{i}Pr on 2,3-cichloroquinoxaline, an attempt to replicate these results with **39**, an electronically similar molecule, was made.[24] C_2 and C_3 of compound **39** are electrophilic sites generated by the moderate electron withdrawing properties of the ketone moieties on the structure. After several attempts to create compound **41** using excessive heat and a par vessel, the only product was compound **42**. This was confirmed by examination of the ^{1}H NMR spectrum, which showed asymmetric peaks in the aromatic region with two doublets at 8.15 ppm and 8.04 ppm corresponding to the proton of C_6 and C_7, respectively, and two triplets at 7.72 ppm and 7.62 ppm corresponding to the protons on C_5 and C_8 respectively.

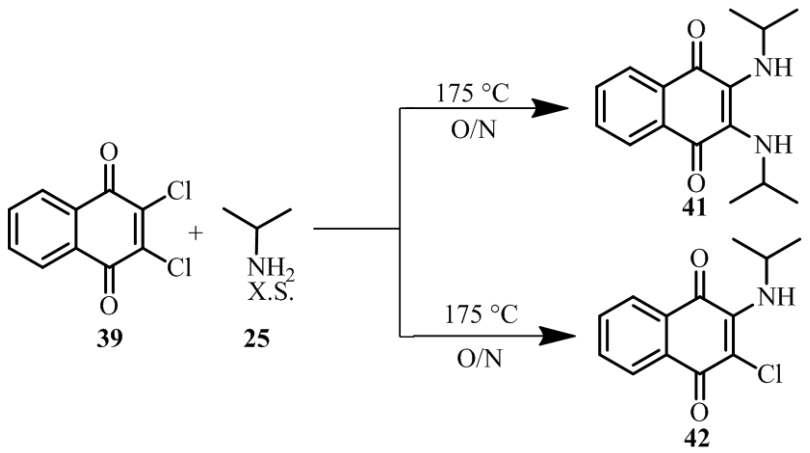

Scheme 2-9: Synthetic route for compound **44** yielding only **42**

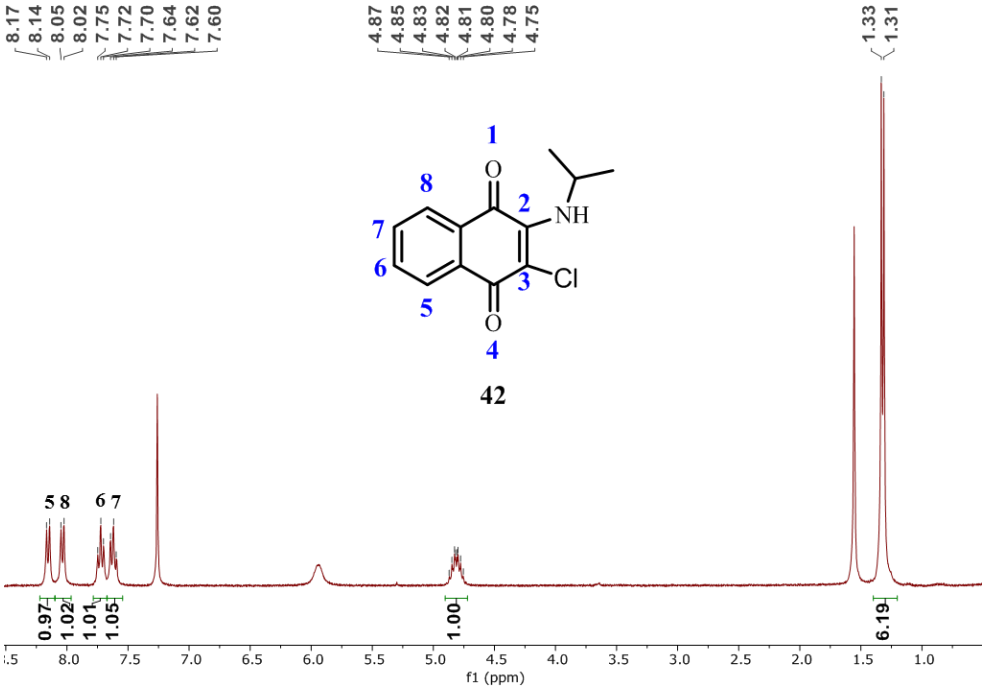

Figure 2-7: 3-chloro-2-isopropylamine-1,4-dionenaphthalene ^{1}H NMR Spectrum

It is likely that the electron donating properties of the newly bound nitrogen in C_2 prevent the second substitution of isopropyl amine by decreasing the electrophilicity of the enone. This is demonstrated in a paper where the N^{i}Pr group is first functionalized with a ketone minimizing the electron donating properties of nitrogen before the second N^{i}Pr addition.[25]

Using the experimental procedure described by Lee *et al.*[21], compound **46** was successfully synthesized. The success of this synthetic route draws from the use of the Gabriel synthesis known for

transforming alky halides into amines. In the first reaction of the Gabriel synthesis, **43** acts as a nucleophile in a substitution reaction replacing the chlorines. In a subsequent reaction, the phthalimides on **44** are reduced to phthalhydrazide leaving behind the primary amine. From **45**, the heterocycle is formed in the same manner as **27**. Compound **46** was characterized by ^{1}H NMR and is consistent with the literature values.

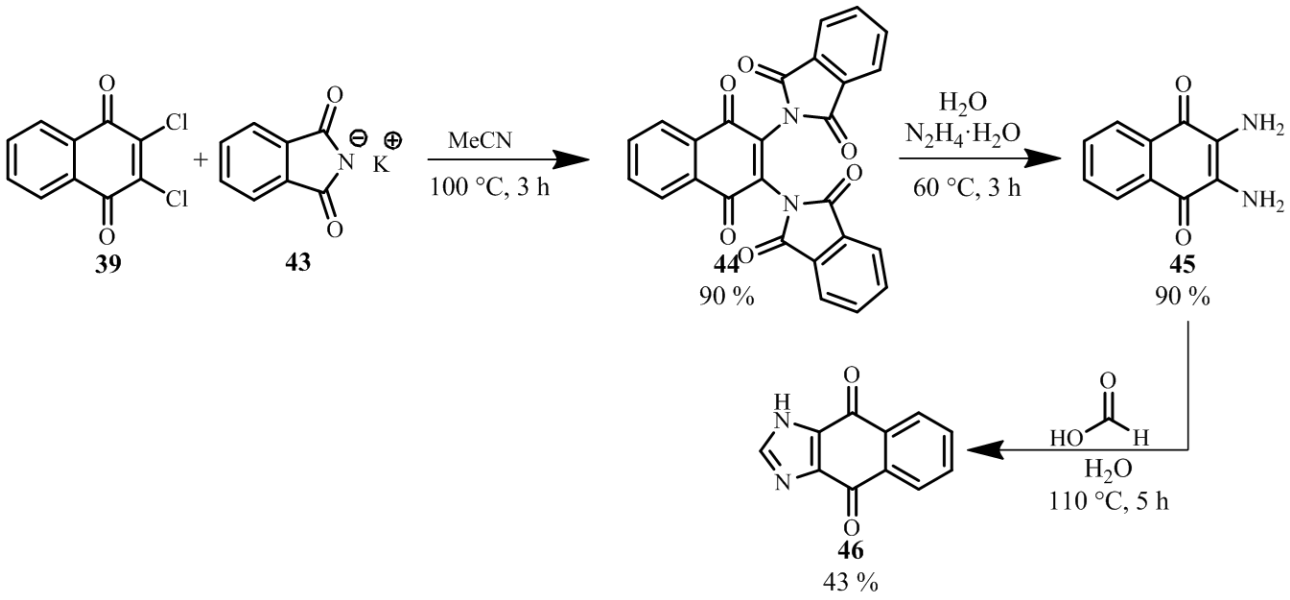

Scheme 2-10: 2,3-imidazole-1,4-dionenaphthalene Synthesis

As mentioned before, the alkylation of the two nitrogen atoms was achieved using the procedure outlined by Crudden *et al*.[4] The first alkylation was performed using **28** and Cs_2O_3 as the base resulting in compound **47**. This was characterized by ^{1}H NMR spectroscopy, revealing a septet corresponding to the NC*H*CH_3 of the isopropyl group at 5.40 ppm and the corresponding doublet at 1.65 ppm, each integrating to 1 and 6 respectively. As expected, the aromatic region is asymmetric with a multiplet at 7.76 ppm integrating to two protons, corresponding to the protons on C_7 and C_8, and two multiplets at 8.20 and 8.28 ppm, with integrations of one proton corresponding to the protons on C_9 and C_6, respectively. A singlet at 8.01 ppm was observed corresponding to the proton on the carbenic carbon.

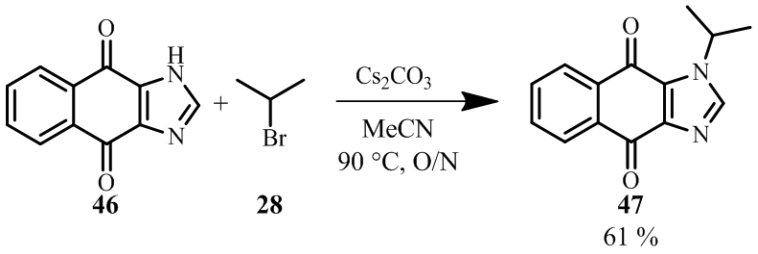

Scheme 2-11: N-isopropyl-[2,3d]-imidazole-1,4-dionenaphthalene Synthesis

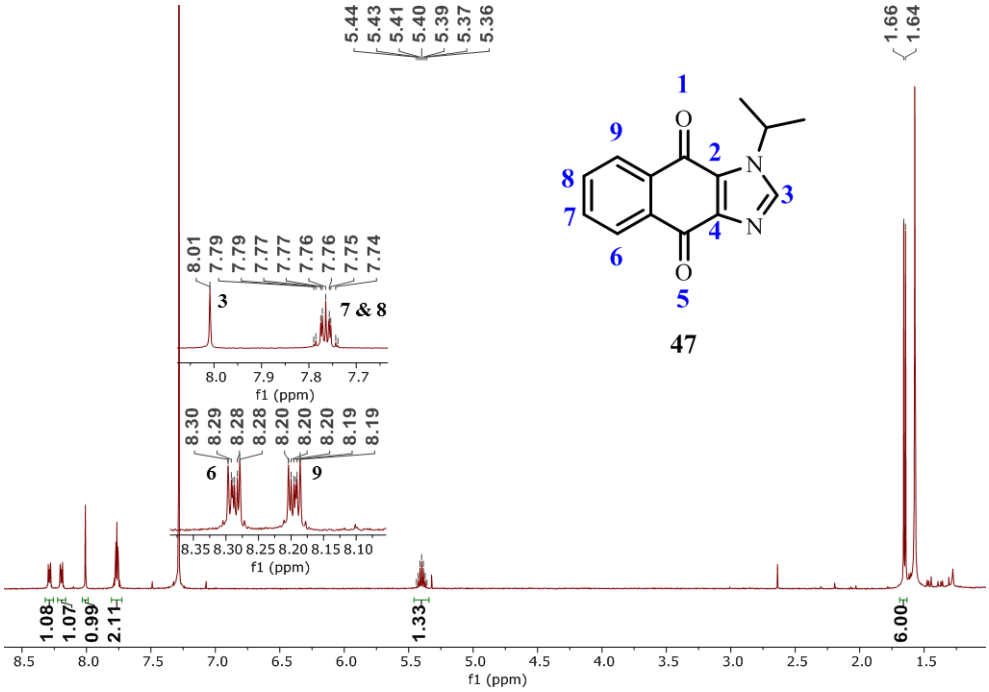

Figure 2-8: N-isopropyl[2,3-d]imidazole-1,4-dionenaphthalene ^{1}H NMR Spectrum

The second alkylation was carried out to yield both compounds **48** and **50** containing an iodine or triflate counterion. The iodine salt was made by refluxing compound **47** in **30** resulting in compound **48**. This was characterized by ^{1}H NMR spectroscopy in acetonitrile, which showed a symmetrical molecule characterized by a doublet of doublets at 8.30 ppm and 7.96 ppm corresponding to the protons on C_6, C_9, and C_7, C_8 respectively, each integrating to two protons. Additionally, a septet integrating for two protons is found at 5.54 ppm and the corresponding doublet integrating for 12 protons is found at 1.68 ppm. Finally, a singlet observed at 9.20 ppm which integrates for one proton is assigned to the carbenic proton.

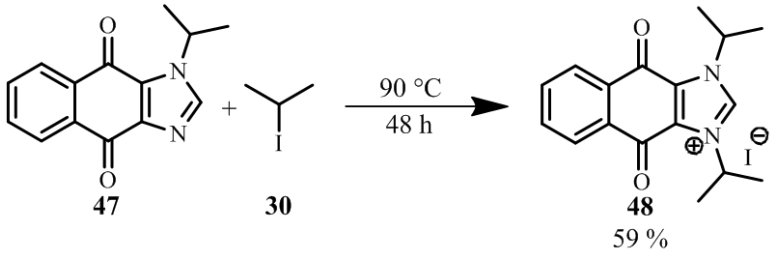

Scheme 2-12: N,N'-diisopropyl[2,3-d]imidazolium-1,4-dionenaphthalene Iodide Salt Synthesis

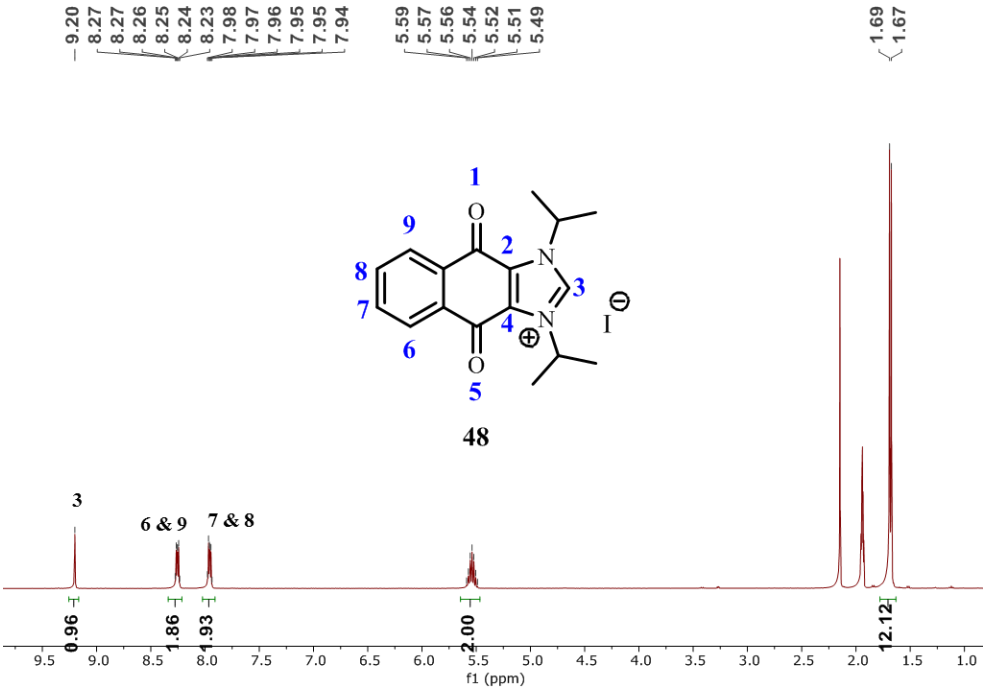

Figure 2-9: N,N'-diisopropyl[2,3-d]imidazolium-1,4-dionenaphthalene Iodide ^{1}H NMR Spectrum

Upon attempted formation of the bicarbonate salt, the compound decomposed. However, a BF_4^- resin developed by Dr. Ali Nazemi, a former member of the Crudden group was used to make the tetrafluoroborate salt.

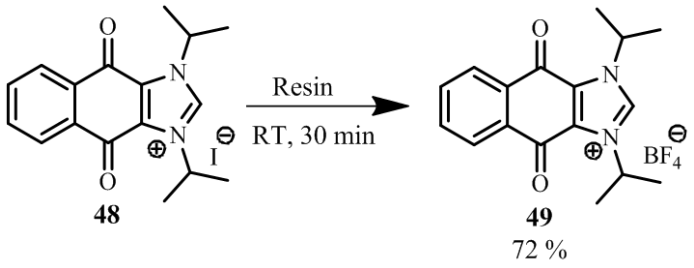

48 **49**
72 %

Scheme 2-13: Synthesis of N,N'-diisopropyl[2,3-d]imidazolium-1,4-dionenaphthalene Tetrafluoroborate

Since iodine is NMR silent it is not possible to determine if the reaction is complete using NMR techniques. The appearance of a fluorine peak in the ^{19}F NMR spectrum does not confirm the absence of a mixture of reactants and products. To circumvent this problem, a powder sample of the reaction was examined by XPS until such time that the iodine peak was no longer significant. The resulting compound was also analyzed using ^{1}H NMR in acetonitrile and was found to have the same spectrum as **48** with the exception of the carbenic proton which is shifted upfield to 9.11 ppm.

We next turned to the synthesis of triflate salt **50**, using the methods outlined by Crudden *et al*.[4] As mentioned before, the isopropyl triflate is generated *in situ* before reacting with compound **47**, which is then alkylated a second time to yield compound **50**. This compound was characterized by ^{1}H NMR spectroscopy in methanol with identical results to **1g**. The ^{19}F NMR has a peak at -151.88 ppm which is characteristic of a triflate counterion.

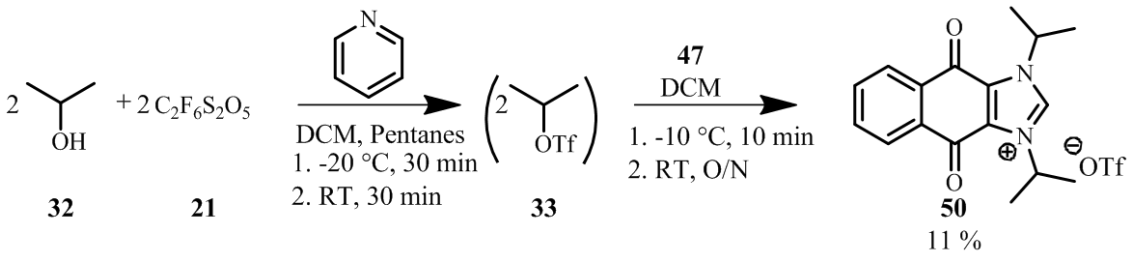

Scheme 2-14: Synthesis of N,N'-diisopropyl[2,3-d]imidazolium-1,4-dionenaphthalene Triflate

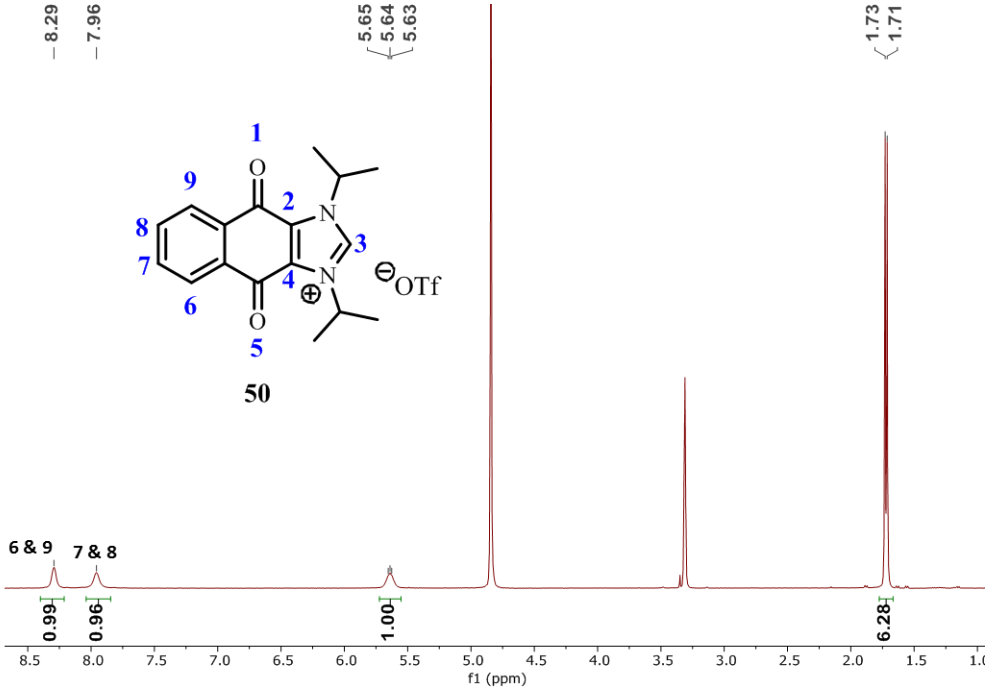

Figure 2-10: N,N'-diisopropyl[2,3-d]imidazolium-1,4-dionenaphthalene Triflate ^{1}H NMR Spectrum

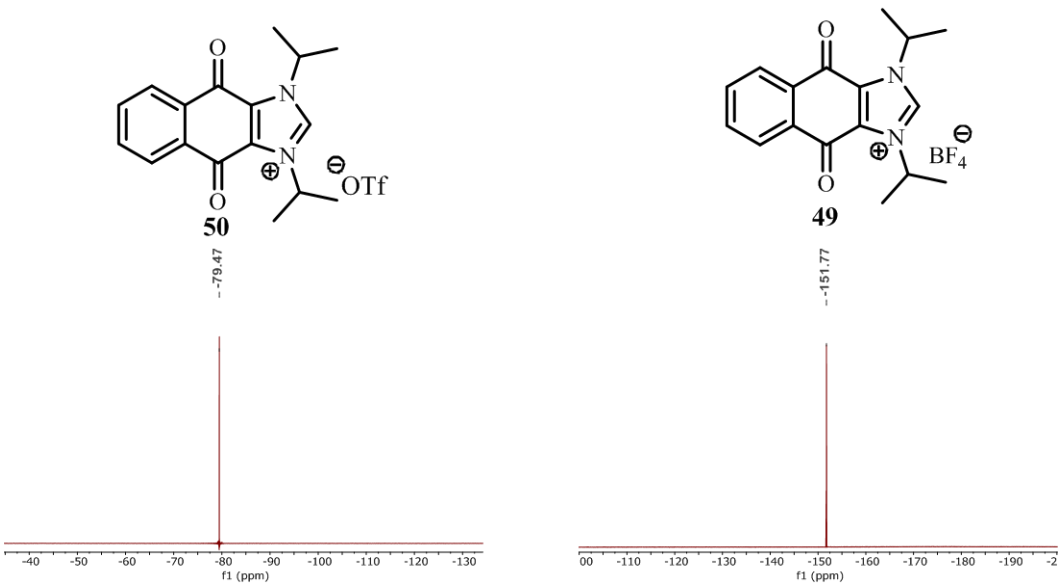

Figure 2-11: N,N'-diisopropyl[2,3-*d*]imidazolium-1,4-dionenaphthalene OTf^- and BF_4^- ^{19}F NMR Spectrum

2.2 Carbene Deposition

2.2.1 Free Carbene Deposition

With carbene precursors **19**, **31**,**34**, **35**, **37**, and **50** in hand, we next turned to the preparation of SAMs from these species. Using the "free carbene" method, an inert atmosphere glove box or Schlenk techniques need to be employed. The carbene salt is deprotonated using a strong base, then the target substrate is placed in the solution containing the carbene and left for 24h to deposit.[6,26] Using this method to create carbene SAMs is advantageous because the counterion for the carbene does not matter. However, the drawbacks to this method is that you need special equipment in order to set up the experiment, as not to expose the free carbene to atmospheric conditions. Compounds **19** and **31** were deposited using this method. The film produced by **19** had experimental elemental ratios after XPS analysis confirming the compound had formed a monolayer on the surface. However, the film produced by **31** had lots of iodine and carbon contamination as determined from the elemental ratios obtained after probing the surface using XPS.

2.2.2 Base Free Deposition

As an alternative, we also examined depositions using carbene salts without external base. As reported by Crudden *et. al*, the direct formation of a carbene SAM with no addition of base is possible using a hydrogen bicarbonate carbene salt in methanol.[4] However, as reported by Fèvre *et al.* the addition of a bicarbonate base such as $KHCO_3$, to a non hydrogen bicarbonate carbene salt will generate the bicarbonate salt in equilibrium with the CO_2 adduct which can then produce an NHC monolayer as described by the Crudden lab.[4,27] In our studies, Dr. Christene Smith from our lab has produced some evidence that carbene deposition of a triflate or tetrafluoroborate salt can occur without an external base although, the exact mechanism of the reaction is unknown and the method is not as well tested as the free carbene or carbonate methods. When deprotonation of the carbenic carbon occurs in the presence of the metal substrate, as soon as the carbene is generated it can start forming a monolayer on the surface. In this thesis, only the free carbene and base free deposition methods were used, deposition using a bicarbonate base was not attempted. Compounds **50**, **49**, **37 35**, **34**, and **19** were deposited using the base free method giving varying results upon XPS analysis.

2.3 Surface Analysis

2.3.1 Elemental Ratios

An XPS spectrum provides the binding energy in electron volts (eV) of different species in the sample, and an indication of their magnitude with respect to signal intensity defined as counts per second (CPS). The binding energy at which a peak appears defines what the element is. By integrating the area under each peak, it is possible to establish a ratio between all the different elements detected. For example, if the molecule expected to be on the surface is benzimidazole, a ratio can be established between the percent mass of carbon and nitrogen atoms. In this case the ratio would be 6:2. Thus if the ratios between the carbon and nitrogen signals is 6:2, it is possible to conclude the benzimidazole has adsorbed onto the surface. However, it is rare that the numbers work out in this manner. It is well known that adventitious carbon forms a layer on the surface upon exposure to the atmosphere and is often present in the XPS

instrument. Thus, it is likely the levels of carbon in the spectra will be larger than anticipated when creating the ratio. To circumvent this problem, it is essential to commence the deposition immediately after the substrate has been cleaned of adventitious carbon minimizing the time which the clean substrate is exposed to the atmosphere.

2.3.2 Powder Samples

When performing an ion exchange using Amberlyst resin, sometimes it can be difficult to monitor whether the exchange is complete. When changing from an iodine counterion to a tetrafluoroborate counterion, relying on the fluorine signal in the ^{19}F NMR is not enough evidence to consider the exchange complete. To overcome this problem, powder XPS of the sample can be performed. For the purposes of this work, XPS is mainly used to analyze SAMs on gold substrates. However, it is possible to load a powder sample where the compound is packed down onto copper tape then measured. This is useful for gaining an idea of how much of an NMR inactive element is present.

N,N'-Diisopropyl[2,3-d]imidazolium-4,9-dione iodine salt (**48**) was subjected to the tetrafluoroborate resin for anion exchange. The resin exchange was set up at three different temperatures 0°C, room temperature, and 40°C, for 30 minutes. It was found that all three compounds still had iodine present, however there was more iodine present in the 0°C sample than the room temperature and 40°C sample. The compounds were re-subjected to a new batch of resin, however the 0°C sample was then heated to 40°C. After the second resin exchange there was no iodine seen in any of the samples by powder XPS. Thus, it is possible to conclude that raising the temperature during the resin exchange does not have a significant effect on the speed at which the exchange occurs. Additional experiments need to be carried out to determine if a longer resin exchange time would provide the same results or if the compound needs to be subjected to two equivalents of resin.

2.3.3 Free Carbene and Base Free Monolayers

X-ray photoelectron spectroscopy was employed to analyze the results of each method of deposition. As shown below, it was found there was no significant difference between them in terms of the elemental ratios and amount of contaminant on the surface.

N,N'-ditolyl-4,5(R,R)-diphenylimidazolium tetrafluoroborate (**19**) deposited onto a gold substrate by means of free carbene and the surface was analyzed by XPS and the ratio between the atomic percentage of carbon with respect to nitrogen was found to be 29:2 over 4 samples. The expected ratio between carbon and nitrogen based on the atomic percent of each element in compound **19** is 25:2. Considering the possibility for adventitious carbon on the surface, this is a very reasonable ratio. A base free deposition of compound **19** was attempted with one sample, producing a carbon to nitrogen ratio from the film of 75:2. However, this film was contaminated with iodine (Table 2-1) but no iodine was seen in the XPS of the solid sample, meaning it is possible the atmosphere in the lab where the deposition was being carried out is contaminated allowing excess iodine and carbon to adsorb onto the surface prior to the deposition of the carbene. Since this was only carried out once, repetitions of the base free method for the deposition of compound **19** are needed.

NHC	Deposition Method	Carbon to Nitrogen Ratio; Expected (25:2)	Iodine Contamination (Iodine to Nitrogen Ratio)
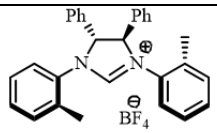 **19**	Free Carbene	29:2	N/A
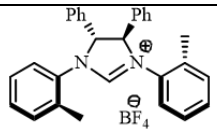 **19**	Base Free	75:2	1:2

Table 2-1: XPS carbon to nitrogen ratios of varying methods for depositing compound **19**

The C1s XPS spectrum of the film deposited by the free carbene method from compound **19** in Figure 2-12, is deconvoluted into three peaks which is to be expected for a monolayer of **19** where 284.1 eV corresponds to C-C, 285.6 eV corresponds to C-N, and 287.3 eV corresponds to C-Ar bonding. However, the base free deposition film (B) has an extra peak at 288.8 eV indicative of adventitious C-O species. Since the base free deposition method was only completed once, no conclusions can be made as to which deposition method is most effective.

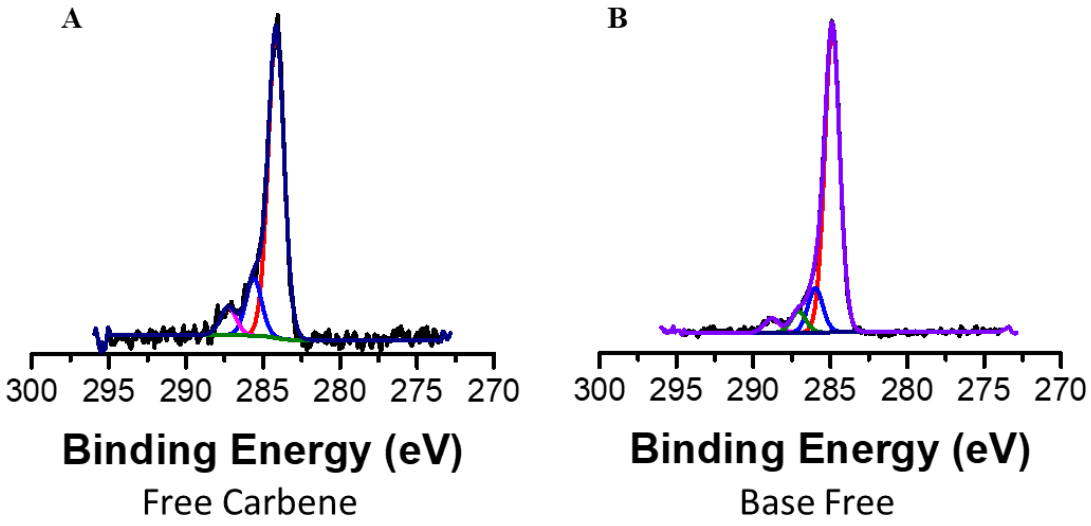

A Binding Energy (eV) (Percentage of total peak area)	B Binding Energy (eV) (Percentage of total peak area)
284.1 (78%)	284.9 (79%)
285.6 (14%)	286 (11%)
287.3 (7%)	287.1 (4%)
	288.8 (5%)

Figure 2-12: C1s XPS spectra of compound **19** after **A** free carbene deposition and **B** base free deposition onto a gold surface.

Monolayers of N,N'-diisopropylnaphthalene[2,3-d]imidazolium salts (**31**, **34**, **35**, and **37**) were also analyzed by XPS. The iodine, tetrafluoroborate, bicarbonate, and triflate salts for this compound were all deposited. Compound **31** was deposited using the free carbene method and the resultant film had a carbon to nitrogen ratio of 26:2 from the XPS data of two samples. However, there was some iodine contamination (Table 2-2) with a ratio of iodine with respect to nitrogen of 1:2 suggesting an incomplete formation of the free carbene before exposure to the gold substrate or incomplete removal of the residual iodide salt. As mentioned previously, the increased amounts of carbon may be attributed to the brief exposure of the gold substrate to atmospheric conditions after the plasma etch. The tetrafluoroborate, bicarbonate, and triflate salts (**34**, **35**, and **37**) were deposited onto the surface using the base free method. The monolayers made from these salts had a carbon to nitrogen ration of 25:2, 29:2, and 27:2 respectively, suggesting successful depositions. These values are comparable with the results from the free carbene deposition monolayer. The bicarbonate and tetrafluoroborate salts had no iodine contamination, however the triflate salt had some

iodine contamination resulting in an iodine to nitrogen ratio of 1:2 (Table 2-2). Since no iodine is present in the powder XPS spectrum of **34** the iodine can be attributed to contamination in the solvent, atmosphere, or possibly the substrate prior to SAM formation. However, the C:N ratios of the salts deposited using the base free method for this compound have much less carbon contamination when compared to the base free deposition of compound **19**.

NHC	Deposition Method	Carbon to Nitrogen ratio; Expected (15:2)	Iodine Contamination (Iodine to Nitrogen Ratio)
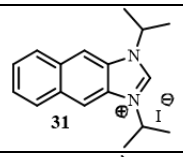 **31**	Free Carbene	26:2	2:1
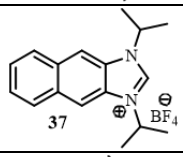 **37**	Base Free	25:2	N/A
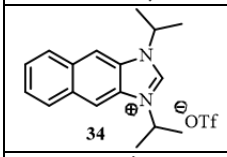 **34**	Base Free	27:2	2:1
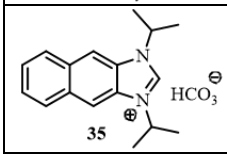 **35**	Internal Base	29:2	N/A

Table 2-2: Carbon to nitrogen ratios from XPS measurements of N,N'-diisopropylnaphthalene[2,3-*d*]imidazolium salt monolayers on gold substrate by varying deposition methods

Three signals are obtained upon the deconvolution of the C 1s XPS spectra for the monolayer of compound **31**. The signals correspond with C-C (284.4 eV), C-N (286.7 eV) and C-Ar (287.1 eV) binding. However, the carbon to nitrogen ratio suggests increased amounts of carbon on the gold surface. Since there is no signal indicating C-O binding from adventitious carbon, the excess carbon found on the surface can be attributed to adventitious C-C carbon.

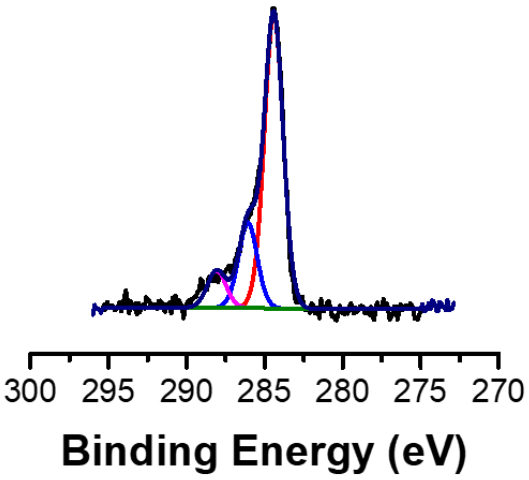

Binding Energy (eV) (Percentage of total peak area)
284.4 (73%)
286.1 (19%)
287.1 (8%)

Figure 2-13: C1s XPS spectrum of the thin film from compound **31** after free carbene deposition onto a gold surface.

The C 1s XPS spectra in Figure 2-14 shows a direct comparison between the powder sample of **37** (A) and surface bound **37** (B). As expected, the powder sample (A) which is a direct analysis of the synthesized molecule is deconvoluted into three features corresponding to C-C (284.5 eV), C-N (286 eV), and C-Ar (287.8 eV) bonding. However, the surface bound species (B) has an extra signal at 288.4 eV which can be attributed to adventitious C-O species accounting for the increased carbon in the carbon to nitrogen ratio.

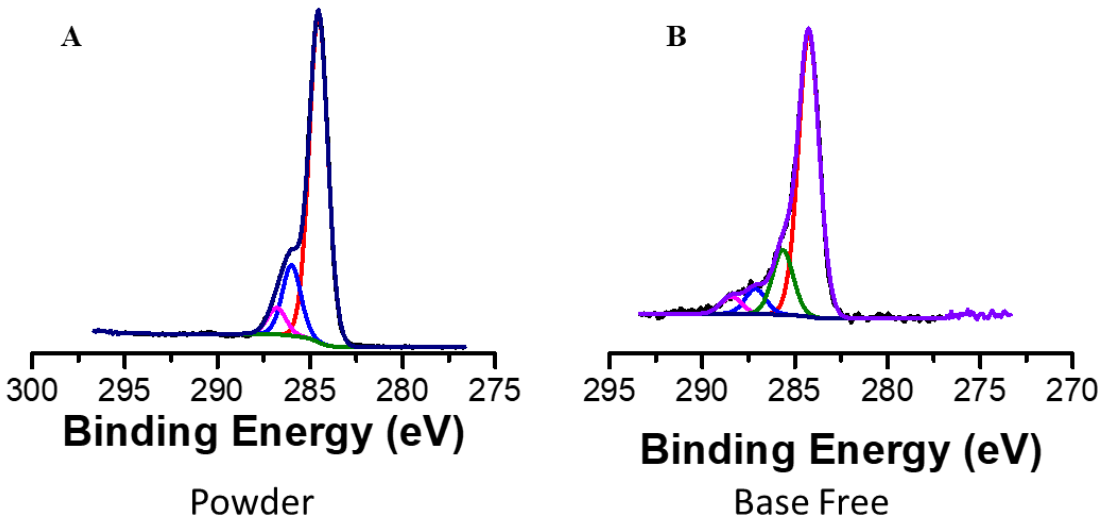

A Binding Energy (eV) (Percentage of total peak area)	B Binding Energy (eV) (Percentage of total peak area)
284.5 (77%)	284.2 (73%)
286 (16%)	285.3 (16%)
287.8 (6%)	287.1 (6%)
	288.4 (4%)

Figure 2-14: C1s XPS spectra of compound **37** after **A** powder analysis of the molecule and **B** base free deposition onto a gold surface.

Likewise, the C 1s XPS spectra in Figure 2-15 shows a direct comparison between the powder sample (A) and surface bound (B) of compound **34**. The deconvolution of the spectrum corresponding to the synthesized molecule has four distinct signals. Three of these signals fall within the same grouping as expected for the C-C (284.7 eV), C-N (285.8 eV), and C-Ar (286.8 eV) binding energies. The fourth signal is seen at a much higher binding energy (292.2 eV) corresponding to the C-F bond in the triflate counter ion. Similarly to Figure 2-14, the surface bound sample has a signal at 288.9 eV corresponding to adventitious C-O accounting for the large carbon presence in the carbon to nitrogen ratio. However, the disappearance of the signal at 292.2 eV in Figure 2-15 B indicates the triflate counter ion is no longer present suggesting a successful deposition of **34** onto a gold surface.

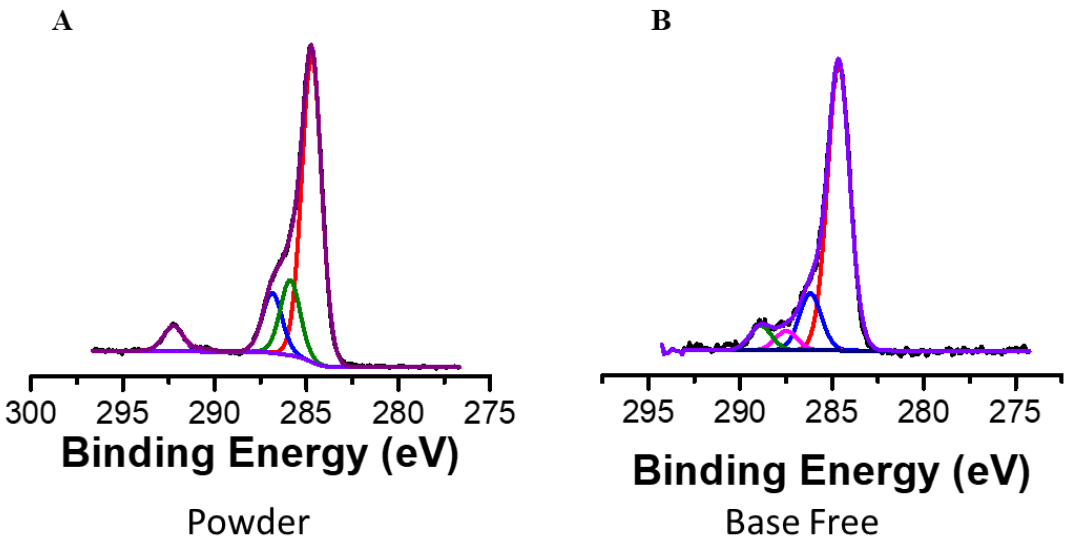

A Binding Energy (eV) (Percentage of total peak area)	B Binding Energy (eV) (Percentage of total peak area)
284.7 (65%)	284.6 (74%)
285.8 (16%)	286.1 (15%)
286.8 (13%)	287.5 (5%)
292.2 (5%)	288.9 (6%)

Figure 2-15: C1s XPS spectra of compound **34** after **A** powder analysis of the molecule and **B** base free deposition onto a gold surface.

Finally, Figure 2-16 displays the C 1s spectrum from the deposition of compound **35** onto a gold substrate. Much like the previous results, this surface bound species has a spectrum which is deconvoluted into four signals. The three signals corresponding to the monolayer of compound **35** are 284.6 eV consistent with C-C binding, 285.5 eV consistent with C-N binding and 286.4 eV which can be assigned to C-Ar binding. The last signal at 288 eV is determined to be adventitious C-O bound to the surface.

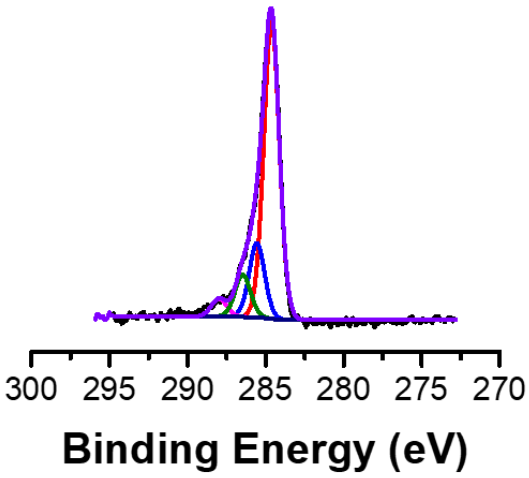

Binding Energy (eV) (Percentage of total peak area)
284.6 (69%)
285.5 (17%)
286.4 (4%)
288 (10%)

Figure 2-16: C1s XPS spectrum of compound **35** after internal base deposition onto a gold surface.

Based on these results, there is a carbon contamination issue with the gold surfaces. There is some iodine contamination present for some of the samples however this can be addressed with more careful lab practices to avoid cross contamination. From all the samples prepared, only the free carbene method of **31** produced a monolayer which was not contaminated with adventitious C-O. Thus, in order to reduce carbon contamination on the surface the free carbene method for deposition is the best route. The extra C-O contamination observed from the base free and internal base deposition methods may come from a combination of the solvent used and atmospheric conditions. It is imperative to perform the depositions under an inert atmosphere in order to achieve the desired monolayer with minimal contaminants.

N,N'-diisopropyl[2,3-d]imidazolium-4,9-dione salts (**49** and **50**) were deposited using the base free method. The triflate salt, compound **50**, and the tetrafluoroborate salt, compound **49** were used. The results from the XPS analysis after SAM formation for compound **50** showed a carbon to nitrogen ratio of 36:2 over 4 samples. The expected values for the ratio between carbon to nitrogen is 15:2. Some iodine and sulfur contamination were also observed (iodine to nitrogen ratio of 1:2 and sulfur to nitrogen ratio of 1:2).

The contamination of sulfur may come from the triflate counterion, however there is no contamination from fluorine, and compound **46** mentioned previously showed no contamination from sulfur. It is possible that carbene formation by means of base free depostion for compound **50** follows a slightly different path than compound **46** leading to decomposition of the counter ion. Since SAMs have traditionally been made with thiols, it is well known that sulfur has an affinity towards gold. Again, the iodine and increased carbon measured may be a product of contamination from the atmosphere since no iodine is present in the powder C1s XPS spectra of **49** and **50**. The results from the XPS analysis of the film from compound **49** was a carbon to nitrogen ratio of 16:2 over 2 samples. This ratio matches the expected values of 15:2 within error of ± 1. However, much like so many samples before, there is still some contamination from iodine. This contamination has a iodine to nitrogen ratio of 1:2. This may come from residual iodine present in the compound after performing the tetrafluoroborate resin exchange.

NHC	Deposition Method	Carbon to Nitrogen Ratio Expected (15:2)	Iodine Contamination (Iodine to Nitrogen Ratio)	Sulfur Contamination (Sulfur to Nitrogen Ratio)
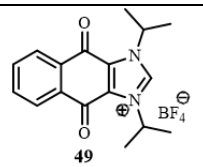 **49**	Base Free	16:2	1:2	N/A
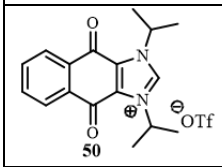 **50**	Base Free	36:2	1:2	1:2

Table 2-3: Carbon to nitrogen ratios from XPS measurements of N,N'-diisopropy[2,3-*d*]imidazolium-1,4-dionenaphthalene salts after base free deposition onto a gold substrate

Figure 2-17 depicts the C 1s XPS spectra in direct comparison of the powder sample (A) and surface modified sample (B) of **49**. Since this NHC has a quinone, it is expected to deconvolute into four species instead of three. This is seen with the powder sample where the C-C bonding can be attributed to the signal at 284.8 eV, C-N at 286 eV, C-Ar at 286.5 eV and C=O at 287.9 eV. However, the spectra of the surface bound species is deconvoluted into five different signals. A carbon to nitrogen ratio within error of the

expected value suggests the successful formation of a monolayer. Thus the signals can be assigned as follows. 284.6 eV for the C-C bond, 285.3 eV for C-N, 286.4 eV for C-Ar, 287.8 eV for C=O and 288.9 eV for π-π^* satellite from the extended pi structure in the molecule and interactions with adjacent molecules in the monolayer.

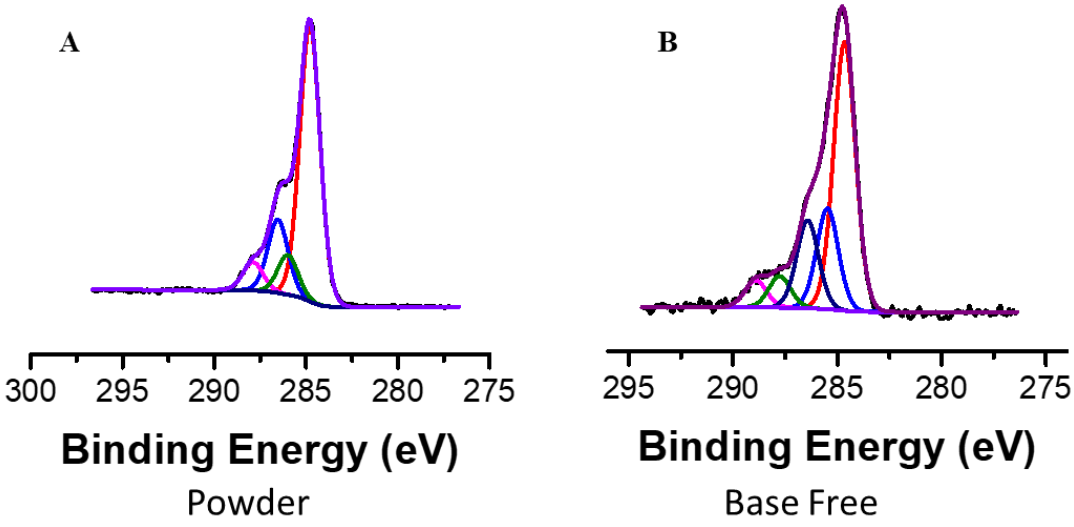

A Binding Energy (eV) (Percentage of total peak area)	B Binding Energy (eV) (Percentage of total peak area)
284.8 (66%)	284.6 (52%)
286 (9%)	285.4 (19%)
286.5 (17%)	286.4 (17%)
287.9 (7%)	287.8 (6%)
	288.9 (5%)

Figure 2-17: C1s XPS spectra of compound **49** after **A** powder analysis of the molecule and **B** base free deposition onto a gold surface.

Finally, the C 1s spectra for compound **50** is seen in figure 2-18. This spectrum is deconvoluted into three signals at 284.9 eV for C-C, 286.4 eV for C-N and 288.2 eV for C=O. Since there is a large excess of carbon on the surface described in table 2-3, it is possible a large excess of adventitious carbon reduces the C-Ar signal such that it is no longer significant. However, the presence of the C-N and C=O signals on the spectra suggest that **50** is on the surface but likely in very small amounts.

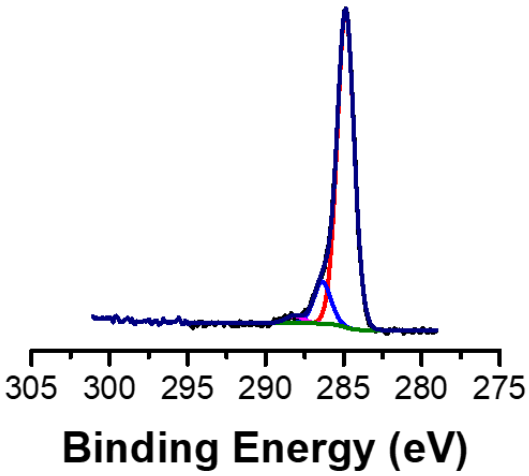

Binding Energy (eV) (Percentage of total peak area)
284.9 (86%)
286.4 (11%)
288.2 (2%)

Figure 2-18: C1s XPS spectrum of compound **50** after base free deposition onto a gold surface.

From these results it is possible to conclude for this NHC the counterion significantly impacts the formation of a monolayer on the surface. The BF_4^- counterion (**49**) NHC successfully produced a monolayer on the surface, however, the OTf^- counter ion (**50**) NHC did not and had traces of sulfur on the surface which suggests some decomposition during monolayer formation.

Since the measured iodine in all the samples is the same, even compounds where iodine was never the counterion, it is possible an iodine to nitrogen ratio of 1:2 can be considered a standard background value for iodine. More repetitions of each SAM formation on a gold substrate should be carried out in order to conclusively determine if iodine contamination is truly a problem or if the ratio of iodine to nitrogen of 1:2 can simply be considered negligible. Additionally, the method by which the monolayer is formed has some significance on the amount of contamination in the resulting surface. The free carbene deposition of the NHCs significantly reduces the amount of adventitious C-O such that the carbon contamination only comes from adventitious C-C. Finally, the counterion for the carbene salts may influence how the

monolayer forms, however, the comparison between **50** and **49** were the only examples where the counterion may have been a factor.

2.4 Monolayer Imaging

STM was performed on compound **19** to determine if it forms a chiral surface on gold. Unfortunately, the STM images obtained only showed bare gold surface. XPS was used to analyze the chip which was imaged, and there was no evidence of **19** on the surface. An attempt to image compound **35** was also made. Studies were carried out at ambient temperature. A well-ordered surface was not seen, but variation in the step edges of gold is observed, suggesting upon imaging at room temperature the molecules migrate to the step edges. Further studies are currently underway in the McLean group at Queen's University at cryogenic temperatures.

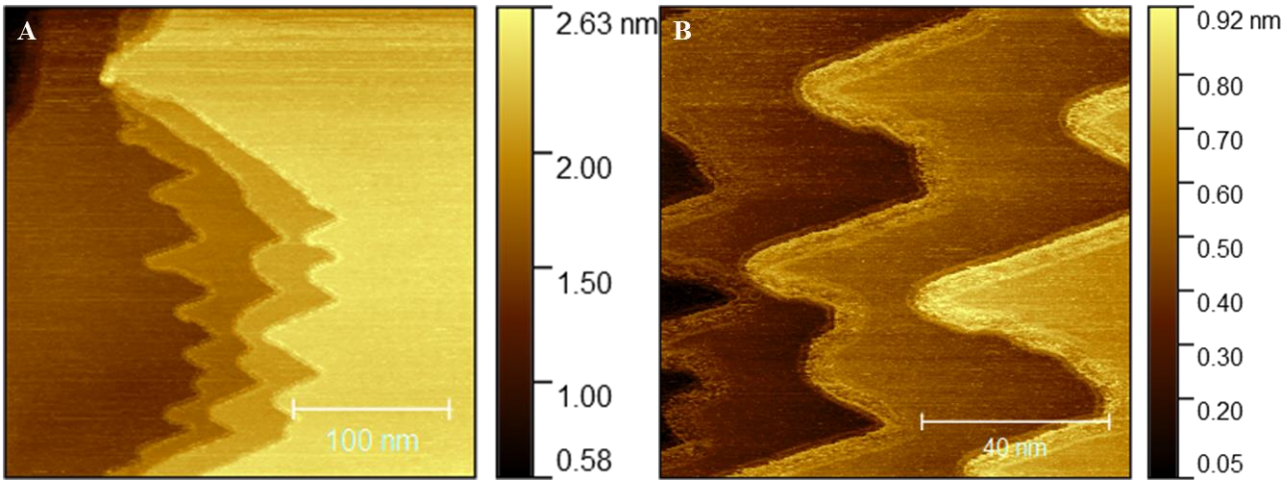

Figure 2-12: STM image of gold step edges with A on the order of 2.63nm and B closer look on the order of 0.92nm

2.5 Electrochemical Probing

In collaboration with the Birss lab at the University of Calgary, voltammetry studies were employed to examine the formation of NHC films from electroactive NHC **50**. The scope of the collaboration was to electrochemically investigate if **50** formed a monolayer on the gold surface and after confirming the presence of a monolayer, a SAM containing different concentrations of **50** and **34** were also to be studied. However, when **50** was deposited onto an electrode and the resulting film measured using cyclic voltammetry, the features indicative of a quinone moiety were present however very minor. This indicated

very low molecular coverage on the electrode surface. It is possible since the quinone is sandwiched between the benzene and imidazole, that the benzene may be insulating the molecule such that the quinone has a reduced signal. No further electrochemistry studies were performed.

2.6 References

1. Stephenson-Brown, A. *et al.* Glucose selective Surface Plasmon Resonance-based bis-boronic acid sensor. *The Analyst* **138**, 7140 (2013).
2. Zhang, D.-Q., Gao, L.-X., Cai, Q.-R. & Lee, K. Y. Inhibition of copper corrosion by modifying cysteine self-assembled film with alkylamine/alkylacid compounds. *Materials and Corrosion* **61**, 16–21 (2010).
3. Meth, S. *et al.* Siloxane-based thin films for corrosion protection of stainless steel in chloride media. *Journal of Applied Electrochemistry* **41**, 885–890 (2011).
4. Crudden, C. M. *et al.* Simple direct formation of self-assembled N-heterocyclic carbene monolayers on gold and their application in biosensing. *Nature Communications* **7**, 12654 (2016).
5. Ehler, T. T. & Noe, L. J. Surface Plasmon Studies of Thin Silver/Gold Bimetallic Films. *Langmuir* **11**, 4177–4179 (1995).
6. Crudden, C. M. *et al.* Ultra stable self-assembled monolayers of N-heterocyclic carbenes on gold. *Nature Chemistry* **6**, 409–414 (2014).
7. Gürses, A., Açıkyıldız, M., Güneş, K. & Gürses, M. S. Dyes and Pigments: Their Structure and Properties. in *Dyes and Pigments* 13–29 (Springer International Publishing, 2016). doi:10.1007/978-3-319-33892-7_2
8. Li, B., Gutierrez, P. L., Amstad, P. & Blough, N. V. Hydroxyl Radical Production by Mouse Epidermal Cell Lines in the Presence of Quinone Anti-Cancer Compounds. *Chemical Research in Toxicology* **12**, 1042–1049 (1999).
9. Seiders, T. J., Ward, D. W. & Grubbs, R. H. Enantioselective Ruthenium-Catalyzed Ring-Closing Metathesis. *Organic Letters* **3**, 3225–3228 (2001).

10. Ye, R. *et al.* Supported Au Nanoparticles with *N* -Heterocyclic Carbene Ligands as Active and Stable Heterogeneous Catalysts for Lactonization. *Journal of the American Chemical Society* **140**, 4144–4149 (2018).
11. Gellman, A. J. Chiral Surfaces: Accomplishments and Challenges. *ACS Nano* **4**, 5–10 (2010).
12. Love, J. C., Estroff, L. A., Kriebel, J. K., Nuzzo, R. G. & Whitesides, G. M. Self-Assembled Monolayers of Thiolates on Metals as a Form of Nanotechnology. *Chemical Reviews* **105**, 1103–1170 (2005).
13. Schwartz, D. K. Mechanisms and Kinetics of Self-Assembled Monolayer Formation. *Annual Review of Physical Chemistry* **52**, 107–137 (2001).
14. Grobler, I., Smith, V. J., Bhatt, P. M., Herbert, S. A. & Barbour, L. J. Tunable Anisotropic Thermal Expansion of a Porous Zinc(II) Metal–Organic Framework. *Journal of the American Chemical Society* **135**, 6411–6414 (2013).
15. He, M. & Bode, J. W. Enantioselective, NHC-Catalyzed Bicyclo-β-Lactam Formation via Direct Annulations of Enals and Unsaturated *N* -Sulfonyl Ketimines. *Journal of the American Chemical Society* **130**, 418–419 (2008).
16. Smith, C. A. Self-Assembled Monolayers of N-Heterocyclic Carbenes on Gold and their Applications. (Queen's University, 2018).
17. Kojima, A., Takemoto, T., Sodeoka, M. & Shibasaki, M. Catalytic Asymmetric Synthesis of Halenaquinone and Halenaquinol. 2
18. Lee, D.-Y. & Hartwig, J. F. Zinc Trimethylsilylamide as a Mild Ammonia Equivalent and Base for the Amination of Aryl Halides and Triflates. *Organic Letters* **7**, 1169–1172 (2005).
19. Navarro, O., Kaur, H., Mahjoor, P. & Nolan, S. P. Cross-Coupling and Dehalogenation Reactions Catalyzed by (*N* -Heterocyclic carbene)Pd(allyl)Cl Complexes. *The Journal of Organic Chemistry* **69**, 3173–3180 (2004).

20. Weber, L. *et al.* Electrochemical and spectroelectrochemical studies of C-benzodiazaborolyl-ortho-carboranes. *Dalton Trans.* **42**, 2266–2281 (2013).

21. Lee, J., Kim, H. & Park, M. J. Long-Life, High-Rate Lithium-Organic Batteries Based on Naphthoquinone Derivatives. *Chemistry of Materials* **28**, 2408–2416 (2016).

22. Pompeo, M., Froese, R. D. J., Hadei, N. & Organ, M. G. Pd-PEPPSI-IPent ^{Cl} : A Highly Effective Catalyst for the Selective Cross-Coupling of Secondary Organozinc Reagents. *Angewandte Chemie International Edition* **51**, 11354–11357 (2012).

23. Dunsford, J. J., Tromp, D. S., Cavell, K. J., Elsevier, C. J. & Kariuki, B. M. N-alkyl functionalised expanded ring N-heterocyclic carbene complexes of rhodium(I) and iridium(I): structural investigations and preliminary catalytic evaluation. *Dalton Transactions* **42**, 7318 (2013).

24. Saravanakumar, S., Kindermann, M. K., Heinicke, J. & Köckerling, M. Influence of anellation in N-heterocyclic carbenes: Novel quinoxaline-anellated NHCs trapped as transition metal complexes. *Chemical Communications* 640 (2006). doi:10.1039/b512884f

25. Ho, S.-H. S. *et al.* Antiproliferative, DNA intercalation and redox cycling activities of dioxonaphtho[2,3-d]imidazolium analogs of YM155: A structure–activity relationship study. *European Journal of Medicinal Chemistry* **104**, 42–56 (2015).

26. Arduengo, A. J., Dias, H. V. R., Harlow, R. L. & Kline, M. Electronic stabilization of nucleophilic carbenes. *Journal of the American Chemical Society* **114**, 5530–5534 (1992).

27. Fèvre, M. *et al.* Imidazol(in)ium Hydrogen Carbonates as a Genuine Source of *N* -Heterocyclic Carbenes (NHCs): Applications to the Facile Preparation of NHC Metal Complexes and to NHC-Organocatalyzed Molecular and Macromolecular Syntheses. *Journal of the American Chemical Society* **134**, 6776–6784 (2012).

Chapter 3

Conclusions

3.1 Furthering the Scope of Surface NHCs

The importance of NHCs in recent decades is outlined by their increased use in areas such as catalysis, where NHCs are found to form a stronger metal carbene bond in comparison to their phosphine counterparts.[1–3] Additionally, NHCs out compete thiols in stability on gold surfaces and nanoparticles.[4,5] Investigation of NHC analogues to thiol based materials such as biosensors, offers the potential to create more robust sensors with longer lifetimes.[6]

The research presented in this thesis demonstrates the synthesis of N,N'-diisopropylnaphthalene[2,3-*d*]imidazolium and N,N'-diisopropyl[2,3-*d*]imidazolium-1,4-dionenaphthalene salts, compounds **31**, **34**, **35**, **37**, **48**, **49** and **50**. Additionally, N,N'-ditolyl-4,5(R,R)-diphenylimidazolium tetrafluoroborate (**19**) and compounds **31**, **34**, **35**, **37**, **49** and **50** were deposited onto a gold surface and analyzed using XPS.

Compounds **34** and **37** were characterized by ^{1}H NMR with a doublet of doublets at 8.07 and 7.65 ppm integrating for 2 protons corresponding to the protons of C_6, C_9 and C_7, C_8 respectively, and a singlet at 8.22 ppm integrating for two protons which corresponds to the protons on C_1 and C_5 as shown in Figure 2-4. The carbenic proton was characterized by a singlet at 9.99 ppm integrating for 1 proton. The isopropyl wingtip groups were defined by a septet at 5.10 ppm integrating for 2 protons and a doublet at 1.86 integrating for 12 protons. These compounds differ in the ^{19}F NMR where compound **34** has a singlet at -78.29 ppm and **37** has a singlet at -151.65 ppm. Compounds **29** and **35** were characterized using ^{1}H NMR with two doublet of doublets in the aromatic region at 8.21 and 7.66 ppm each integrating for two protons, corresponding to the protons on C_6, C_9 and C_7, C_8 respectively, and a singlet at 8.59 ppm which integrates for two protons corresponding to the protons on C_1 and C_5 as outlined in Figure 2-3. The isopropyl moieties

are characterized by a septet integrating for two protons at 5.19 ppm and a doublet integrating for 12 protons at 1.82 ppm.

Compounds **48**, **49**, and **50** were characterized using ^{1}H NMR. Compounds **48** and **49** have the same peak positions with a doublet of triplets at 8.26 ppm which integrates for two protons and corresponds to C_6 and C_9 and a doublet of quartets at 7.96 ppm which integrates for two protons and corresponds to the protons on C_7 and C_8 as depicted in Figure 2-9. A singlet at 9.20 ppm integrates for one proton and corresponds to the proton on the carbenic carbon. The isopropyl groups were characterized by a septet at 5.54 ppm which integrates for 2 protons and a doublet at 1.68 ppm which integrates for twelve protons. **49** is further characterized by ^{19}F NMR by a singlet at -151.77 ppm indicative of fluorine on a BF_4 moiety. Compound **50** was characterized using ^{1}H NMR with two doublet of doublets both integrating for two protons at 8.29 and 7.96 ppm, which corresponds to the protons on C_6, C_9 and C_7, C_8 respectively as depicted in Figure 2-10. The isopropyl groups were characterized by a septet at 5.64 ppm which integrates for two protons and a doublet at 1.72 ppm which integrates for twelve protons. Since the ^{1}H NMR spectrum was acquired using deuterated methanol as the solvent, the carbenic proton is not present. The ^{19}F NMR spectrum has a singlet at -79.47 ppm, indicative of the fluorine on a triflate anion.

NHC SAMs were created by a solution phase deposition of the corresponding salt. There are three methods for depositing the carbenes. The first method is through the free carbene which requires an inert atmosphere. The second method is bench stable in methanol where the counterion acts as an internal base generating the free carbene which allows for SAM formation. The third method is bench stable where the salt is dissolved in methanol and left to deposit on the metal surface. All methods were used in depositing the synthesized molecules. However, it should be noted that gold is a highly iodophilic surface so compound **31** was only deposited by the free carbene method.

Compounds **49**, and **50** were deposited using the third deposition method as depicted in Table 2-3. From two samples **49** had an excellent C:N elemental ratio of 16:2 in comparison to the calculated value of 15:2. However, over 4 chips compound **50** has an average C:N ratio of 36:2 which does not compare with

the expected value. Compound **19** was deposited using two methods as illustrated in Table 2-1. The free carbene method was used on four chips with an average C:N elemental ratio of 29:2 which is comparable with the calculated value of 25:2. Only one chip was made by the third deposition method resulting in a C:N ratio of 75:2 suggesting a large excess of carbon on the surface. Finally, compounds **31**, **34**, **35**, and **37** were deposited using either the free carbene, internal base, or base free methods as depicted in Table 2-2. None of the surfaces from these compounds were comparable to the calculated C:N elemental ratio of 15:2. The results from two chips modified with **31** using the first deposition method had an average C:N ratio of 26:2. Compound **37** and **34** was deposited by the third method and resulted in a similar C:N ratio of 25:2 and 29:2. Compounds **35** was deposited by the second method with C:N ratio of 27:2.

The source of the increased carbon on the gold substrates is unclear. However, the free carbene method shows reduced contamination, where only C-C adventitious carbon is present. Additionally, the combination between the counterion of the carbene precursor and method for SAM formation which produces an elemental ratio comparable with the expected value appears to be individualized to each molecule. No success was had with any of the N,N'-diisopropylnaphthalene[2,3-*d*]imidazolium salts and evidence of decomposition of **50** upon monolayer formation was present. Monolayers were successfully formed via free carbene deposition of **19**, and base free deposition of **49**.

Moving forward, more depositions of the synthesized molecules need to be completed in order to determine which method and counterion produces the best monolayers for each NHC compound. Specifically, the free carbene method for these molecules should be further investigated with **19** showing the most promise for this method. Compound **49** shows the most promise for the base free method and should be studied further. Additionally, high quality STM images of N,N'-diisopropyl[2,3-*d*]imidazolylidene-1,4-dionenaphthalene modified surfaces will provide insight into the packing of the molecule on the surface. Imaging a SAM of compound **19** by STM can confirm whether a chiral surface has been created. In addition, using a SAM of compound **19** on a gold surface for heterogenous enantioselective catalysis is conceivable. Performing electrochemical experiments of **49** which produced a

more promising monolayer as determined from the XPS results, may provide more insight into the redox activity of the molecule. Alternatively altering the quinone position on N,N'-diisopropyl[2,3-*d*]imidazol-1,4-dionenaphthalene salts may allow easier access to the redox active site on the molecule. Further studies of the molecules synthesized in this thesis can potentially lead to furthering the field of materials chemistry.

3.2 References

1. Herrmann, W. A. & Köcher, C. N-Heterocyclic Carbenes. *Angewandte Chemie International Edition in English* **36**, 2162–2187 (1997).
2. Herrmann, W. A. N-Heterocyclic Carbenes: A New Concept in Organometallic Catalysis. *Angewandte Chemie International Edition* **41**, 1290–1309 (2002).
3. Bourissou, D., Guerret, O., Gabbaï, F. P. & Bertrand, G. Stable Carbenes. *Chemical Reviews* **100**, 39–92 (2000).
4. Crudden, C. M. *et al.* Ultra stable self-assembled monolayers of N-heterocyclic carbenes on gold. *Nature Chemistry* **6**, 409–414 (2014).
5. Man, R. W. Y. *et al.* Ultrastable Gold Nanoparticles Modified by Bidentate *N* -Heterocyclic Carbene Ligands. *Journal of the American Chemical Society* **140**, 1576–1579 (2018).
6. Crudden, C. M. *et al.* Simple direct formation of self-assembled N-heterocyclic carbene monolayers on gold and their application in biosensing. *Nature Communications* **7**, 12654 (2016).

Chapter 4

Experimental

General Experimental Considerations. All manipulations were carried out in benchtop conditions unless otherwise specified. Nuclear magnetic resonance (NMR) spectroscopy data were acquired on a Bruker AVANCE NMR spectrometer ranging from 300-700 MHz and processed using MestReNova 11.0.4-18998. X-ray photoelectron spectroscopy (XPS) was carried out on a KRATOS AXIS Nova spectrometer with all data being processed in CasaXPS 2.3.18PR1.0. XPS spectra was calibrated to Au 4F peak unless otherwise specified. HPLC grade acetonitrile and methanol were used and purchased from Fisher Chemical™. Amberlyst ion exchange resin was purchased from Alfa Aesar. All other chemicals are standard reagent grade from Millipore Sigma.

4.1 Resin Preparation

Hydrogen Carbonate Resin The hydrogen bicarbonate resin was prepared as described by Crudden *et al*.[1] Amberlyst A26 hydroxide resin (20 g) was suspended in 20 mL of Milli-Q water with carbon dioxide being bubbled through the solution for 30 minutes or until the pH of the solution measured 6 using a pH strip. A qualitative test of the resin was done by adding the resin (0.2 mL, 0.2 mmol) to potassium iodide (0.2 mL, 0.4 M). An excess of 1 M silver nitrate was added to the solution. If a brown or off-white precipitate formed the resin needed more time bubbling with carbon dioxide, however, if it was white, the resin was deemed to be ready.

Tetrafluoroborate Resin Amberlyst A26 hydroxide resin (10 g) was suspended in a 1:1:0.1 solution of Milli-Q water (48 mL), HPLC grade methanol (48 mL), and 48 wt. % in water tetrafluoroboric acid (4mL) and stirred until a pH of 1 had been reached monitoring with a pH strip. The resin beads turned a peachy orange at about pH 2 and a pale yellow at pH 1. If the original volume of acid solution was not enough to

turn the resulting solution to pH 1, more was added in the appropriate ratio. Once a pH of 1 had been reached, the resin was ready to be used.

4.2 Surface Functionalization

Gold on Mica Surface Preparation. The gold on mica chips were cleaned as described by Crudden *et al*.[1] The gold chips were cleaned by washing 3 x 2 mL with HPLC grade methanol, followed by drying under a stream of argon after each rinsing. The chips were then cleaned with a plasma generated from ambient air at medium RF level and a pressure kept between 300 and 500 mTorr for 1 minute. Immediately after the plasma etch, the chips were used for surface functionalization.

Gold on Silica Preparation. Gold on silica chips were cleaned as described by Crudden *et al*.[1] 150 oxidation and reduction cycles were carried out in 5 mM/ 5 mM $Fe(CN)_6^{3+/4+}$. The chip was then thoroughly rinsed with Milli-Q water 3 times drying with a stream of argon in between. It was then directly used for surface functionalization.

***General Preparation for Free Carbenes and Self Assembly on Gold*.** The free carbene was prepared as described by Crudden *et al*.[2] In a glove box, a 10 mM solution was prepared by dissolving 0.02 mmol of the imidazolium salt in 2 mL of anhydrous THF in a 20 mL vial with a stir bar. In a separate 20 mL vial, potassium tert-butoxide (2.2 mg, 0.02 mmol) was dissolved in 1.4 mL of anhydrous THF. Both solutions were cooled to -40°C in the freezer of the glovebox. The base was added to the imidazolium solution drop wise, and the resulting solution was left to stir for 1 hour. The THF was evaporated *in vacuo*. Toluene was added to the solid to create a 10 mM solution and filtered through a celite plug directly into a vial containing the gold surface. The chip was left in solution for 24 hours. The chip was then rinsed with anhydrous toluene, then 3 x 2 mL anhydrous methanol, drying with a stream of argon in between.

General Procedure for Hydrogen Carbonate Carbene Deposition. The deposition of imidazolium and benzimidazolium hydrogen carbonates proceeded as described by Crudden *et al*.[1] A 2 mM solution of the desired imidazole in anhydrous methanol was created. A freshly cleaned gold chip was immediately added to the solution post cleaning and left for 24 hours. The chip was then cleaned with 3 x 2 mL of anhydrous methanol, drying under a stream of argon between each rinsing.

4.3 Synthetic Procedures

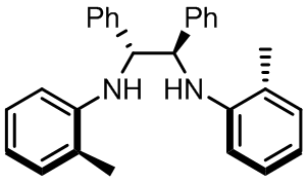

N,N'-ditolyl-(R,R)-diphenylethylenediamine (**18**). Compound **18** was synthesized as described by Seiders *et al*.[3] In a glovebox, palladium acetate (26 mg, 0.1 mmol), *rac*-BINAP (141 mg, 0.2 mmol), and sodium *t*-butoxide (0.7 g, 7.2 mmol) were added to deoxygenated toluene (31 ml) in a Schlenk flask and stirred for 20 min. (*R,R*)-Diphenylethylenediamine (0.5 g, 2.3 mmol) and 2-bromotoluene (0.6 mL, 0.9 g, 5 mmol) were added to the solution and it was removed from the glovebox. Under a stream of argon, the solution was heated at 100 °C for 14 h. The solution was cooled to ambient temperature and diluted with reagent grade hexanes (92 mL), then filtered through a silica plug. The silica was washed with dichloromethane to elute the product. The volatiles were removed *in vacuo* with a yield of 87% (0.9 g). NMR data were consistent with literature values.

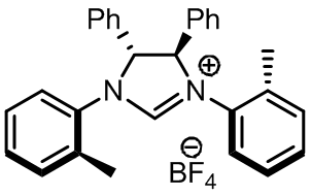

N,N'-ditolyl-4,5(R,R)-diphenylimidazolium tetrafluroborate (**19**). Compound **19** was synthesized as described by Seiders *et al*.[3] A 25 mL round bottom flask was charged with compound **18** (46 mg, 0.1 mmol), ammonium tetrafluoroborate (15 mg, 0.1 mmol), and triethylorthoformate (0.17 mL). It was then heated to 120 °C and left to stir for 5 hours. The product precipitated as the solution cooled to room temperature and was removed by filtration. The solid was washed with diethyl ether until the washings were clear. The solid was then dissolved in dichloromethane and filtered. The volatiles were removed *in*

vacuo yielding an off white solid with a yield of 94% (58 mg). NMR data were consistent with literature values.

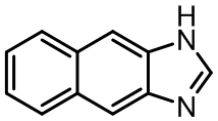

1H-naphth[2,3-d]imidazole (**27**). Compound **27** was synthesized as described by Grobler *et al*.[4] 2,3-Diaminonaphthalene (1 g, 6.3 mmol) dissolved in formic acid (20 mL) were added to a 50 mL round bottom flask. Under a stream of argon, the mixture was heated to reflux and left to react for 36 hours. After cooling to room temperature, the contents of the flask were **slowly** added to saturated sodium carbonate (200 mL). The precipitated solid was collected by filtration and washed with water until the washings were clear. The solid was dried under vacuum yielding a brown sold with a yield of 73% (0.8 mg). NMR data were comparable with literature.

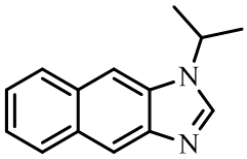

1-isopropylnaphth[2,3-d]imidazole (**29**). Compound **27** (0.8 mg, 4.6 mmol), 2-bromopropane (1.3 mL, 1.7 g, 13.8 mmol), and cesium carbonate (2.2 g, 6.8 mmol) were added to a 50 mL round bottom flask with 30 mL of HPLC grade acetonitrile. The mixture was brought to reflux and left to stir for 14 h under a stream of argon. After cooling to room temperature, the solvent was removed *in vacuo*. The solid was dissolved in dichloromethane and filtered through celite. The volatiles were removed *in vacuo* resulting in a light brown powder with a yield of 94% (0.9 mg). ^{1}H NMR (400 MHz, $CDCl_3$) δ 8.30 (s, 1H, N-C*H*=N), 8.19 (s, 1H, Ar-*H*), 8.01 (d, J = 7.98 Hz, 1H, Ar-*H*), 7.95 (d, J = 7.96 Hz, 1H, Ar-*H*), 7.82 (s, 1H, Ar-*H*), 7.42, (m, 2H, Ar-*H*), 4.75 (sept, J = 6.67 Hz, 1H, NC*H*^{i}Pr), 1.70, (d, J = 6.76 Hz, 6H, CH_3^{i}Pr). ^{13}C NMR (101 MHz, $CDCl_3$) δ 144.25 (s, N_2*C*H), 133.90 (s, C_q), 130.31 (s, C_q), 130.06 (s, C_q), 128.49 (s, C_{Ar}), 127.48 (s, C_{Ar}), 124.41 (s, C_{Ar}), 123.44 (s, C_{Ar}), 117.31 (s, C_q), 105.9 (s, C_{Ar}), 47.71 (s, *C*H^{i}Pr), 22.31 (s, *C*H_3^{i}Pr).

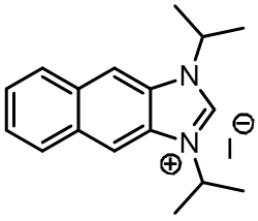

N,N'-diisopropyl[2,3-d]imidazolium iodide (**31**). A mixture of compound **29** (0.3 g, 1.5 mmol) and 2-iodopropane (35 mL) were added to a 50 mL round bottom flask and heated at reflux for 14 h. The solvent was removed *in vacuo* and the resulting solid was triturated with ether resulting in an off-white solid with a yield of 92% (0.5 g). ^{1}H NMR (499 MHz, MeOD) δ 8.59, (s, 2H, Ar-*H*), 8.21 (dd, J = 3.26, 6.35 Hz, 2H, Ar-*H*),

7.66, (dd, J = 3.20, 6.49 Hz, 2H, Ar-*H*), 5.19, (sept, J = 6.64 Hz, 1H, NC*H*^{i}Pr), 1.82, (d, J = 6.73, 12H, C*H*$_3$^{i}Pr). Note the NC*H*N proton is not present due to the rapid exchange with methanol. ^{13}C NMR (101 MHz, MeOD) δ 133.15 (s, C_q), 131.50 (s, C_q), 129.49, (s, C_{Ar}), 128.01, (s, C_{Ar}), 112.56, (s, C_{Ar}), 52.98, (s, *C*H^{i}Pr), 22.04 (s, *C*H$_3$^{i}Pr).

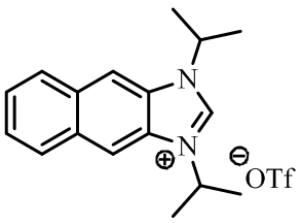

N,N'-diisopropyl[2,3-d]imidazolium triflate (**34**). Anhydrous isopropanol (0.55 mL, 0.4 g, 7.2 mmol) and anhydrous pyridine (0.58 mL, 0.6 g, 7.2 mmol) were added to an oven dried Schlenk flask with 12 mL of dry dichloromethane under a stream of argon. At -20°C, triflic anhydride (1.2 mL, 2.0 g, 7.2 mmol) was slowly added to the stirring solution and a precipitate formed. The reaction was stirred at -20°C for 30 minutes, then allowed to warm to room temperature and stirred for an additional 30 minutes. Dry pentane (12 mL) was added to further precipitate the salts. The resulting suspension was filtered through a celite plug into an oven dried Schlenk flask containing compound **29** (0.7 g, 3.1 mmol) and 12 mL of dry dichloromethane at -10°C under a stream of argon. This was left to stir for 10 minutes at -10°C, then room temperature for 14 h. The solution was quenched with a saturated sodium bicarbonate solution (15 mL), and the aqueous layer extracted with dichloromethane until the organic layer was clear. The solution was dried over sodium sulfate, then the volatiles were removed *in vacuo* and the resultant solid was triturated with ether, resulting in an off-white product (0.5 g, 37% yield). Another method performed was the same as above up to the filtration. However, the filtration was performed at -20°C and left to stir for 30 minutes. Then the reaction was brought to reflux and left for 14 h. Once cooled the precipitate was filtered through a glass frit and washed with dichloromethane. The solid was triturated in ether and dried under vacuum. The filtrate was worked up as previously described yielding additional product. This produced a combined yield of 74% (1.1 g). ^{1}H NMR (700 MHz, $CDCl_3$) δ 9.99 (s, 1H, N-C*H*=N), 8.22 (s, 2H, Ar-*H*), 8.07, (dd, J = 3.18, 6.21 Hz, 2H, Ar-*H*), 7.65, (dd, J = 3.03, 6.41Hz, 2H, Ar-*H*), 5.10, (sept, J = 6.80 Hz, 1H C*H*^{i}Pr), 1.86, (d, J = 6.79 Hz, 12H, C*H*$_3$^{i}Pr). ^{13}C NMR (101 MHz, $CDCl_3$) δ 143.27 (s, N_2*C*H), 131.60, (s, C_q),

129.95 (s, C_q), 128.40 (s, C_{Ar}), 127.56 (s, C_{Ar}), 111.54 (s, C_{Ar}), 52.71 (s, *C*H^{i}Pr), 21.82 (*C*H$_3$^{i}Pr). ^{19}F NMR (376 MHz, $CDCl_3$) δ -78.29.

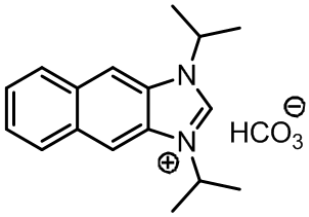

N,N'-diisopropyl[2,3,-d]imidazolium hydrogen bicarbonate (**35**). 2 mL (1.5 mequiv) of hydrogen bicarbonate resin suspended in Milli-Q water was measured out in a graduated cylinder, then transferred a 20 mL scintillation vial. After settling, the water was removed by decantation and the resin was washed with HPLC grade methanol (3 x 2 mL). Compound **31** or **34** , 0.2 g (0.5 mmol) was dissolved in 2 mL HPLC methanol and added to the resin. The mixture was stirred at 0°C for 30 minutes. The solution was filtered through a pipette plugged with cotton into another 20 mL vial. The remaining resin was washed with methanol until the solvent was clear. The volatiles were removed under a stream of air, then triturated with ether yielding an off-white solid. The process was repeated with the same sample until there was no fluorine in the ^{19}F NMR if the starting reagent was **34**, or no iodine in the powder XPS if the starting reagent was **31**. The resulting white solid had a yield of 34% (54.4 mg). ^{1}H and ^{13}C NMR spectra are identical to compound **31**.

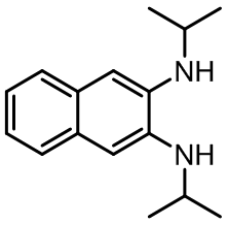

N,N'-diisopropyl-2,3-diaminonaphthalene (**36**). 2,3-Diaminonaphthalene (0.13 g, 0.8 mmol), cesium carbonate (0.2 g, 0.6 mmol) and 2-iodopropane (0.3 mL, 0.6 mg, 3.3 mmol) were added to a 25 mL round bottom flask with 4 mL of HPLC grade acetonitrile. The reaction was stirred at reflux for 12 hours. After cooling to room temperature, the solvent was removed *in vacuo* the resulting solid was dissolved in dichloromethane and filtered through Celite. The filtrate was dried over sodium sulfate and the volatiles were removed *in vacuo*. The resulting solid was purified by silica gel column chromatography using an eluent of 2:1 dichloromethane : hexanes. The second eluent to come off the column was pure product (63.4 mg, 32% yield). ^{1}H NMR (400 MHz, $CDCl_3$) δ 7.59 (dd, J = 3.31, 6.04 Hz, 2H, Ar-*H*), 7.20 (dd, J = 3.24, 6.12 Hz,

2H, Ar-*H*), 6.91 (s, 2H, Ar-*H*), 3.72 (sept, J = 6.15 Hz, 2H, C*H*^{i}Pr), 1.31 (d, J = 6.23 Hz, 12H, C*H*$_3$^{i}Pr). ^{13}C NMR data were not collected.

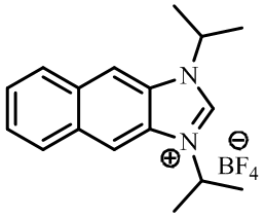

N,N'-diisopropyl[2,3,-d]imidazolium tetrafluoroborate (**37**). Ammonium tetrafluoroborate (5.6 mg, 0.05 mmol), triethylorthoformate (0.6 mL), and compound **36** (63.4 mg, 0.3 mmol) were added to a 15 mL round bottom flask and heated to 150°C for 20 hours. After cooling to room temperature, the precipitate was filtered and washed with ether until the washings ran clear. The solid was then dissolved in dichloromethane and filtered through a glass frit. The volatiles were removed *in vacuo* resulting in an off white solid as pure product. A yield of 35% (31.8 mg) was obtained. The ^{1}H and ^{13}C NMR spectra data were identical to compound **34**. ^{19}F NMR (376 MHz, $CDCl_3$) δ -151.65.

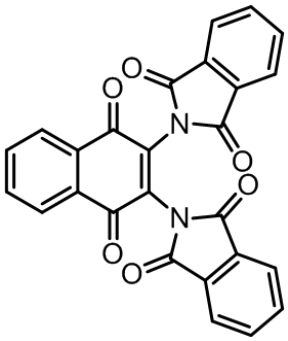

2,3-diphthalimido-1,4-naphthoquinone (**44**). Synthesized as described by Chesneau *et al*.[5] Potassium phthalimide (17.1 g, 92.5 mmol) was dried under vacuum then added to a 50 mL round bottom flask along with 2,3-dichloro-1,4-naphthoquinone (5 g, 22 mmol) in 30 mL of HPLC grade acetonitrile. The solution was heated at reflux for 3 hours, then filtered while hot. The precipitate was sequentially washed with acetonitrile, water, then methanol each until the filtrate runs clear. After washing the yellow solid was dried under vacuum at 50°C with a yield of 87% (8.6 g). NMR data were comparable to literature values.

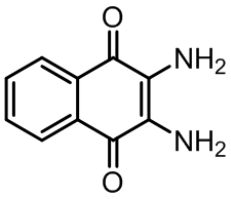

2,3-diamino-1,4-naphthoquinone (**45**). Synthesized as described by Chesneau *et al*.[5] Compound **44** (8.6 g, 19.1 mmol) was added to a 1 L round bottom flask with 600 mL of distilled water. A 64% solution of hydrazine hydrate (86 mL, excess) was added and the solution was brought to 70°C for 3 hours. Once cooled to room temperature the precipitate was filtered then washed with copious amounts of water. The resulting dark purple solid was dried under vacuum at 100°C with a yield of 95% (3.4 g). NMR data were consistent with literature values.

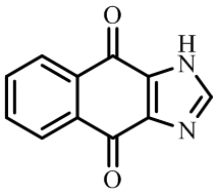

1H-naphtho[2,3-d]imidazole-4,9-dione (**46**). Synthesized as described by Lee *et al*.[6] Compound **45** (3.4 g, 18.2 mmol) was added to a 100 mL round bottom flask, with reagent grade formic acid (62 mL, 75.6 g, 1.6 mol) and 25 mL of distilled water. The solution was heated at reflux for 5 hours. After cooling to room temperature, the solution pH was brought to 9 measuring with a pH strip using 30% ammonium hydroxide. The resulting precipitate was removed by filtration and washed with water until the filtrate ran clear. The resulting dark yellow powder was dried under vacuum with a yield of 54% (2 g). NMR data were consistent with literature values.

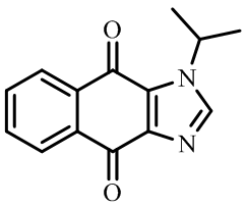

1-isopropylnaphtho[2,3-d]imidazole-4,9-dione (**47**). Compound **46** (2.0 g, 9.9 mmol), cesium carbonate (4.9 g, 15 mmol), and 2-bromopropane (2.8 mL, 3.7 g, 29.8 mmol) were added to a 25 mL round bottom flask with 6 mL HPLC grade acetonitrile. The solution was heated at reflux over-night. After cooling to room temperature, the solvent was evaporated *in vacuo*. The solid was dissolved in dichloromethane then filtered through Celite. The organics were dried over sodium sulfate and evaporated *in vacuo* resulting in a dark brown solid with a 75% yield (1.8 g). ^{1}H NMR (500 MHz, $CDCl_3$) δ 8.29 (m, 1H, Ar-*H*), 8.19 (m, 1H, Ar-*H*), 8.01 (s, 1H, N-C*H*=N), 7.77 (m, 2H, Ar-*H*), 5.40 (sept, J = 6.86 Hz, 1H, C*H*^{i}Pr), 1.65 (d, J = 6.76 Hz, 6H, C*H*$_3$^{i}Pr). ^{13}C NMR data were not collected.

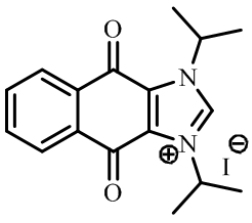

N,N'-diisopropylnaphtho[2,3-d]imidazolium-4,9-dione iodide (**48**). Compound **47** (0.35 g, 1.5 mmol) and 2-iodopropane (12 mL) were added to a 25 mL round bottom flask and heated at reflux for 48 hours. Once cooled to room temperature the precipitate was filtered through a glass frit resulting in a red solid dried *in vacuo* with a yield of 53% (0.31 g). ^{1}H NMR (400 MHz, CD_3CN) δ 9.20 (s, 1H, N-C*H*=N), 8.26 (dt, J = 3.47 5.73 Hz, 2H, Ar-*H*), 7.96 (dq, J = 3.77, 7.00 Hz, 2H, Ar-*H*), 5.54 (sept, J = 6.77, 2H, C*H*^{i}Pr), 1.68 (d, J = 6.73 Hz, 12H, C*H*$_3$^{i}Pr). ^{13}C NMR (101 MHz, MeOD) δ 176.37 (s, *C*=O), 136.28 (s, C_q), 133.45 (s, C_q), 132.59 (s, C_{Ar}), 128.35 (s, C_{Ar}), 55.54 (s, C*H*^{i}Pr), 22.55 (s, C*H*$_3$^{i}Pr).

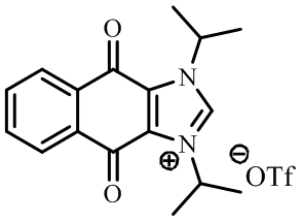

N,N'-diisopropylnaphtho[2,3-d]imidazolium-4,9-dione triflate (**50**). Anhydrous isopropanol (0.2 mL, 0.15 g, 2.5 mmol) and anhydrous pyridine (0.2 mL, 0.2 g, 2.5 mmol) were added to an oven dried Schlenk flask with 5 mL of dry dichloromethane under a stream of argon. After cooling to -20°C, triflic anhydride (0.4 mL, 0.69 g, 2.42 mmol) was slowly added to the stirring solution and a precipitate formed. The reaction was stirred at -20°C for 30 minutes, then allowed to warm to room temperature and stirred for an additional 30 minutes. Dry pentane (5 mL) was added to further precipitate the salts. The resulting suspension was filtered through a Celite plug into an oven dried Schlenck flask containing compound **47** (0.2 g, 0.8 mmol) and 5 mL of dry dichloromethane at -20°C under a stream of argon. This was left to stir for 10 minutes at -10°C, then heated at reflux for 14 h. The filtrate was then quenched with a saturated sodium bicarbonate solution (7 mL), and the aqueous layer extracted with dichloromethane until the organic layer was clear. The organics were dried over sodium sulfate, filtered, and the volatiles were removed *in vacuo* then triturated with ether, resulting in light brown product. The total yield was 10% (53.3 mg). A one-time trial of a slightly different work up was also carried out, where the room temperature solution was filtered through a glass frit and washed with dichloromethane. The resulting light brown solid was collected and triturated with ether producing pure product. The filtrate was worked up as described above resulting in a combined yield of 30% (0.91 g). ^{1}H NMR (600 MHz, CD_3CN) δ 8.29 (dd, J = 3.35, 5.53 Hz, 2H, Ar-*H*), 7.96 (dd, J = 3.27, 5.44 Hz, 2H, Ar-*H*), 5.64 (sept, J = 6.98 Hz, 2H, C*H*^{i}Pr), 1.72 (d, J = 6.75 Hz, 12H, C*H*$_3$^{i}Pr). ^{13}C NMR spectrum was taken in MeOD and was found to be identical to compound **48**. ^{19}F NMR (376 MHz, $CDCl_3$) δ -79.47.

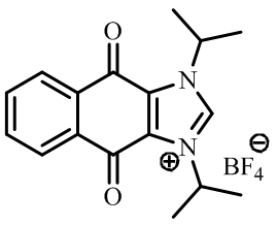

N,N'-diisopropylnaphtho[2,3-d]imidazolium-4,9-dione tetrafluoroborate (**48**). 1 mL (3 equiv) of tetrafluoroborate resin suspended in a methanol Milli-Q water mixture was measured out in a graduated cylinder, then transferred a 20 mL screw cap vial. The resin was allowed to settle to the bottom then the supernatant was decanted off and the resin was washed with HPLC grade methanol (3 x 2 mL). Compound **48** (66.3 mg, 0.2

mmol) was dissolved in 2 mL HPLC methanol and added to the resin. The mixture was stirred at 40°C for 30 minutes. The solution was filtered through a pipette plugged with cotton into another 20 mL vial. The remaining resin was washed with methanol until the solvent was clear. The volatiles were removed under a stream of air, then triturated with ether yielding an off white solid. Upon XPS analysis, iodine was still present, so the process was repeated with the same sample for an additional 30 minutes at 40°C. The resulting solid was off white with an 87% yield (52.2 mg). ^{1}H and ^{13}C NMR spectra were found to be identical to compound **48**. ^{19}F NMR (376 MHz, $CDCl_3$) δ -151.77.

4.4 References

1. Crudden, C. M. *et al.* Simple direct formation of self-assembled N-heterocyclic carbene monolayers on gold and their application in biosensing. *Nature Communications* **7**, 12654 (2016).
2. Crudden, C. M. *et al.* Ultra stable self-assembled monolayers of N-heterocyclic carbenes on gold. *Nature Chemistry* **6**, 409–414 (2014).
3. Seiders, T. J., Ward, D. W. & Grubbs, R. H. Enantioselective Ruthenium-Catalyzed Ring-Closing Metathesis. *Organic Letters* **3**, 3225–3228 (2001).
4. Grobler, I., Smith, V. J., Bhatt, P. M., Herbert, S. A. & Barbour, L. J. Tunable Anisotropic Thermal Expansion of a Porous Zinc(II) Metal–Organic Framework. *Journal of the American Chemical Society* **135**, 6411–6414 (2013).
5. Chesneau, B., Hardouin-Lerouge, M. & Hudhomme, P. A Fused Donor−Acceptor System Based on an Extended Tetrathiafulvalene and a Ruthenium Complex of Dipyridoquinoxaline. *Organic Letters* **12**, 4868–4871 (2010).
6. Lee, J., Kim, H. & Park, M. J. Long-Life, High-Rate Lithium-Organic Batteries Based on Naphthoquinone Derivatives. *Chemistry of Materials* **28**, 2408–2416 (2016).

Appendix: Selected NMR and XPS Spectra

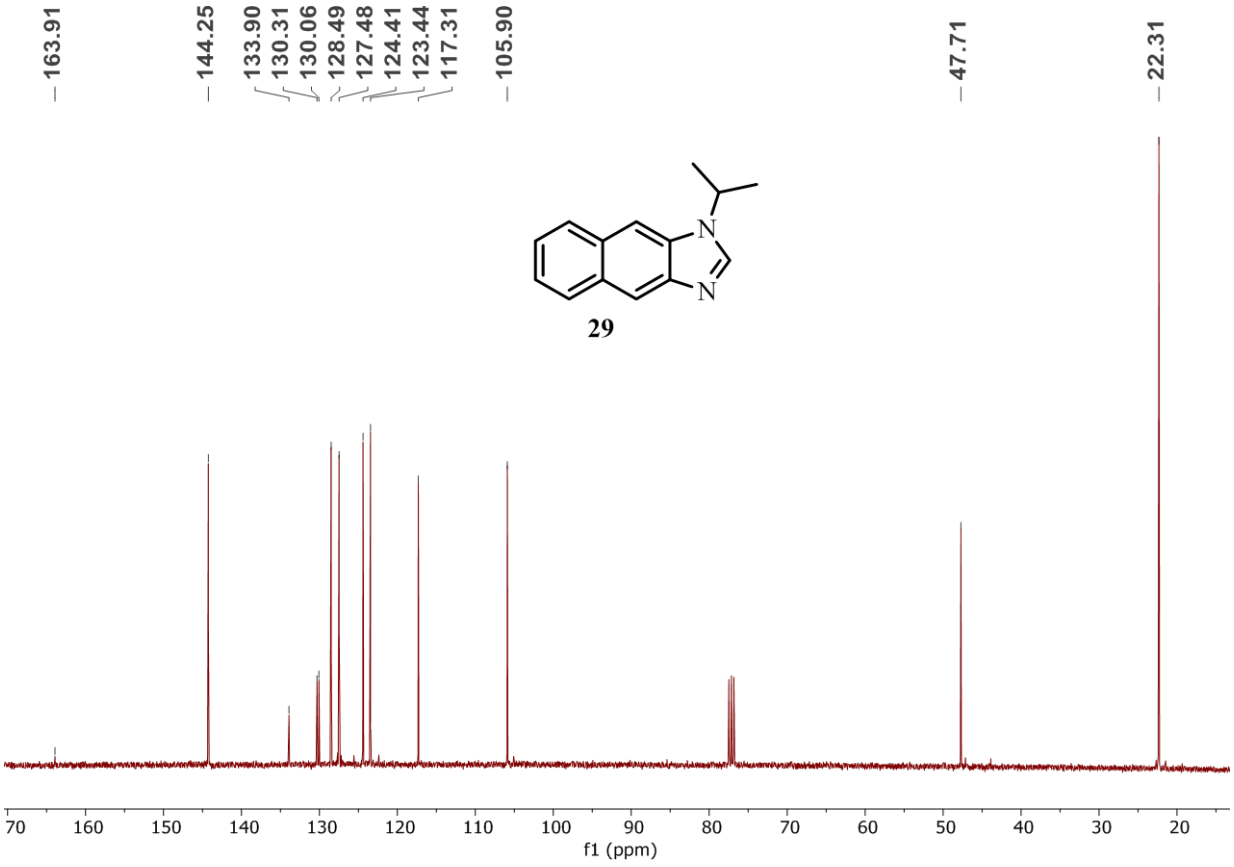

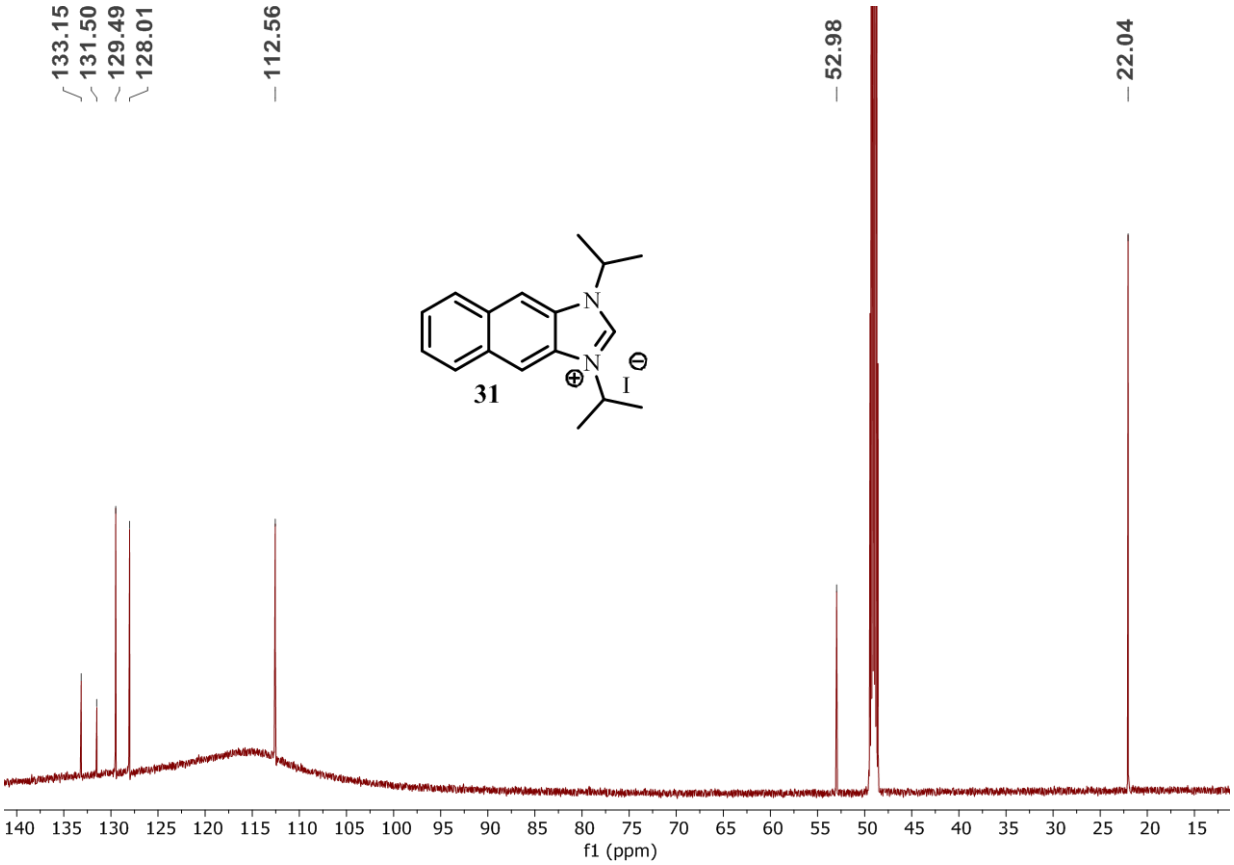
133.15
131.50
129.49
128.01
112.56
52.98
22.04
31
140 135 130 125 120 115 110 105 100 95 90 85 80 75 70 65 60 55 50 45 40 35 30 25 20 15
f1 (ppm)

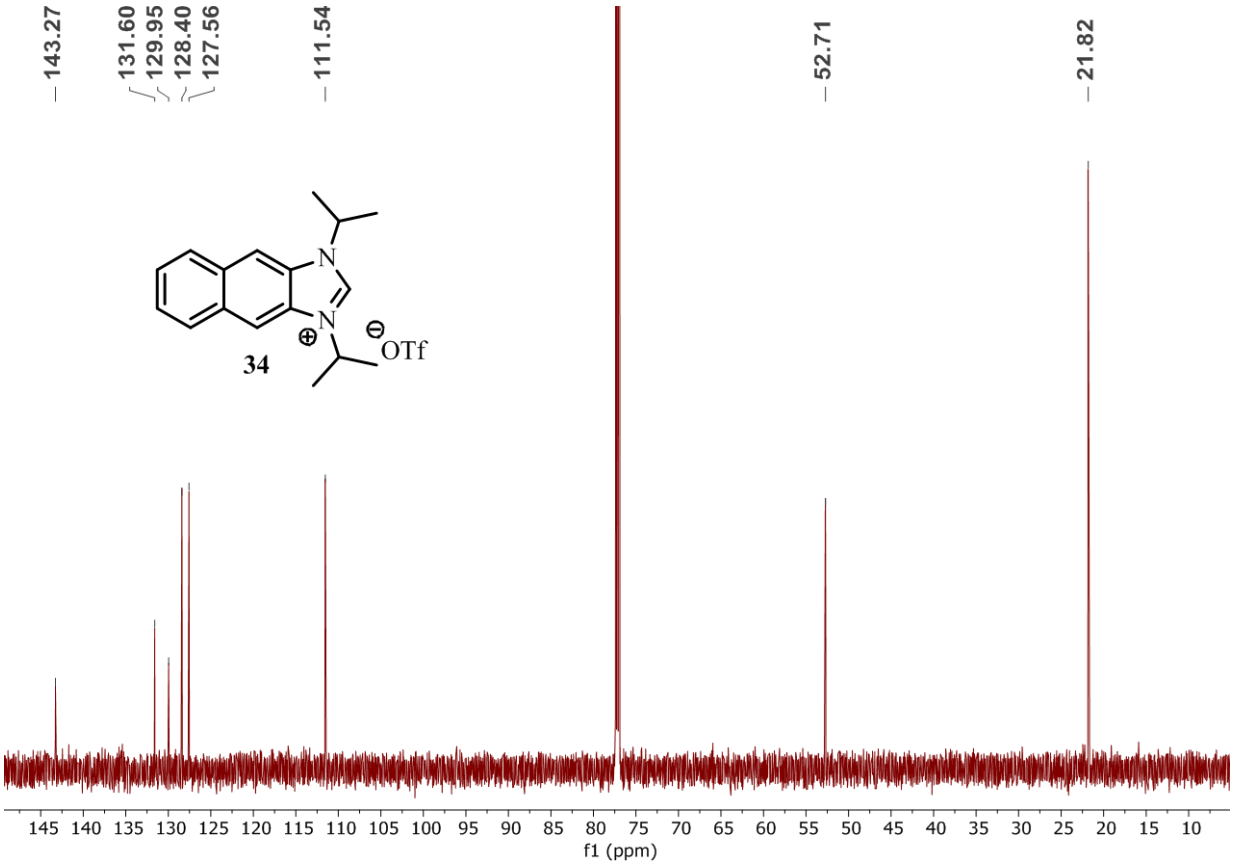
143.27
131.60
129.95
128.40
127.56
111.54
52.71
21.82
N
N
OTf
34
145 140 135 130 125 120 115 110 105 100 95 90 85 80 75 70 65 60 55 50 45 40 35 30 25 20 15 10
f1 (ppm)

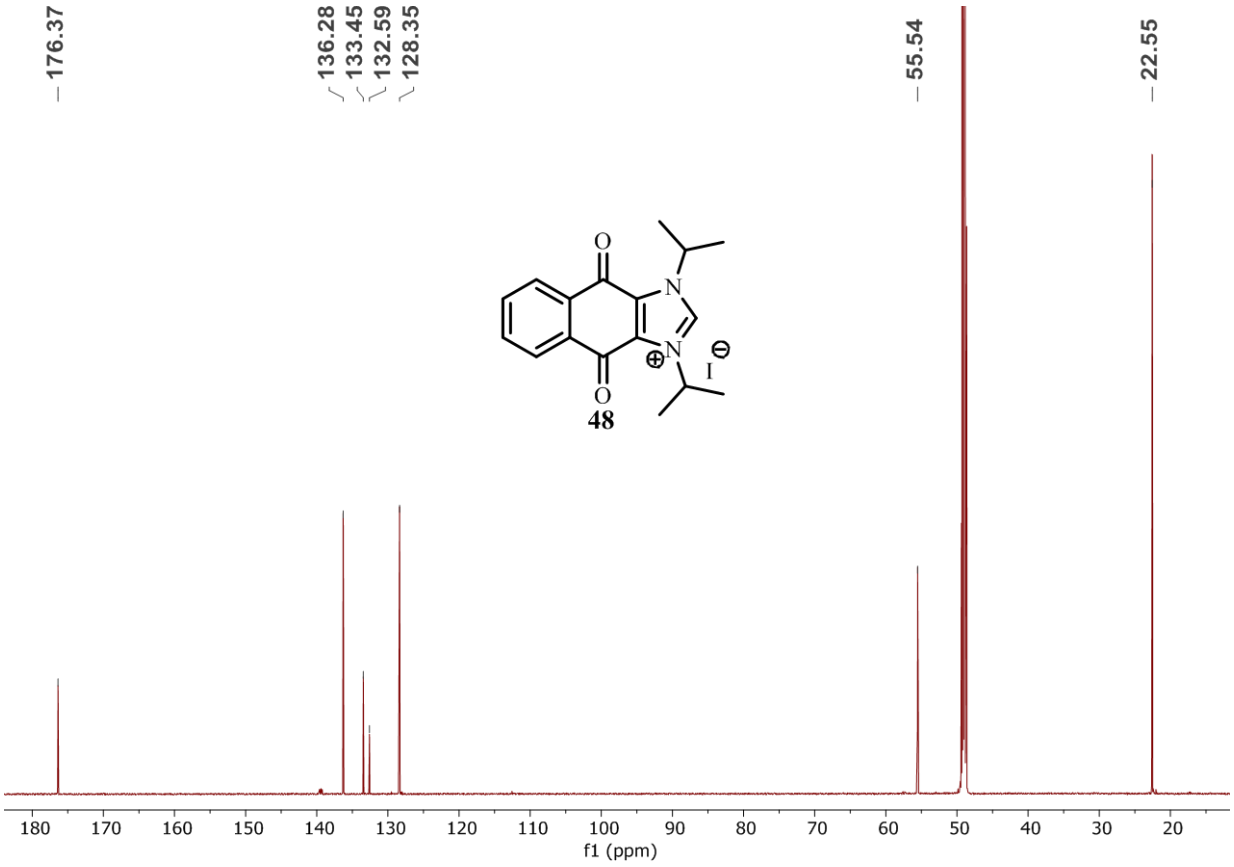

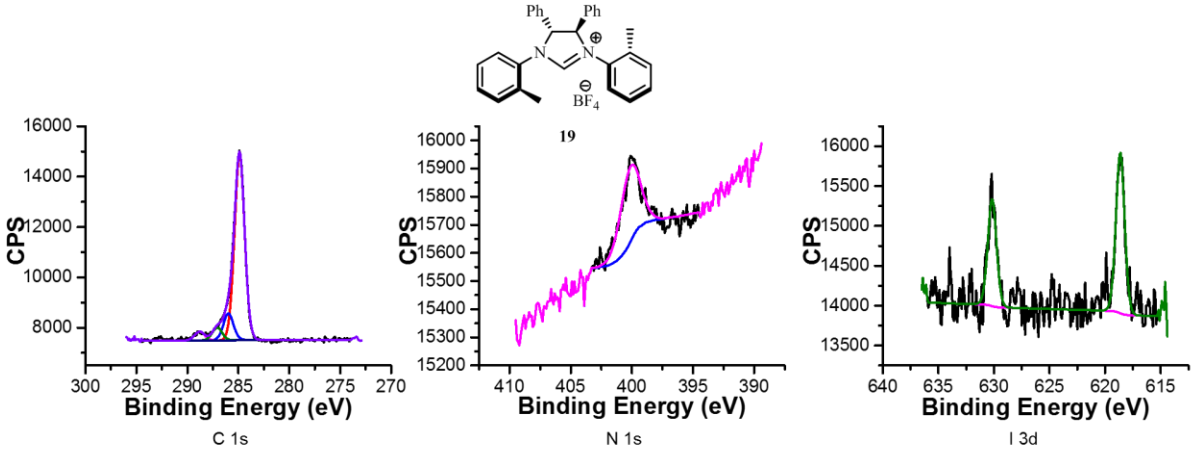

Base Free Deposition

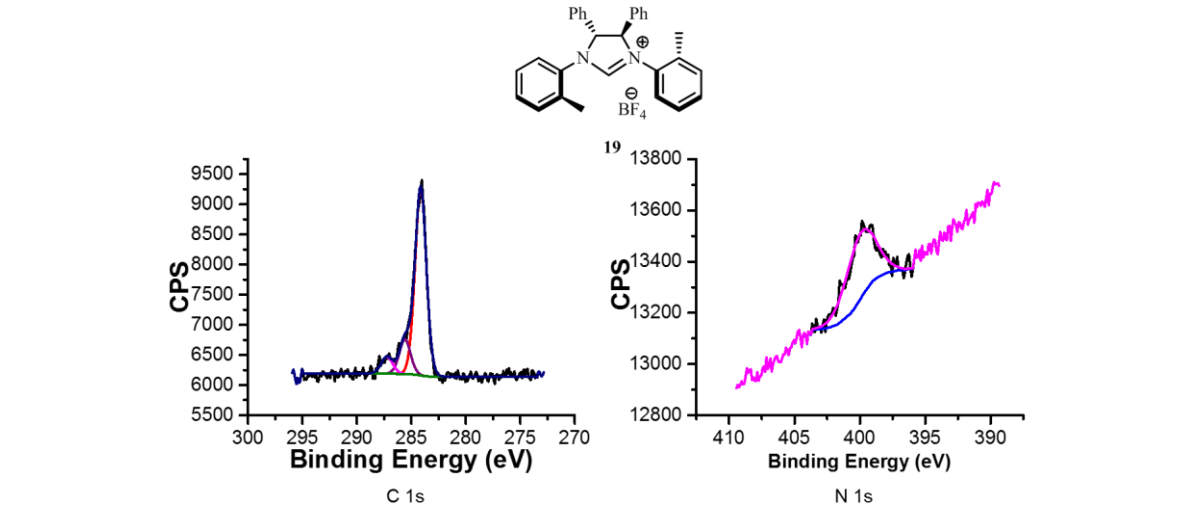

Free Carbene Deposition

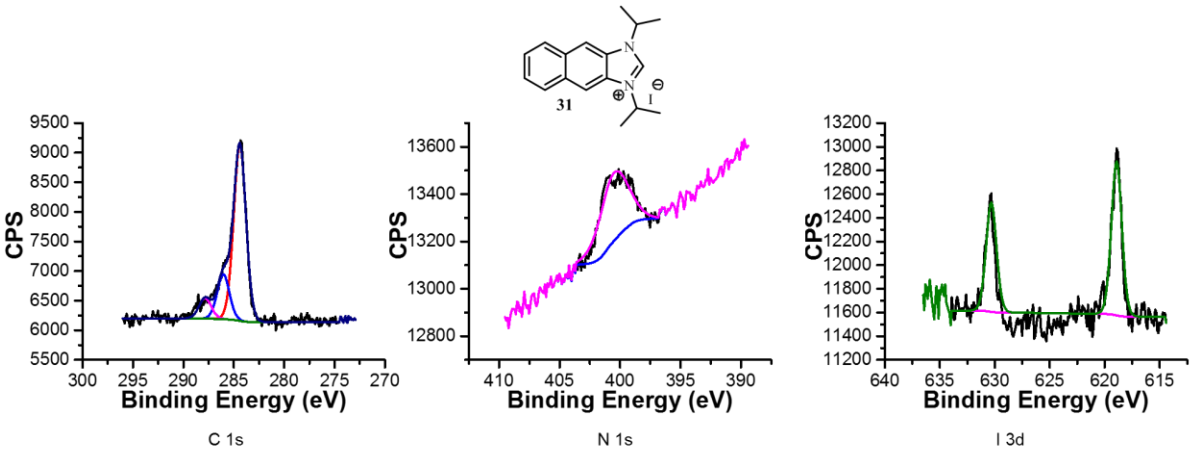

Free Carbene Deposition

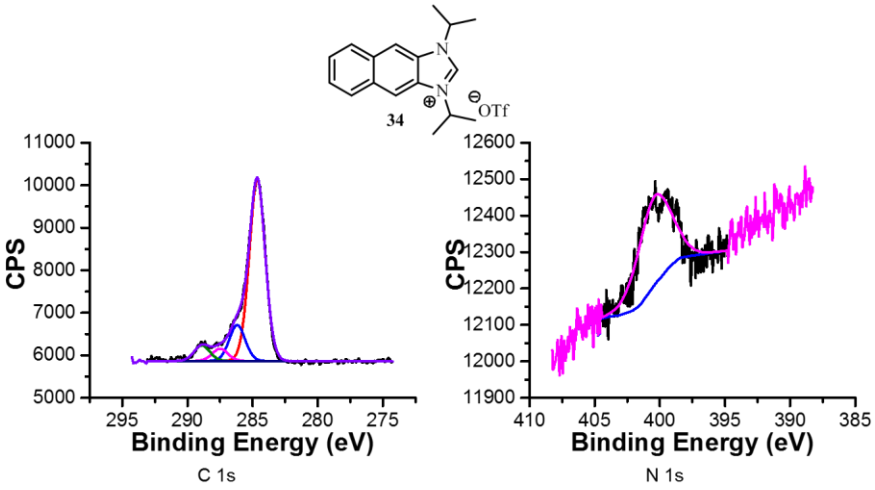

Base Free Deposition

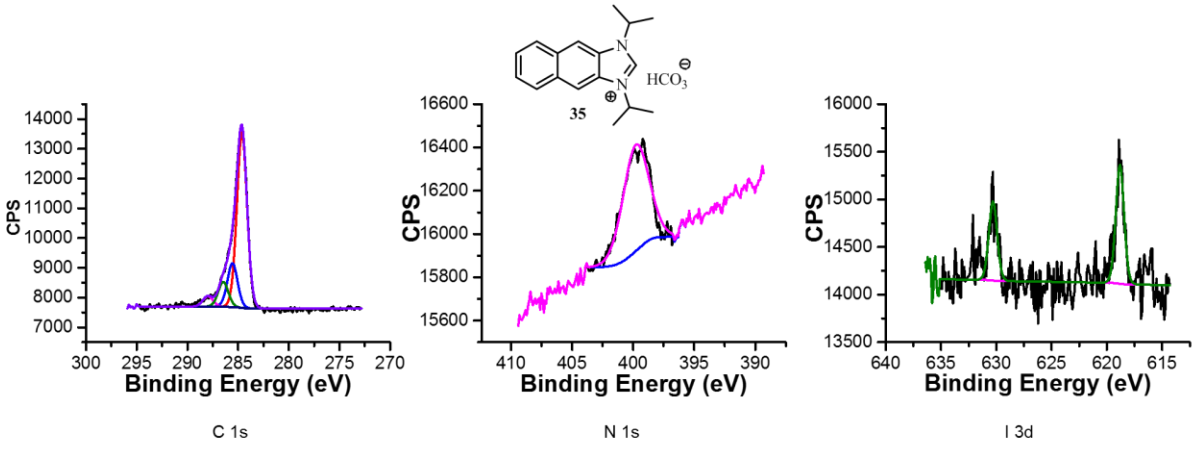

Base Free Deposition

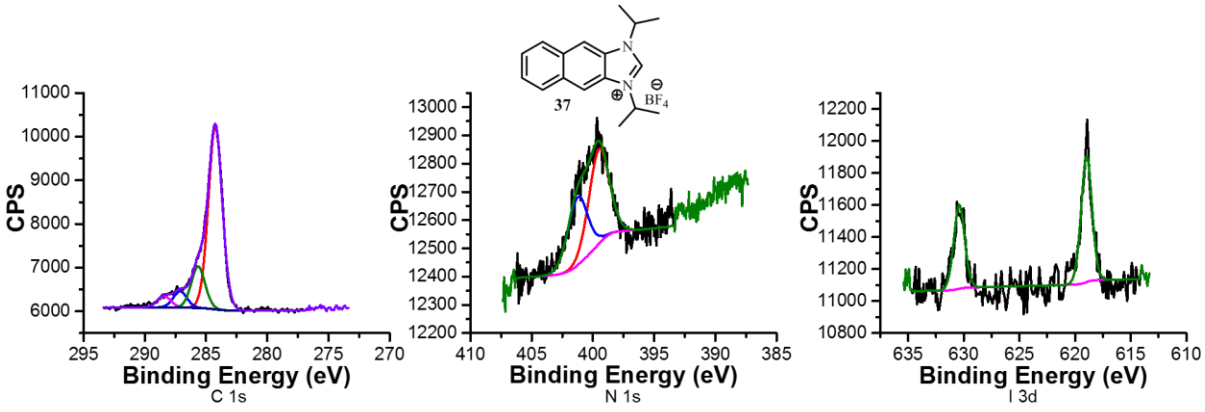

Base Free Deposition

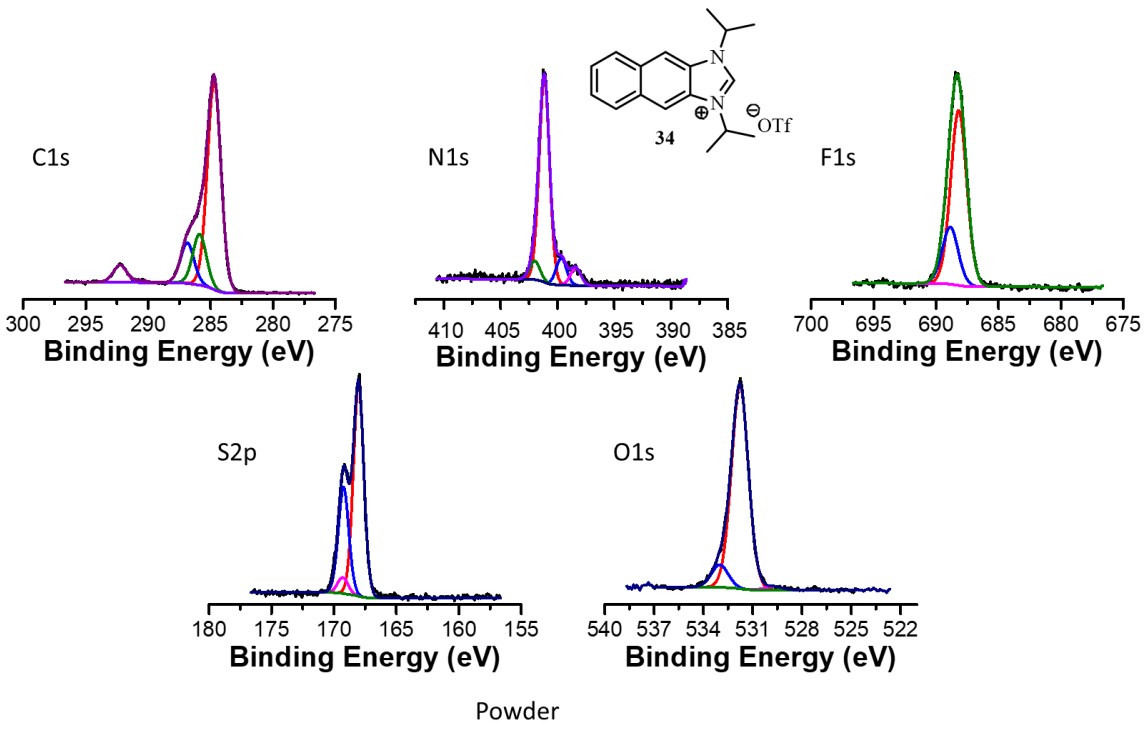

Powder

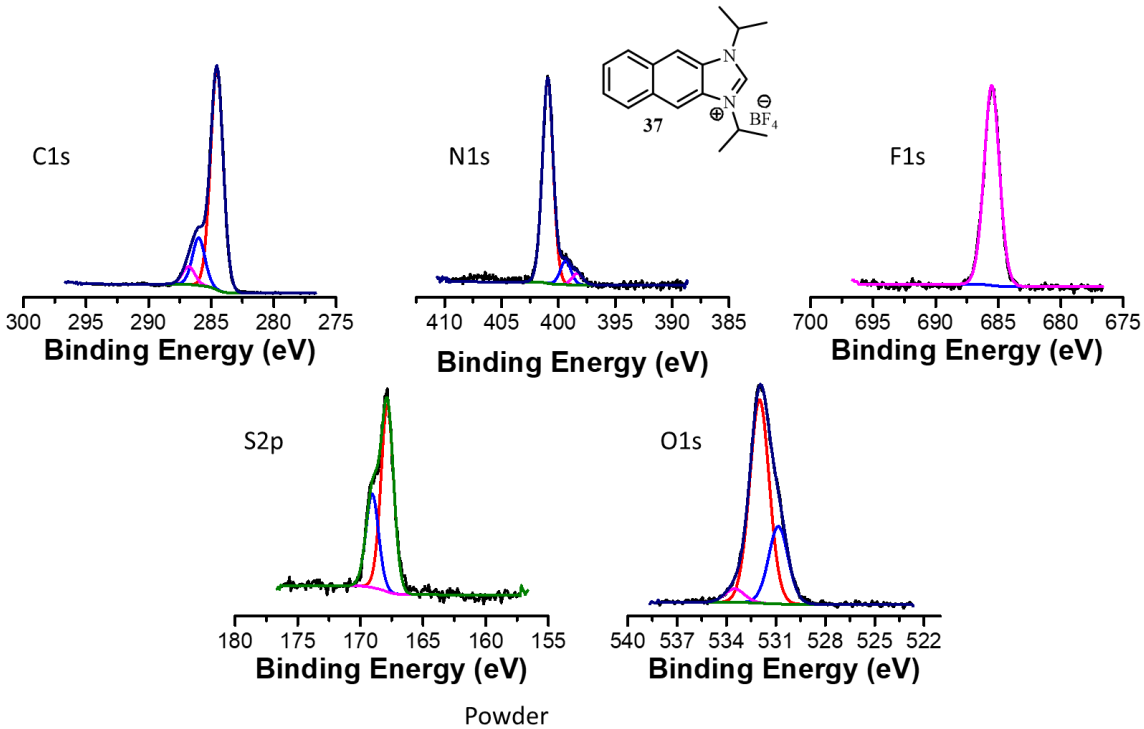

Powder

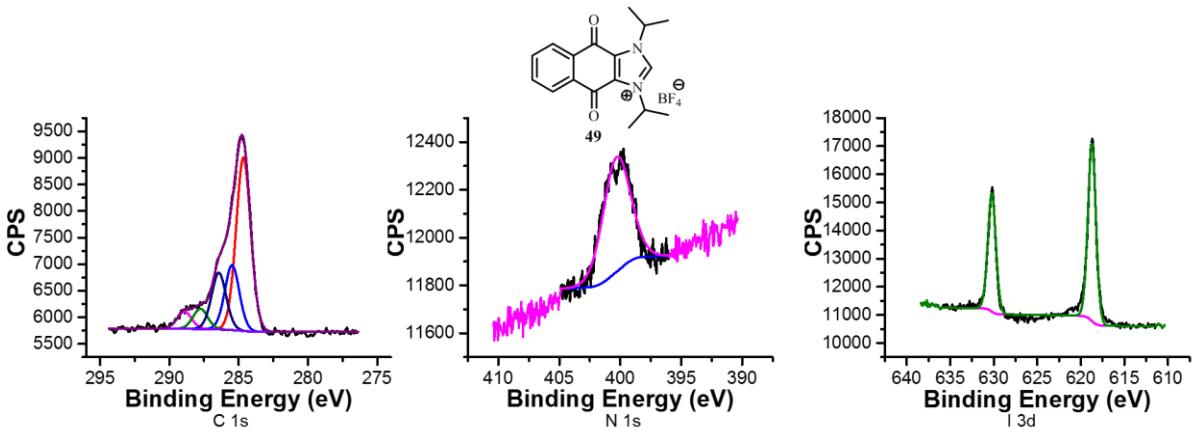

Base Free Deposition

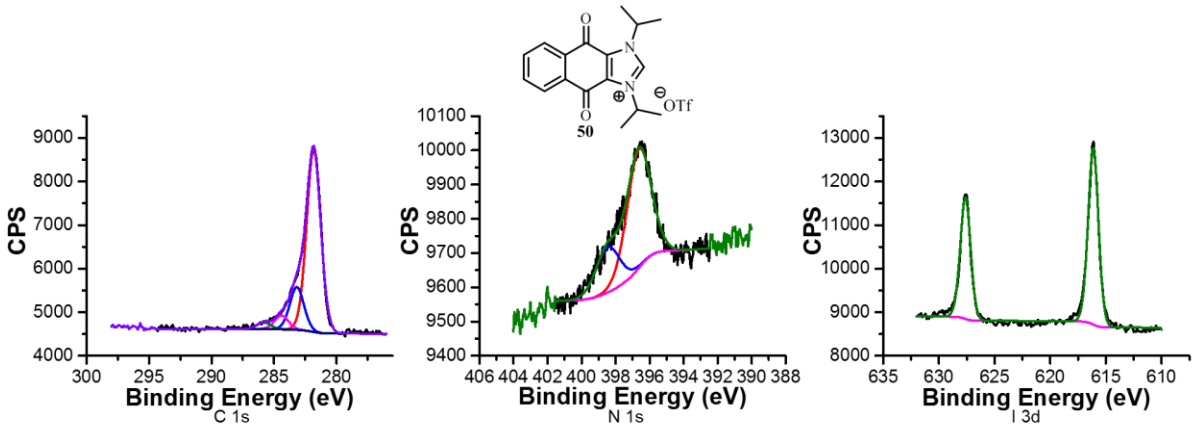

Base Free Deposition

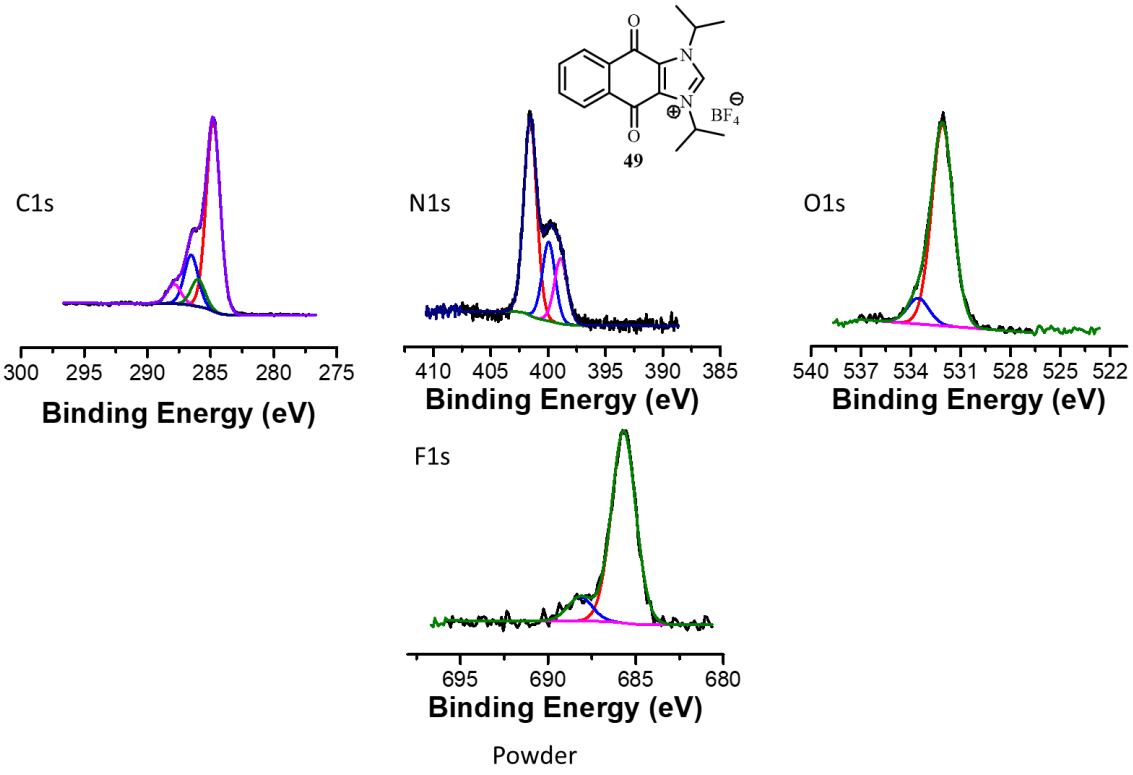
C1s
300 295 290 285 280 275
Binding Energy (eV)
49
N1s
410 405 400 395 390 385
Binding Energy (eV)
O1s
540 537 534 531 528 525 522
Binding Energy (eV)
F1s
695 690 685 680
Binding Energy (eV)
Powder